T2R2 東京科学大学 リサーチリポジトリ
Science Tokyo Research Repository

論文 / 著書情報
Article / Book Information

題目(和文)	
Title(English)	Development of Large-flow Plasma Source Based on Dielectric Barrier Discharge and Its Application to Air Pollutant Degradation
著者(和文)	徐茂
Author(English)	Mao Xu
出典(和文)	学位:博士(工学), 学位授与機関:東京工業大学, 報告番号:甲第12770号, 授与年月日:2024年3月26日, 学位の種別:課程博士, 審査員:沖野 晃俊,中村 健太郎,徳田 崇,田原 麻梨江,柘植 丈治,ジャン 天卓
Citation(English)	Degree:Doctor (Engineering), Conferring organization: Tokyo Institute of Technology, Report number:甲第12770号, Conferred date:2024/3/26, Degree Type:Course doctor, Examiner:,,,,,
学位種別(和文)	博士論文
Type(English)	Doctoral Thesis

Powered by T2R2 (Science Tokyo Research Repository)

Doctoral Thesis

Development of Large-flow Plasma Source Based on Dielectric Barrier Discharge and Its Application to Air Pollutant Degradation

Human Centered Science and Biomedical Engineering
Department of Electrical and Electronic Engineering
Tokyo Institute of Technology

Mao Xu

Supervisor: **Prof. Akitoshi Okino**

February 2024

Table of contents

Chapter 1 Introduction

1.1. Preface

This dissertation unfolds a comprehensive exploration into the realm of large-flow plasma sources, centered on the development and optimization of dielectric barrier discharge (DBD) reactors. The investigation, spanning two distinct phases, showcases a determined pursuit of understanding fundamental properties and decomposition characteristics of volatile organic compounds (VOCs) at large flow rates.

In the initial phase, the research endeavors led to the successful creation of single- and two-layer DBD reactors, laying the foundation for subsequent advancements. The intricacies of the processing parameters of these reactors were dissected to unravel the essential attributes that influence their performance in VOC degradation. The empirical outcomes not only contributed to the understanding of large-flow DBD systems but also laid the groundwork for the subsequent phase of development.

The second phase marked a significant stride forward with the introduction of ten-layer DBD reactors, representing a substantial upscaling of the technology. The dissertation details the meticulous optimization of flow paths, employing both simulation tools and empirical measurements to achieve uniform and stable plasma generation across each layer, even at high flow rates. This innovative approach not only expanded the processing capacities of the DBD reactors but also established an effective methodology for upscaling, with the potential for processing capacities reaching up to 1000 L/min.

Integral to this dissertation is the rigorous exploration of the multilayer configuration, specifically designed for VOC abatement. A comparative analysis of the degradation performance between single-layer, two-layer, and ten-layer reactors confirmed the feasibility and superiority of the multilayer approach in handling large-flow VOC treatment. This validation not only underscores the practical applicability of the developed reactors but also contributes valuable insights to the broader field of environmental technology.

As these pages unfold, they bear witness to the endeavor, ingenuity, and scientific thoroughness invested in the pursuit of advancing large-flow DBD plasma sources for the critical task of VOC abatement. It is my sincere hope that this work not only contributes to the academic discourse but also serves as a catalyst for further innovations in the realm of plasma technology and environmental sustainability.

1.2 Thermal and non-thermal plasmas

Plasma is a state of gas containing a significant amount of charged particles in any combination of ions or electrons, referred to as one of the four fundamental states of matter after solid, liquid, and gas. Furthermore, it is the most common form of ordinary matter in the universe, found predominantly in stars, with lightning and auroras being the most commonly witnessed instances of plasma phenomena that occur within Earth's interior.

Plasmas can be classified into two categories based on electron temperature (T_e) and ion temperature or gas temperture ($T_i \approx T_g$), namely thermal plasmas and non-thermal plasmas (NTP), aslo called hot and cold or low-temperature plasmas (LTP). In a thermal plasma, electrons and heavier particles (ions and neutral atoms) have exchanged enough energy through collisions to reach the same temperature, usually subjected to high gas pressure (Figure 1.1, reported by Ibrahim et al. (2021) [1]). Stated differently, there is a state of local thermal equilibrium between the heavy particles and electrons. The temperature of particles in plasma may reach values in the order of $T_i \approx T_e \approx T_g \geq 10^7$ K, giving rise to the term "hot plasma." A common example of thermal plasma is fusion plasma, whose electon termperature electron temperature is about 25 keV at the center (ITER core plasma).

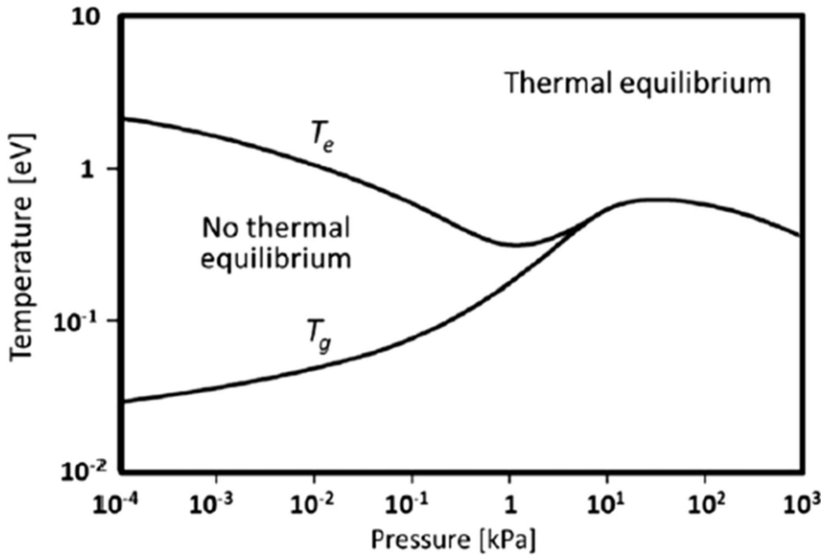

Figure 1.1. Schematic of plasma electron and gas temperature evolution versus pressure [1].

Whereas, non-thermal plasma, is only partially ionized, with mean electron energies of around 20 eV, i.e., $T_e \gg T_i \approx T_g$, which are substantially greater than the surrounding gas

components [2], and are typically created in a vacuum chamber at low pressure (i.e., < 1 atm = 101325 Pa). Since the temperature of heavier particles, such as ions and neutral particles, is almost equal to ambient temperature, non-thermal plasma has a temperature range of 25 °C–100 °C [3]. In the meanwhile, it contains a variety of ions, electrons, active molecules, electric fields, and ultraviolet radiation (UV). Non-thermal plasma is best known for its applications in the semiconductor industry, including plasma etching, plasma deposition, plasma ashing, etc., which are all implemented in vacuum chambers, as presented in Figure 1.2.

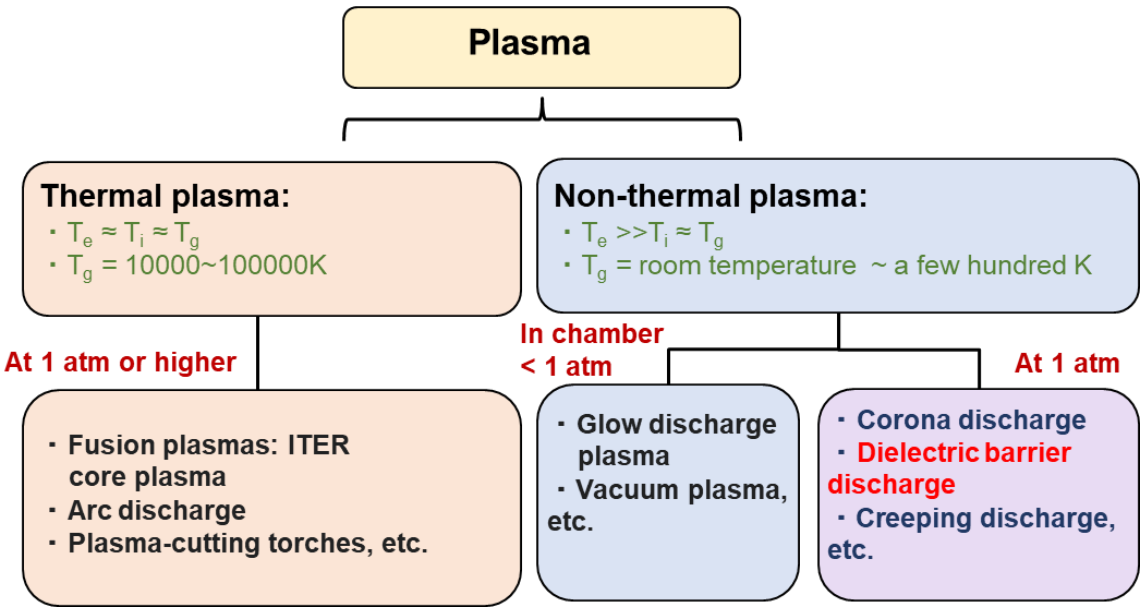

Figure 1.2. Simplified classification of thermal and non-thermal plasmas

Further on, another classification of non-thermal plasmas that are formed at stanardard pressure is low-temperature atmospheric-pressure plasma (LT-APP). In contrast to onther forms of NTP generated in vacuum chamber under low pressure, LT-APP exhibits the following merits. Firstly, a LT-APP system does not require a chamber, making it possible to treat materials of any size and shape at a low running cost, even effective with soft biomateril. Additionally, because LT-APP, the same as NTP, can be generated at temperatures as low as room temperature and possesses abundant reactive species (e.g., OH, O, O_3, and N in air plasma), it is also utilized in numerous fields, which include disinfection, medicine, chemical analysis, and surface modification, in different forms. Examples of LT-APP include corona discharge, dielectric barrier discharge (DBD), creeping discharge, etc., as shown in Figure 1.2. Here, because DBD possesses the following advantages, the application of DBD plasma in air pollutant degradation is the

main focus of this discussion. First, stable plasma can be used to create a homogeneous bulk plasma volume, allowing for uniform treatment of the gaseous pollutants. Moreover, compared to other LT-AAPs, DBD consumes less energy and works more effectively.

1.3. Large-flow treatment for VOC abatement

Volatile organic compounds (VOCs), which comprise a staple of air pollutants, are emitted in various industrial sectors. The main sources of VOCs include the extraction of petroleum and natural gas, combustion of fossil fuels, and the manufacturing of lubricants, adhesives, paints, oil derivatives, and paint coatings. Among these, the paint-coating industry accounts for approximately 50% of all VOC emissions in urban areas [4,5]. The emissions of VOCs in the atmosphere can cause environmental problems and present a major risk to human health. Therefore, the minimization of the adverse impacts of VOCs on public health and air quality improvement is a major concern. The typical measures enforced to process VOCs include adsorption by liquids and activated carbon, combustion by fuels, biofilters, and catalytic oxidation [6,7]. However, these methods are associated with various limitations, such as large energy consumption, production of undesirable by-products in catalytic oxidation, and high-running absorption costs.

Decomposition through nonthermal plasma (NTP) technology, also referred to as low-temperature atmospheric plasma, provides a promising option for VOC treatment owing to its various advantages, e.g., low-energy consumption, high-decomposition efficiency, and ease of operation [7–12]. Additionally, because NTP can be generated at temperatures as low as room temperature and possesses abundant reactive species (e.g., in air-driven plasma, reactive oxygen species: O, O^{2-}, O_3 and OH, and reactive nitrogen species including NO and NO_2 [13,14]), it is also utilized in numerous fields, which include disinfection, medicine, chemical analysis, and surface modification, in different forms [15–19]. For example, Kurosawa et al. and Nomura et al. [15,16] reported the effect of NTP on hemostasis in the form of a plasma jet in medicine. Moreover, NTP exhibited its enhancement effect on the coating of polydopamine on a graphite substrate as well as its conducive influence on protein introduction into plant cells and surface modification [17,18]. Conversely, NTP has been proven to cause deconstructive phenomena on biological cells, e.g., bactericidal effect and DNA damage [19,20]. Among them, dielectric barrier discharge (DBD) plasma is considered the most suitable form for the decomposition of VOCs and has gained considerable attention in the scientific and industrial fields [20,21]. DBD has the following strengths. First, a homogeneous bulk plasma volume can be generated with stable plasma, which enables the gas to be treated

uniformly. Moreover, in comparison with other NTPs, DBD exhibits better effectiveness and consumes less energy [22]. Consequently, DBD has become the mainstream for the configuration of processing systems for different VOC degradations by focusing on single VOC abatement, e.g., toluene, benzene, formaldehyde, etc. The configurations of the DBD systems can be mainly divided into three types: planar, coaxial, and surface, and were well described by Kogelschatz and Pemen et al. [8,22,23]. Meanwhile, they can also be categorized into standalone DBD and DBD catalysis systems in terms of the presence or absence of a catalyst, as the characteristics of DBD systems may be considerably influenced when combined with catalysts [7]. Based on the use of various techniques to adjust parameters (e.g., configuration, geometric features, catalyst incorporation, etc.), it has been proven that the DBD system is an effective and efficient technology for reducing VOCs [6]. Nevertheless, almost all of these efforts were concentrated at the lab scale at small flow rates, and the processing capability was restricted to low gas flow rates (less than a few L/min) [24]. Moreover, all the characterizations and optimizations were also performed at the lab scale, which is far from practical industrial applications. Therefore, there is a high demand to investigate the characteristics of DBD systems for VOC degradation at large flow rates that are more practical in the fields of building ventilation, industrial effluents, etc.

In the first phase of this study, a scalable DBD reactor (single-layer reactor) capable of treating gases at flow rates that are two orders of magnitude larger than small-flow DBD reactors (typically less than 1 L/min) was developed for VOC abatement, and it was characterized at large flow rates. Additionally, another large-flow, multilayer (two-layer) DBD reactor was developed based on the single-layer reactor to verify its scalability and superiority. Using the two reactors, the degradation performance of toluene treatment was analyzed in large-flow scales, including the decomposition rate and energy efficiency at different applied voltages (15–21.5 kV), flow velocities (1–4.48 m/s), flow rates (10–110 L/min), and discharge lengths (150–450 mm). Thus, the feasibility of the configuration of large-flow DBD reactors was also verified. Furthermore, by comparing the degradation performances of the two reactors in different conditions, the feasibility and superiority of the multilayer structure in the large-flow DBD reactor configurations (intended for use for VOC abatement) are demonstrated.

Further on in the second phase, based on the above findings, an upscale multilayer reactor, namely large-flow, ten-layer DBD reactor with a processing capacity of up to 1000 L/min was designed and fabricated. This development is novel and has not been previously reported, serving as an upgraded version of the single- and two-layer DBD reactors in the first phase. The flow path design of the ten-layer DBD reactor was validated via computational fluid dynamics (CFD) simulations and empirical

measurements. In addition, multi-gas ignition involving various gases such as Air, Ar, He, N_2, O_2, and CO_2, as well as electrical and spectroscopic characterizations at large flow rates (50−1000 L/min), were conducted. Following the fundamental characterizations, the decomposition characteristics of toluene treatment at large flow rates (50−1000 L/min) were evaluated, including decomposition rate, energy efficiency, and ozone yield. Furthermore, the effects of high-frequency intermittent-pulse voltage on the decomposition characteristics of the ten-layer DBD reactor were also investigated to verify the feasibility of introducing high-frequency power to improve the degradation performance of large-flow DBD reactors. Therefore, the proposed design methodology and characterization are expected to lay the foundation for developing practical DBD reactor systems aimed at VOC control.

1.4. Outline of this dissertation

The dissertation is structured into six comprehensive chapters, each contributing a crucial piece to the exploration of Dielectric Barrier Discharge (DBD) plasma applications. Chapter 1 serves as the introduction, providing context and setting the stage for the subsequent chapters. In Chapter 2, a comprehensive literature review examines previous studies on DBD-based air pollutant abatement, offering insights into the existing body of knowledge. Chapters 3 and 4 focus on the design and characterization of large-flow DBD reactors, progressing from single- and two-layer configurations to a more advanced ten-layer upgraded version. Chapter 5 delves into the decomposition characterization of the ten-layer upgraded reactor specifically in the decomposition of toluene. The dissertation concludes with Chapter 6, presenting an overall summary that consolidates key findings and contributions from the preceding chapters.

Chapter 2 Literature review of the previous studies on DBD-based air pollutant abatement

2.1. Dielectric barrier discharge (DBD)

DBD, also known as barrier discharge or silent discharge, is a process of electrical discharge that occurs between two electrodes separated by an insulating barrier that limits the current flow in the plasma and prevents the discharge from transitioning to an arc discharge. As illustrated in Figure 2.1, the inclusion of an insulating substance in the discharge path is a common characteristic of DBD designs. Usually, dielectric materials are employed, such as silicon rubber, teflon, glass, quartz, ceramics, enamel, mica, and plastics. DBD devices can be produced in a variety of forms; they are usually either planar, with parallel plates separated by a dielectric, cylindrical with coaxial plates and a dielectric tube between them, or surface discharges involving exposed and embedded electrodes in dielectric materials.

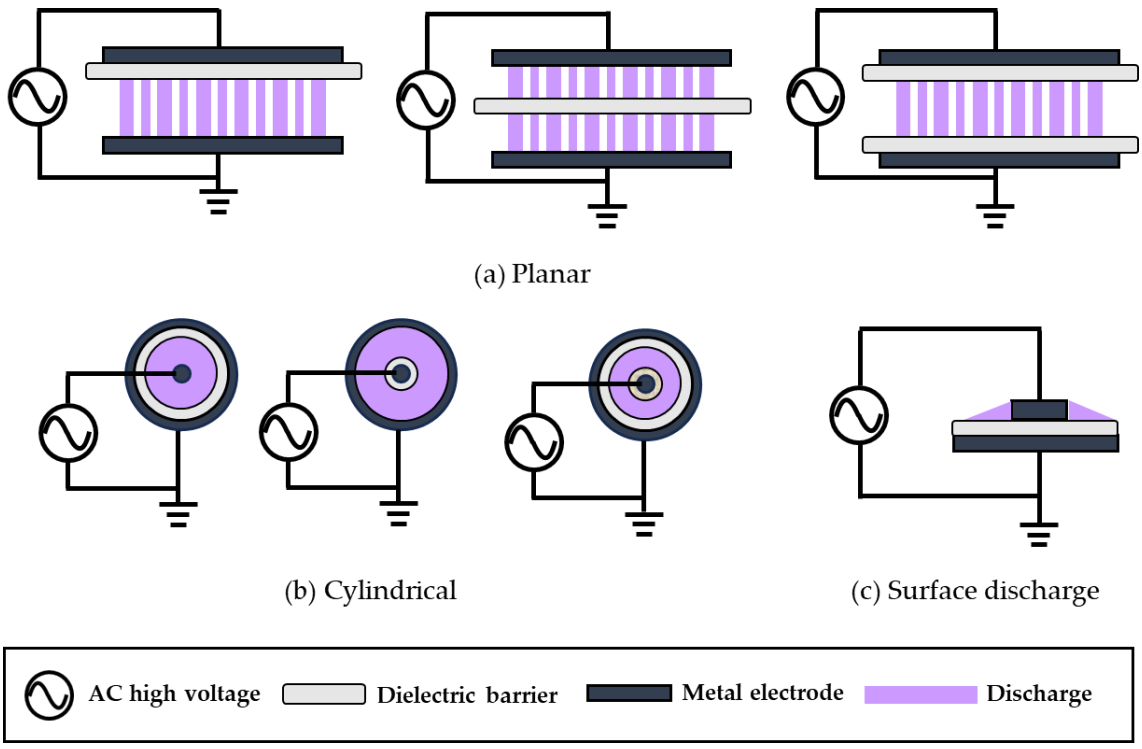

Figure 2.1. Typical dielectric barrier discharge (DBD) configurations: (a) Planar; (b) Cylindrical; (c) Surface discharge.

When a high alternating voltage is applied to the two barrier-separated electrodes in atmospheric or high-pressure gases, a very brief (~ns) microdischarge is formed and continues intermittently. Those microdischarges are filamentary plasmas with a diameter of approximately 100 nm, an electron temperature of 1~10 eV, and an electron density of about 10^{20} m^{-3}. The presence of a dielectric barrier stops the progression to spark and arc discharges, and because the duration of microdischarges is as short as the order of nanoseconds, the energy transfer from electrons to ions and gas molecules is negligible, and the ions and gas molecules remain at room temperature. Normally, dielectric barrier discharge at atmospheric pressure operates at a low temperature (gas temperature), however, has a high electron temperature and has an excellent ability to generate active species (atoms and molecules with high chemical reactivity, called radicals).

Table 2.1. Operating conditions of DBD and the parameters of the filamentary plasma

Operation conditions	
Pressure	10^5 Pa
Electric field	10 kV/m ~ 10 MV/m
Mean electron density	10^{19} ~ 10^{20} m^{-3}
Degree of ionization	10^{-5} ~ 10^{-4}
Filamentary plasma	
Diameter of a filamentary plasma	~ 100 μm
Electric Current	0.1 ~ 0.5 A
Current density	~ 10^{17} Am^{-2}
Electron density	~ 10^{20} m^{-3}
Electronic temperature	1 ~10 eV
Lifetime	~ ns

Therefore, it is used in many fields such as ozone generators, surface treatment of polymer materials, and degradation of environmental pollutants. In the meantime, DBD is also applied to the AC surface discharge type, which is the main discharge method for plasma displays. In conclusion, a dielectric barrier discharge has a pair of electrodes, and at least one of the electrodes is covered with a dielectric, as discussed above, and shown in Figure 2.1. Plasma is generated in the gap when an alternating current voltage of a few kV with a frequency of about 50 Hz to 500 kHz is applied between the electrodes. The operating conditions and plasma parameters of DBD is summarize in Table 2.1.

2.2. Q-V plot (Lissajous figure) of a DBD load

Because of its multiple uses, dielectric barrier discharge (DBD) has received a lot of attention. For such discharges, measuring current and voltage waveforms is a key diagnostic approach. The observed waveforms are influenced by the parameters of the external electrical circuit, and the presence of dielectric barriers frequently makes extracting information about the discharge itself difficult or impossible. Manley proposed in 1943 that the electrical characteristics of the discharge be inferred by graphing the relationship between the charge on the DBD reactor electrode and the applied voltage (Q-V plot) [25]. Thus, the Manley method has gradually become a standard and widely used tool for DBD discharge electrodiagnosis. The Q-V plot, also known as a Lissajous figure, is widely used to calculate the discharge power absorbed by the DBD load since the Q-V plot's closed zone corresponds to the power linked into the DBD load. In addition, unlike current waveform detection, charge measurements do not require expensive high-bandwidth probes and can be easily measured by placing an additional capacitor in series with the DBD load.

Figure 2.2 presents a general measurement circuit for Q-V plots. Therein, the monitoring capacitor C_m, which integrates the current and detects the charge, is connected in series with the capacitance C_{eff} of the DBD load. Since $C_m >> C_{eff}$, when the applied voltage is divided into C_{eff} and C_m, most of the applied voltage is applied to C_{eff}. In particular, the capacitance of C_m should be several thousand times that of C_{eff}. This is to prevent the circuit constants from being disturbed by the connection of the measuring capacitor.

Typically, the Q-V plot appears as a parallelogram, as shown in Figure 2.3 (a). The general interpretation of this Q-V plot is as follows: a DBD load can be represented as a series connection of two capacitors, C_g and C_d, where C_g is the air gap capacitance and C_d is the dielectric barrier capacitance (Figure 2.2 (b)). As shown in Figure 2.3, when the voltage across the air gap exceeds a certain value V_{min} (i.e., the minimum external voltage at which the ignition starts, the ignition voltage), series of filamentous discharge channels begin to bridge the air gap and continue to develop until the voltage reaches a maximum of V_{max} at point B.

From B to C, there is no discharge, and the gap charge generated in the previous period changes to the opposite sign due to the displacement current. The dielectric breakdown condition of polarity reversal is reached at C, and a new discharge phase from C to D

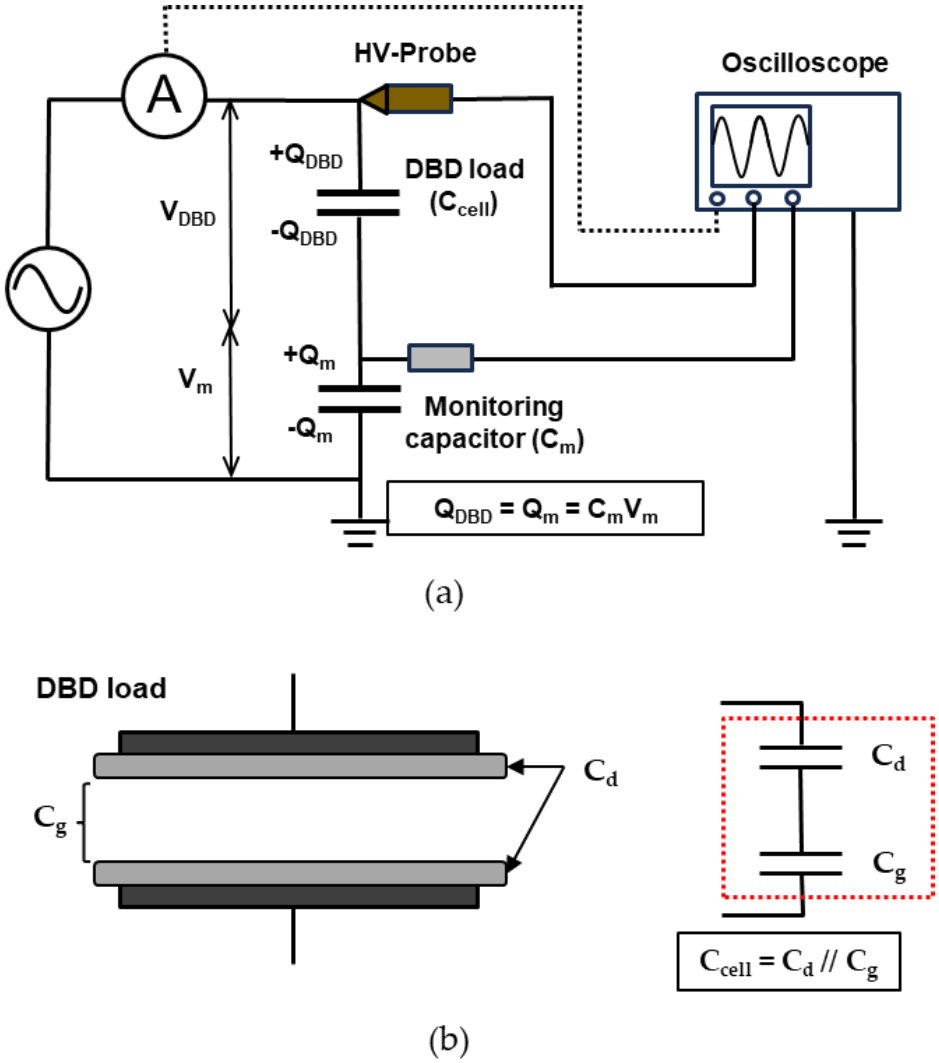

Figure 2.2. (a) Measurement circuit for Q-V plots (Lissajous figures) and (b) the capacitance composition of a DBD load.

begins [26,27]. Thus, the lines BC and DA represent the state of discharge-off, where only displacement current (I(t)) are present, the slope dQ/dV corresponds to the series capacitance of C_d and C_g, and they can be expressed as follows [21,27]:

$$I(t) = C_{cell}\frac{dV(t)}{dt} \tag{2.1}$$

$$C_{cell} = \frac{C_d C_g}{C_d + C_g} \tag{2.2}$$

In the meantime, the capacitance of the gas gap C_g during discharge-off stage can be calculated by:

$$C_g = \frac{C_d C_{cell}}{C_d - C_{cell}} \tag{2.3}$$

While the lines AB and CD represent the state of discharge-on where the air gap is bridged. The slope dQ/dU of the lines is the effective capacitance, which should be equal to Cd for a fully bridged gap. The voltage drop V_m across the monitoring capacitance C_m can be used to calculate the charge Q_{DBD} flowing through the DBD load, as presented in Figure 2.2(a):

$$Q_{DBD} = Q_m = V_m C_m \tag{2.4}$$

In addition, the potential difference (V_g) across the gas gap is constant. V_g is equal to the effective breakdown voltage (V_b) (Figure 2.3(a)), which can be determined as the voltage at zero charge intercept. On the other hand, the variation in charge in the discharge state is equal to the maximum charge (q_{max}) that transfers through the gas gap, as described below [28–30]:

$$q_{max} = \frac{1}{1 - \frac{C_{cell}}{C_d}} Q_0 \tag{2.5}$$

The minimum external voltage (V_{min}) at which ignition occurs is greater than the gas gap voltage corresponding to the breakdown voltage (V_b), and can be derived from Equation 2.6, as shown in Figure 2.3(a).

$$V_{min} = \frac{1}{1 - \frac{C_{cell}}{C_d}} V_b \tag{2.6}$$

With all the above parameters, the classical Q-V plot can be described by the following equation[28,29]:

$$Q(t) \pm \frac{Q_0}{2} = C_{DBD}(V(t) \pm V_g) \tag{2.7}$$

, where during discharge-on, $C_{DBD} = C_d$, $V_g = V_b$, $Q_0 = 0$; while during discharge off, $C_{DBD} = C_{cell}$, $V_g = 0$, Q_0 has the relation of Equation (2.5) with q_{max}.

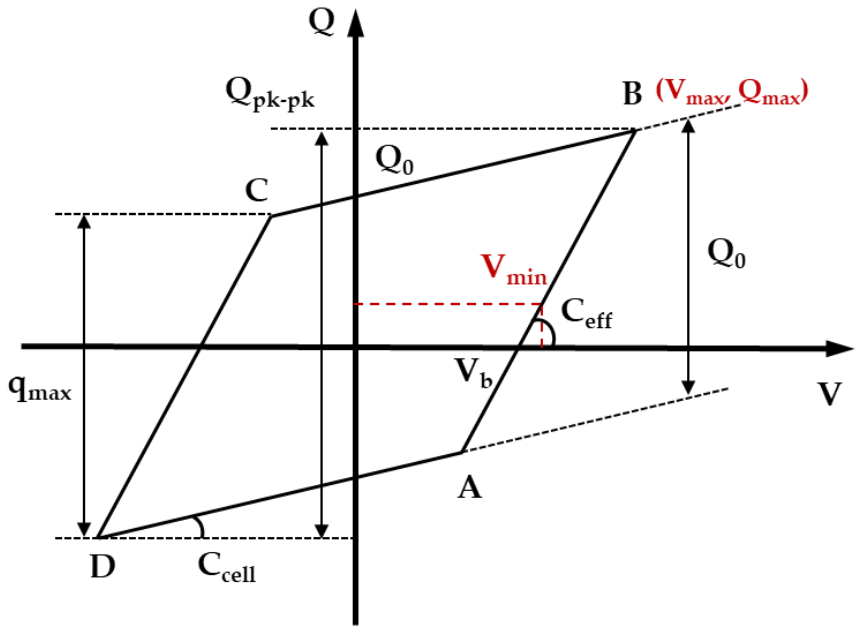

(a)

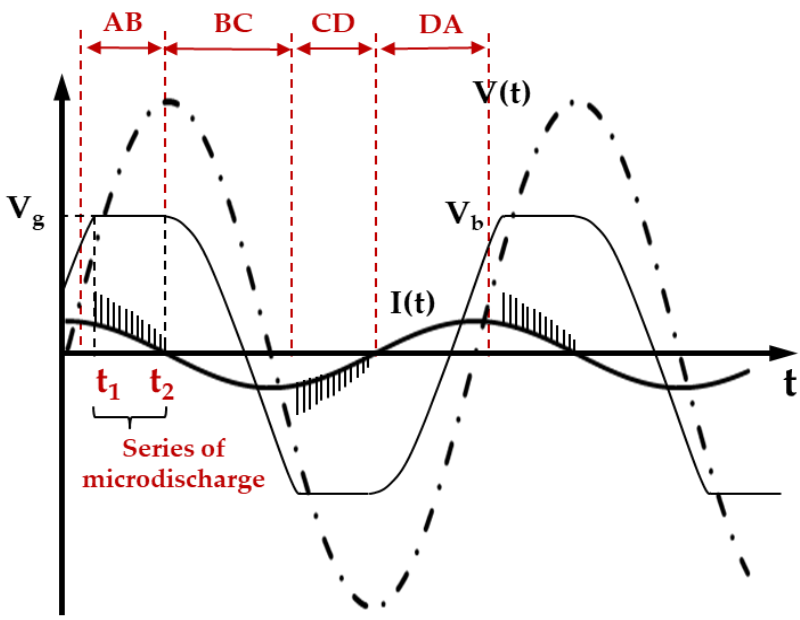

(b)

Figure 2.3. (a) Typical Q-V plot (Lissajous figure) of a DBD load and (b) corresponding voltage V(t) and discharge current I(t) waveforms.

Meanwhile, from this Q-V plot (Figure 2.3(a)), the minimum external voltage V_{min} at which ignition occurs, the energy consumption E_{el} per voltage cycle (f), and the power W can also be estimated [30].

$$W = \oint V(t)dQ = C_{means} \oint V(t)dV_{means}$$

$$= 4C_d \left(\frac{1}{1 + \frac{C_g}{C_d}} V_{min} \right) (V_{max} - V_{min})$$

$$= 2V_b C_d (2V_{max} - 2V_{min}) = 2V_b q_{max}$$

$$\equiv area\ of\ Q - V\ plot$$

$$W = E_{el} \frac{1}{T} = E_{el} f \tag{2.8}$$

Briefly, the power P_{el} that deposited to a DBD load can be calculated from the following Equation (2.9), using the parameters from a Q-V plot.

$$W = 2V_b q_{max} f \tag{2.9}$$

2.3 Typical VOCs to be studied

A variety of hazardous compounds that harm both the environment and human life are released into the atmosphere by the exhaust of both stationary (e.g., plants) and mobile e.g., vehicles) sources [31]. Volatile organic compounds (VOCs) are a significant and sizable class of pollutants, following NO_x, SO_x, H_2S, etc. They evaporate quickly and reach the earth's atmosphere due to their high volatility. They can produce photochemical haze, secondary aerosols, and tropospheric ozone, among other effects, depending on their chemical composition and concentration [32]. They also impact the thinning of the stratospheric ozone layer and the acceleration of global warming. Their harmful impacts on human health are demonstrated by the fact that some of them have poisonous and unpleasant odors, while others have cancerous properties. Table 2.2 lists common volatile organic compounds (VOCs) that have been investigated for elimination using NTP and plasma-catalysis, along with the associated health effects, which has been reported by Vandenbrouke at al. (2011) [33].

Well-established abatement technologies including adsorption, thermal and catalytic oxidation, membrane separation, bioreaction, and photocatalysis are examples of conventional approaches for controlling VOC emissions [34]. The disadvantage of these

Table 2.2. Typical VOCs to be targeted and their health effects [33].

VOC	Formula	Effects
Acetone	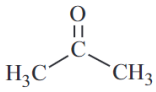	Carcinogen
Formaldehyde	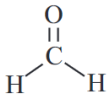	Sore throat, dizziness, headache
Dichloroethane	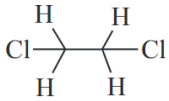	Paralysis of nerve center
Trichloroethylene	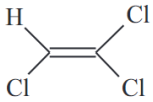	Liver and kidney disease, paralysis of nerve center
Tetrachloroethylene	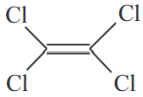	Probable heart and liver disease, skin irritation
Benzene		Carcinogen
Toluene		Headache, dizziness
Xylene	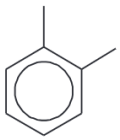	Headache, dizziness
Styrene	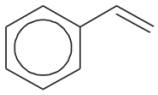	Probable carcinogen

methods is that they become inefficient, expensive, and difficult to attain the necessary performance when low concentrations of volatile organic compounds (VOCs) need to be treated. [13,14]. Due to this and given the increased emission regulations, an alternate technique that overcomes these shortcomings is required. In contrast, NTP technology has continued to attract a great deal of interest as a potential method to reduce VOCs, since it produces a large number of energetic electrons and reactive species (e.g., in air-driven plasma, reactive oxygen species: O, O_2^-, O_3 and OH, and reactive nitrogen species

including NO and NO_2 [24]) that can be used to dissociate VOC molecules effectively and economically. Essentially, the energy supplied to the NTP system is used almost entirely to accelerate electrons, which typically reach temperatures in the range of 10,000 and 250000 K (1 and 20 eV), while the background gas remains at ambient temperature (e.g., room temperature). Meanwhile, the rapidly accelerated primary electrons continue to collide with the surrounding background gas molecules (air, N_2, O_2, H_2O, etc.), thereby forming a highly reactive collective of ions, radicals, excited molecules, and secondary electrons. This process exhibits a highly non-selectivity, which allows for rapid decomposition of harmful pollutants in a chemically reactive environment.

NTP can be generated through a variety of forms, including electron beam, microwave discharge, arc/plasma torch, dielectric barrier discharge (DBD), corona discharge, and gliding discharge reactor [6,24]. Of all these NTP types, DBD plasma has recently attracted a great deal of attention for its ability to generate large-volume and spatially well-distributed plasma, which is highly suitable for the decomposition of gaseous pollutants. While DBD has been suggested in the literature as an end-of-pipe treatment for degrading VOCs, it still has certain drawbacks, primarily the generation of unwanted products and partial mineralization, which reduce the system's effectiveness and shorten the electrode's lifespan. In order to address these problems, scientists are linking the advantages of DBD to the placement of catalyst either in the plasma discharge zone (in-plasma catalyst (IPC)), close to the reaction zone (post-plasma catalyst (PPC)), or both; this technique is referred to as DBD-catalysis. Although DBD and DBD-catalysis systems have been reported for the treatment of numerous VOCs (as shown in Table 2.2) in previous studies by numerous researchers, the focus here is on the treatment of toluene using DBD technologies because it is one of the most studied targets (i.e. trichloroethylene, benzene, and toluene) in many studies as a typical VOC, because it is a toxic and refractory aromatic hydrocarbon. Therefore, the DBD reactors designed in this dissertation were also evaluated for toluene degradation for horizontal comparisons with our studies.

2.4 Effects of processing parameters on VOC treatment

Various geometric and processing parameters of DBD systems are considered to affect the VOC degradation performance, since geometric parameters (e.g., electrode material and shape, discharge gap, discharge length, dielectric material, the presence of catalyst) plays a vital role in the plasma discharge characteristics themselves, whereas processing parameters including initial VOC concentration, gas feeding flow rate, input power, O_2 and H_2O content have an influential effect on the VOC degradation process [6,36].

Evaluation of VOC degradation performance generally includes two key metrics: removal efficiency (also referred to as degradation efficiency, decomposition efficiency, decomposition rate, etc. in different studies) and energy efficiency (also referred to as energy yield). The removal efficiency of VOCs is generally defined as follows [37–41]:
Removal efficiency:

$$\eta(\%) = \frac{VOC_{in} - VOC_{out}}{VOC_{in}} \times 100 \tag{2.10}$$

where VOC_{in} (ppm)and VOC_{out} (ppm) are the initial and final concentrations of VOCs detected before and after DBD treatment, respectively.
While the energy efficiency (EE, g/kWh) is expressed by equation (2.11), where M represents the relative molecular mass of VOC (e.g., M (toluene) = 92.15), and Q (L/min) and P (W) are the gas feeding flow rate and the discharge power consumed by DBD plasma.
Energy efficiency:

$$EE(\%) = \frac{M \times VOC_{in} \times Q \times \eta \times 60}{P \times 22.4 \times 100} \times 10^{-3} \tag{2.11}$$

In addition to the two metrics mentioned above, specific input energy (SIE) and CO_2 selectivity (the degree of mineralization) are also essential.
Specific input energy:

$$SIE(J/L) = \frac{P}{Q} \tag{2.12}$$

CO_2 selectivity:

$$S_{co2}(\%) = \frac{CO_{2,out} - CO_{2.in}}{Number\ of\ carbon\ in\ VOC \times (VOC_{in} - VOC_{out})} \times 100 \tag{2.13}$$

Where $CO_{2,\ in}$ (ppm) and $CO_{2,\ out}$ (ppm) are the initial and final concentrations of CO_2 detected before and after DBD treatment, respectively.

Table 2.3 and 2.4 lists the geometric and material parameters for DBD systems and their effects on the treatment of VOCs, based on the data attracted from Refs. [42–45] to discuss the effects of electrodes, from Refs. [42,46] for the discussion on the effects of discharge gap, from Refs. [47–50] to demonstrate the effects of discharge length, and from Refs. [51–54] to explain the effects of dielectric barrier material. This indicates that proper geometric design, electrode and dielectric barrier material selection for DBD

system construction are influential factors in optimizing its degradation performance on VOC treatment.

Table 2.3. Geometric and material parameters for DBD systems

Geometric parameters	Value	Effect
Electrode material and geometry	Metallic rod, brass wire, tungsten, ferroelectric material, sintered metal fiber	• Higher energy of the ionized electrons • Increasing intensity of plasma
Discharge gap	1-6 mm (mostly 2-3 mm)	• Stable plasma generation • Stronger electric field strength in the gap
Discharge length	Widely varied depending the DBD reactor size (e.g., 1.8 – 30 cm)	• Discharge zone or reaction zone • Residence time • Input power
Dielectric barrier material	Quartz tubes, silica glass, alumina, ceramics, etc. (dielectric constant: 4 - 100)	• Equivalent dielectric capacitance

Table 2.4. Effects of processing parameters on VOC treatment.

Processing parameters	Value	Effect
Initial concentration	31 to 939.06 ppm	• High initial VOC concentrations need either a longer residence time or a higher input power
Input power	Varies widely depending on different DBD system (e.g., 26 to 65 W, 60 to 110 W)	• Number of highly energized electrons and the internal electric field • Pursuance for pre-liminary chemical reactions • Increasing input power enhances the VOCs conversion efficiency
Gas feeding rate	1–10 L/min or lower (in laboratory scale)	• Conversion efficiency related to the residence time • Probability of collision between the targeted molecules and active species
O_2 content	Varies widely (e.g., 0.5%, 2-3%, 2-4%, >4%, 20%)	• $e^- + O_2 \rightarrow 2O + e^-$, $O + O_2 \rightarrow O_3$ • The number and type of active species are highly influenced by the type of the carrier gas • Proper O_2 concentration resulting in a higher reduction of VOCs
H_2O content	Varies widely (e.g., 1 – 100%)	• $e^- + H_2O \rightarrow H + OH + e^-$, $O(1D) + H_2O \rightarrow 2OH$ • OH radicals are the main actors in the destruction • Proper H_2O content leading higher conversion efficiency
Presence of catalysts	Al_2O_3, Fe_2O_3/MnO honeycomb, SMF, $MnPO_4$, Ag/TiO_2, etc.	• Plasma discharge characteristics • Decomposition rate • CO2 selectivity, etc.

In addition, the effects of processing parameters on VOC treatment are also discussed based on the data collected from Refs. [55–59] for the initial concentration of VOCs, from [60–62] for gas feeding rate, from Refs. [55,63,64] for input power effects, from Refs. [40,59,65–68], from Refs. [33,60,65] ,and from Refs. [40,59,66–69] to discuss the effects of combining with catalysts. As can be seen in Table 2.4, various processing parameters can affect the degradation performance on VOC treatment via either changing the plasma discharge characteristics (e.g., number and velocity of electrons, highly reactive species generation with O_2, H_2O or both, the synergetic effects with catalysts, etc.). This suggests that optimization of processing parameters is essential for a variety of applications.

2.5 Degradation pathways for toluene in DBD plasma

Toluene is the most studied VOC for abatement on a laboratory scale since it is widely employed as a solvent in the paint, dye, rubber, chemical, glue, printing, and pharmaceutical sectors. Yue et al. (2023) [70] have theoretically and experimentally studied the toluene degradation mechanism in air/H_2O DBD plasma by combining detailed kinetics modeling and in-situ optical emission spectroscopy (OES) measurements. Therein, a cylindrical DBD reactor was employed to investigate the dependences toluene conversion, product distribution on discharge power, inlet toluene concentration and gas flow rates, with gaseous products being monitored by an online

Table 2.5. Experimental condition [70].

Parameters	Values
Power frequency, kHz	10
Gas type	Air/H_2O
Total gas flow rate F_{gas}, mL/min	500–1500
Relative humidity, %	1
Preheating temperature, °C	300
Inlet toluene concentration $C_{in,toluene}$, ppm	1000–2000
Discharge power P, W	40–120

mass spectrometer and condensable products being analyzed by GC-MS. The corresponding experimental condition is listed in Table 2.5, where toluene decomposition efficiency > 82% and 38% of CO_2 selectivity have been achieved at P = 115 W, initial toluene concentration = 1000 ppm, and F_{gas} = 500 mL/min.

According to the authors, in an air/H_2O driven DBD plasma, the following two stages of the primary cleavage reactions of toluene can be expected.

Discharge stage:

$$e^- + C_6H_5CH_3 \rightarrow C_6H_5CH_2 + H + e^- \quad \text{R2.1}$$

$$e^- + C_6H_5CH_3 \rightarrow C_6H_6 + CH_2 + e^- \quad \text{R2.2}$$

$$e^- + C_6H_5CH_3 \rightarrow C_6H_5 + CH_3 + e^- \quad \text{R2.3}$$

$$N_2(A) + C_6H_5CH_3 \rightarrow C_6H_5CH_2 + H + N_2 \quad \text{R2.4}$$

$$N_2(A) + C_6H_5CH_3 \rightarrow C_6H_5 + CH_3 + N_2 \quad \text{R2.5}$$

$$O_2^+ + C_6H_5CH_3 \rightarrow C_6H_5CH_3^+ + O_2 \quad \text{R2.6}$$

$$N_4^+ + C_6H_5CH_3 \rightarrow C_6H_5CH_3^+ + 2N_2 \quad \text{R2.7}$$

In the discharge phase, toluene breakdown is mostly achieved through electron collision processes (reaction R2.1-2.3), excited species (reaction R2.4, R2.5), and ion fragmentation reactions (reaction R2.6, R2.7).

Afterglow stage:

$$OH + C_6H_5CH_3 \rightarrow C_6H_5CH_2 + H_2O \quad \text{R2.8}$$

$$OH + C_6H_5CH_3 \rightarrow C_6H_4CH_3 + H_2O \quad \text{R2.9}$$

$$O + C_6H_5CH_3 \rightarrow OC_6H_4CH_3 + H \quad \text{R2.10}$$

Whereas at the afterglow stage, toluene degradation mainly involves oxidation reactions with radicals OH and O (reaction R2.8-2.10). These reactions result in the primary breakdown products of toluene being benzyl, benzene, me-phenoxy, and phenyl, as presented in Figure 2.4. Subsequently, these species react with the strong oxidizing agents OH, O, and O_2 to create phenoxy (C_6H_5O), phenol (C_6H_5OH), benzoquinone ($C_6H_4O_2$), benzaldehyde (C_6H_5CHO), and other compounds that play key roles in the ring-opening events. This process follows a general ring-opening reaction course: toluene → benzene (phenyl, me-phenoxy) → cyclopentadienyl (cyclopentadiene, benzoquinone) → unstable intermediates polycarbenes (butadienyl), as described in Figure 2.4. Following that, the products of the ring-opening process are then oxidized by O-containing species to produce CO_2 and H_2O.

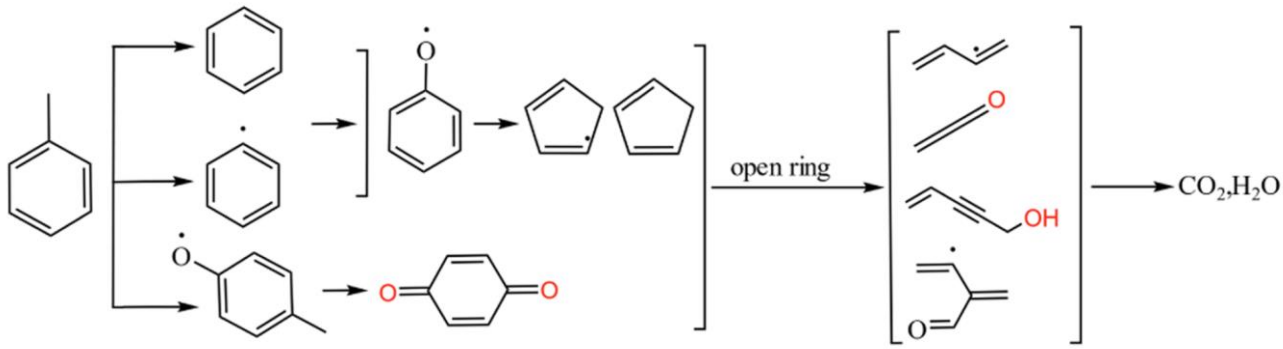

Figure 2.4. The ring-opening pathway and important intermediates for toluene degradation [70].

Among these compounds involved in the reaction course, cyclopentadiene (C_5H_5), benzaldehyde (C_6H_5CHO), benzoquinone ($C_6H_4O_2$), and cyclopentadienyl (C_5H_6) are crucial intermediaries in the ring-opening of toluene.

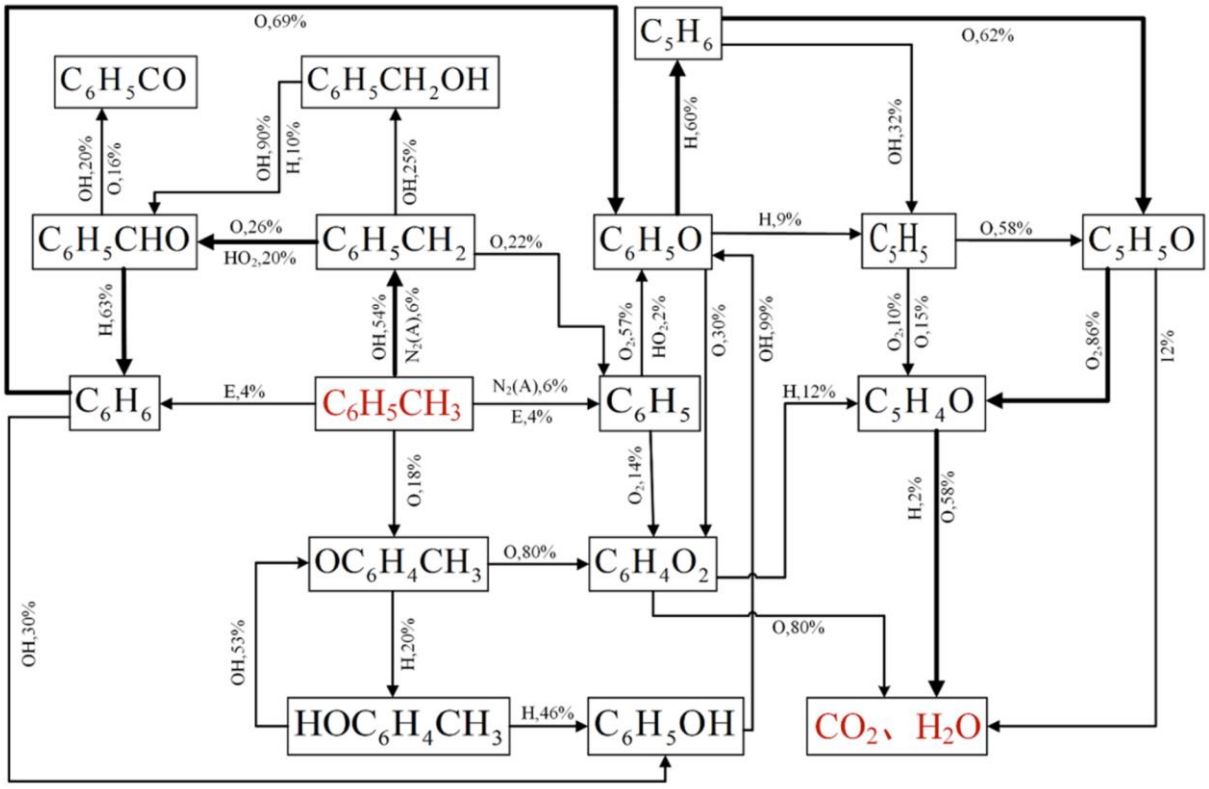

Figure 2.5. Reaction pathway and their corresponding ratios diagram for toluene degradation [70].

Furthermore, based on the discussions above, a general reaction pathway and the contribution of these key active particles to toluene degradation and its intermediates have been also proposed and constructed by Yue et al. [70], as shown in Figure 2.5. The C-H bond of the methyl group in the toluene molecule is most likely to be cleaved by energetic electrons or other active particle collisions to form benzyl, which accounts for 60% of the initial decomposition of toluene. Next, 46% of benzyl is oxidized by O and HO_2 to form benzaldehyde, which further reacts with O, OH, and H to form phenylmethanone (C_6H_5CO) and benzene, contributing 32% and 63% of benzaldehyde consumption, respectively. Benzene then compounds with OH to form phenoxy (69%), then phenol (30%), and phenoxy reacts with H to form cyclopentadiene and CO. The oxidation of cyclopentadiene with O is an important ring-opening reaction, producing polycarbene (C_5H_5O) or alkynol (C_5H_4O) and these were eventually converted to CO_2,

H_2O, and other products. Thus, a most plausible pathway for toluene degradation in Air/H_2O DBD plasma has been proposed as follows:

Toluene (60%)→benzyl (46%)→benzaldehyde (63%)→benzene (69%)→phenoxy (60%) →cyclopentadiene (62%)→polycarbenes (86%)→alkynols (60%)→CO_2/H_2O.

In summary, there are four pathways by which toluene degrades in air/H2O DBD: electron impact reactions, oxidation via radicals, excited-molecule, and ion-molecule reactions. Of the four pathways, the one that has the most impact on the dissociation of toluene is the ring-opening and bond-breaking process of organic matter caused by the impact and oxidation of radicals such as O and OH. Mostly during the afterglow phase, these radicals target the toluene molecule and break C=C, C-H, or C-C bonds. This causes the final decomposition and oxidation of toluene to generate CO_2, H_2O, etc. On the contrary, the short lifetime of charged electrons and the low concentration of toluene in the reaction environment prevented the direct collision between energetic electrons and toluene molecules, which mostly happened during the discharge phase.

In contrast, Jiang et al. (2020) [36] have also reported a possible pathway for toluene degradation in air/H_2O DBD plasma, as shown in Figure 2.6. Therein, a multistage rod-type DBD reactor was used for the decomposition of toluene, and approximately 65 % of decomposition efficiency, 35% of CO_2, and 65% of COx selectivity have been obtained at an initial toluene concentration = 100ppm, gas flow rate = 1.0 L/min, specific input energy (SIE) = 2.3 kJ/L respectively. the gaseous intermediates and products were identified by GC–MS and FTIR, and thereby a possible toluene degradation pathway after plasma treatment was proposed, as shown in Figure 2.6.

According to the authors, the first degradation pathway of toluene is caused by the breakdown of the C-H bond between the methyl and benzene rings and the C-C bond

between the benzene ring and the methyl group, producing benzyl and phenyl radicals. Benzyl and phenyl are then rapidly oxidized to benzaldehyde, benzoic acid, 1,4-benzenediol, 2-methyl, and diethoxymethyl in the presence of O-containing active species including ·O and ·OH. The $\cdot NO_2$ radical may also be involved in the chemical reaction, as nitroaromatics were identified.

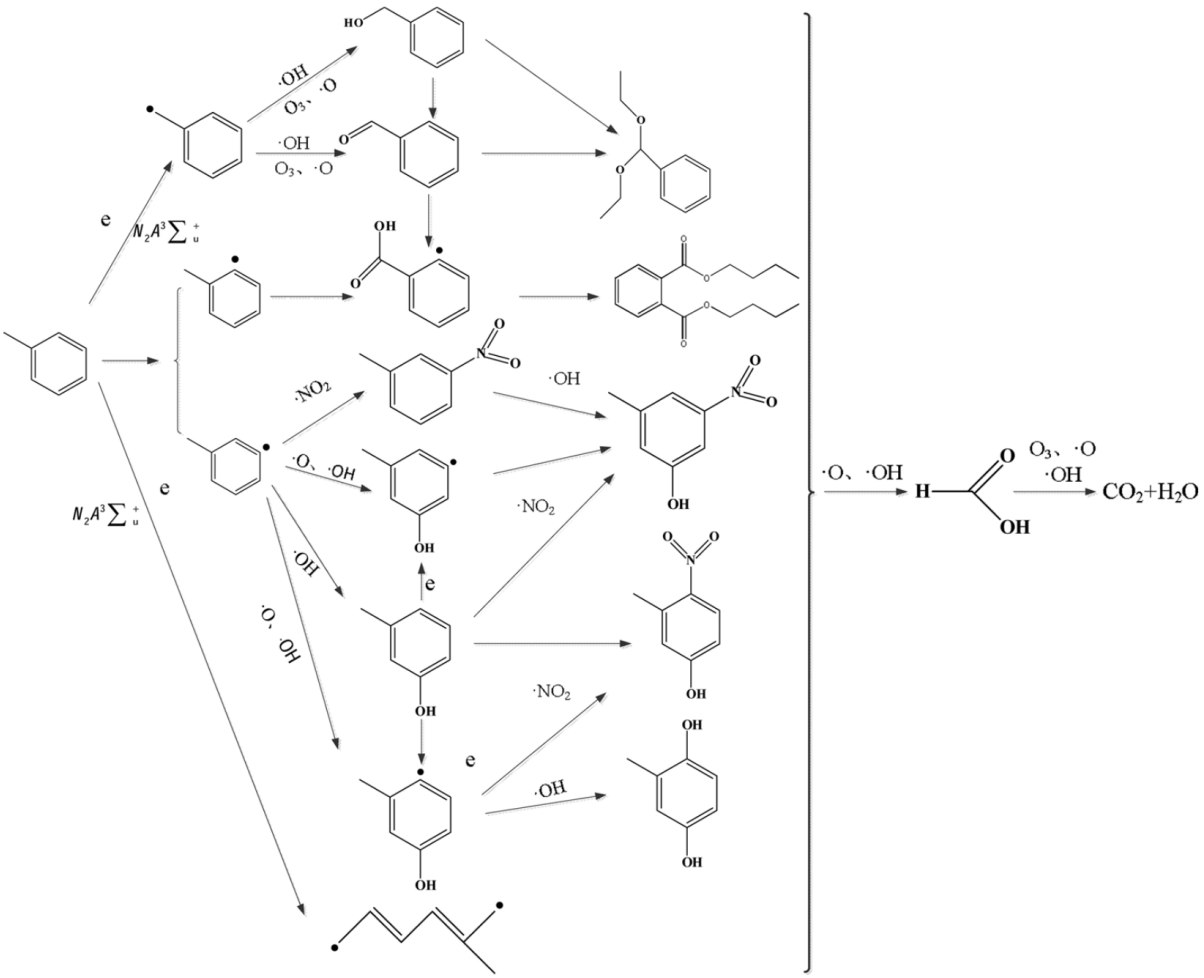

Figure 2.6. The possible degradation pathways of toluene by pulse-modulated multistage DBD plasma [69].

In addition, toluene is also directly oxidized by active species to produce benzaldehyde. Organic intermediates are attacked by energetic electrons and active species to undergo ring-opening reactions and are eventually oxidized by O-containing active species to produce CO_x and H_2O. Formic acid, on the other hand, was identified as a gaseous organic intermediate. Oxidation of the methyl group of toluene is a major

contributor to the formation of formic acid, which is further oxidized to CO_2 and H_2O by O-containing radicals.

The degradation pathway of toluene in DBD plasma reported by Jiang et al. [70] exhibits a good agreement with that proposed by Yue et al. [70], despite some different intermediates. They all attributed the main reactions involved in the toluene decomposition by DBD plasma to the ring-opening reactions, which mainly initiated by energetic electrons and $N_2(A)$. Following that, benzyl, benzaldehyde, etc. as important intermediates are further oxidized by O-containing active species including ·O and ·OH, eventually to produce CO_2 and H_2O. Accordingly, both of them emphasized the predominant oxidation effect of O-containing species, while the final products of toluene degradation are mainly CO_2 and H_2O.

On the other hand, complex chemical processes in the VOC treatment by the DBD systems may result in the formation of some products that may manifest as solid deposits, in addition to gaseous emissions, as reported by numerous studies [71–75]. Both the surface of the inner electrode and the inner wall of the dielectric barrier can accumulate the solid by-products. The overall performance of the DBD reactor can therefore be affected by these deposits. As reported by Karatum and Deshusses, some dark brown solid deposits with an odor akin to petroleum or tar were observed in a DBD reactor during the treatment of mixtures of VOCs (toluene and ethylbenzene). [73]. Similarly, Guo et al. also observed a yellow-colored solid deposit product in the DBD, which was determined as an aromatic polymer [74]. These deposits may affect the dielectric constant of the dielectric barrier materials, resulting in the accumulation of thermal energy and mechanical failure of the dielectric barriers. Whereas, Dors et al. found sulfur deposits on the reactor wall when treating hydrogen sulfide with a DBD system, which therefore acts as a resistive layer and leads to a reduction in the discharge current of the DBD, which could have an undesirable effect on the conversion efficiency [71]. Furthermore, solid deposits are accumulated not only on the walls and electrodes of the DBD reactor, but also on the surfaces of catalysts, resulting in catalytic deactivation in the DBD-catalyst system [75]. For these reasons, solid residue deposition is a non-negligible problem during VOC treatment with DBD systems that needs to be addressed before the technology is upgraded for real-world applications.

2.6 Practical requirements and drawbacks of published works

As discussed above, based on the use of various techniques to adjust parameters (e.g., configuration, geometric features, catalyst incorporation, etc.), it has been proven that the DBD system is an effective and efficient technology for reducing VOCs [24].

Nevertheless, almost all of these efforts were concentrated at the lab scale at small flow rates, and the processing capability was restricted to low gas flow rates (less than a few L/min, 10 L/min at most) [24,33]. In this regard, Schiavon et al. (2017) [27,71] and Vandenbroucke et al. (2011) [33] have conducted comprehensive reviews of the current status of NTP technologies for VOC treatment according to the representative published papers. Several key points can be drawn from the information presented by Schiavon et al. and Vandenbroucke et al. in Tables 2.6-2.8. First, DBD-based systems are the most selected form of NTP for VOC treatment due to their several advantages over other forms of NTP as mentioned above. Second, the incorporation of catalyst without reference to IPC or PPC is an effective approach to achieve higher removal efficiency and CO_2 selectivity, while still requiring appropriate processing parameters. Third, despite the high removal efficiency and CO_2 selectivity, even up to 100% in some papers, the treatment capacity is still limited to laboratory scale (i.e., a few L/min, even less than 1 L/min), which is far from practical applications. all characterizations and optimizations were performed at the laboratory scale, which is also different from practical use cases, resulting in a high degree of uncertainty as to whether the optimized parameters at low flow rates are still applicable at large flow rates (e.g., hundreds of L/min or over 1000 L/min) and in practical use environments.

Table 2.6. Operation parameters and characteristics of the selected experimental activities on VOC abatement [27,72].

VOCs	Type of NTP reactor	Catalysts (configuration)	C_{in} (ppm) (carrier, RU [%])	Total flow rate (L min^{-1})	Residence time (*s*)	Voltage (kV)	Frequency (Hz)	Reference
TOL	DBD	None	95 (compressed air, 30%)	6.6	0.016	7–10	22	Karatoum and Deshusses (2016)
TOL	DBD	Co-MCM-41 (PDC)	100 (synthetic air, 0%)	0.2	0.22	0–100	50	Xu et al. (2017)
TOL	Photocatalytic DBD	TiO_2/SMF (PDC)	40 (synthetic air, 0%)	1	4	10–40	20	Chen et al. (2016)
TOL	Pulsed DBD	Pd/γ-Al_2O_3 (PDC)	1000 (air, n.d.)	1	1.08	20	10–200	Pham Huu et al. (2017)
FOR	Packed-bed DBD	$NaNO_2$ (PDC)	0.05 (compressed air, 30%)	8.5	0.29	0–20	15,000	Liang et al. (2010)
FOR	DBD	Cu/CeO_2 (PDC)	57.7 (synthetic air, 0%)	1	0.23	0–30	10,000	Zhu et al. (2015a)
FOR	Packed-bed DBD	Ag/CeO_2 (PDC)	276 (synthetic air, 35.5%)	0.605	0.22	0–40	50	Huixian and Zengfeng (2009)
FOR	Corona discharge	MnO_x/Al_2O_3 (PAC)	2.2 (synthetic air, 30%)	6	0.05	0–25	–	Wan et al. (2011)
BZ	DBD	None	95 (compressed air, 30%)	6.6	0.016	7–10	22,000	Karatoum and Deshusses (2016)
BZ	Hybrid DBD	TiO_2/MnO_x/SMF (PDC)	50 (air, 0–100%)	0.5	0.46	14–22	50	Karuppiah et al. (2014)
BZ	Packed-bed DBD	Ag/TiO_2 (PDC)	60–210 (synthetic air, 0%)	4	n.d.	28	100–1500	Kim et al. (2005)
BZ	Packed-bed DBD	$Ag_{0.9}Ce_{0.1}$/γ-Al_2O_3 (PDC)	400 (synthetic air, 0–80%)	0.5	5.8	17–25	50	Jiang et al. (2016a)
TCE	Corona discharge	Pd/$LaMnO_3$ (PAC)	500–560 (compressed air, 18%)	2	2.16	30	–	Vandenbroucke et al. (2016)
TCE	DBD	Au-mesoporous silica (PAC)	430 (compressed air, 0%)	0.51	4	10–25	50	Magureanu et al. (2007b)
TCE	Corona discharge	$LaMnO_{3+\delta}$ (PAC)	510 (synthetic air, 0–18%)	2	2.16	30	–	Nguyen Dinh et al. (2014)
TCE	Corona discharge	$CeMn_4$ (PAC)	360–400 (compressed air, 10%)	2	2.16	30	–	Nguyen Dinh et al. (2015)
Mixture	DBD	AgO_x/MnO_x/SMF (PDC)	50 (CBZ), 100 (BZ), 50 (TOL) (air, 0–85%)	0.250	0.47	14–22	50	Karuppiah et al. (2012)
Mixture	Corona discharge	MnO_x/Al_2O_3 (PAC)	1.5 (BZ), 1.4 (TOL), 1.2 (XYL) (synthetic air, 25%)	6	2.1	25	–	Fan et al. (2009)
Mixture	DBD	MnO_x/SMF (PDC)	100 (HX), 75 (DX), 75 (TOL) (air, 0–100%)	0.300	0.77	14–22	50	Ramaraju and Subrahmanyam (2014)
Mixture	DBD	None	25 (BZ), 164 (TOL), 183 (OCT) (synthetic air, 33%)	0.300	0.98	15	4000	Schiavon et al. (2015)

Table 2.7. Results of the selected studies in terms of η_{max} (RE_{max}), corresponding SIE(SED), EE_{max} (EY_{max}), $S_{CO2,max}$, and main byproducts formed during the treatment of VOCs [6,73].

Reference	RE_{max} (%)	SED (J L^{-1})	EY_{max} (g $(kWh)^{-1}$)	$S_{CO2,max}$ (%)	Main by-products
Karatoum and Deshusses (2016)	74	360	2.6	n.d.	Benzoic acid crystals
Xu et al. (2017)	100	226	1.69[a]	n.d.	2-Hexanone, 1-methyl-4-nitrobenzene, 4-methyl-2 -nitrophenol
Chen et al. (2016)	~ 92%	~ 210	0.67[a]	> 90%	Formic acid, formaldehyde
Pham Huu et al. (2017)	100	148	17.5[a]	45	Benzene and benzaldehyde
Liang et al. (2010)	93	786	0.47	n.d.	Methanol
Zhu et al. (2015a)	92.9	486	0.14[a]	96.4	Formic acid
Huixian and Zengfeng (2009)	99	108	2.51[a]	86	Not reported
Wan et al. (2011)	87	20	0.12[a]	n.d.	Not reported
Karatoum and Deshusses (2016)	58	360	0.51[a]	n.d.	Not reported
Karuppiah et al. (2014)	95[b]	170	1.00[a]	n.d.	Not reported
Kim et al. (2005)	98	70	2.73[a]	~ 77	Formic acid, phenol, nitrous oxide, NO_x
Jiang et al. (2016a)	100[c]	400	3.00[a]	83.1	Nitrogen dioxide
Vandenbroucke et al. (2016)	96.2	460	4.49[a]	~ 20	Hydrochloric acid, dichloroacetyl chloride, phosgene, chloral
Magureanu et al. (2007b)	100	~ 670	3.50[a]	n.d.	NO_x, octanal, nonanal, decanal, 1-chloro octane, 1-chloro nonane
Nguyen Dinh et al. (2014)	93[c]	460	4.43[a]	n.d.	Hydrochloric acid, chlorine, dichloroacetyl chloride, phosgene, chloral
Nguyen Dinh et al. (2015)	96.9	240	5.50[a]	~ 37	Hydrochloric acid, chlorine, dichloroacetyl chloride, phosgene, chloral
Karuppiah et al. (2012)	100 (CB), 100 (BZ), 100 (TOL)[c]	300	1.08[a] (BZ)	80	NO_x, nitric acid, benzaldehyde, aromatics, and aromatic acids
Fan et al. (2009)	94 (BZ), 97 (TOL), 95 (XYL)	10	2.8 (BZ), 4.2 (TOL), 5.4 (XYL)	~ 100	Formic acid, benzaldehyde, benzyl alcohol
Ramaraju and Subrahmanyam (2014)	100 (TOL), 100 (HX), 100 (DX)[c]	~ 300	0.96[a] (TOL)	~ 88	Not reported
Schiavon et al. (2015)	99.1 (BZ), 100 (TOL), 100 (OCT)	1840	0.51 (BZ)	63	Benzaldehyde, cresols, phenol, benzyl alcohol

Table 2.8. Overview of published papers on toluene removal with NTP [33].

Plasma type	Carrier gas	Flow rate (mL/min)	Concentration range (ppm)	Maximum removal efficiency (%)	Energy density (J/L)	Energy yield (g/kWh)
DBD	Dry air (5% O_2)	4000–5000	200	75	310	6.6[b]
DBD	N_2	2000	400	21	240	4.7[b]
	dry air			23		5.2[b]
DBD	N_2/5% O_2 (0.2% RH)	100	50	73	600	0.8[b]
DBD	Humid air (55% RH)	1000	100	46	2100	0.3[b]
DBD packed with glass pellets	Dry air	600	1100	75–80	1000	11.5[b]
DBD packed with glass pellets	Humid air (95% RH)	500	500	91	18.5	11.5
DBD packed with glass beads	Dry air	315	240	36	172	6.8[b]
Multicell DBD packed with glass beads[a]	Dry air	1000	110	72	2502	0.4[b]
DC back corona	Dry air	100–750	5–200	93	2400	0.4[b]
Pulsed corona	Dry air	450	500	>99	1000	6.7[b]
Positive corona	Humid air (26% RH)	10^4	0.5	80	65	0.1[b]
$BaTiO_3$ packed-bed	Dry air	–	101	95	125	–
Dielectric capillary plasma electrode discharge	Air	–	266.5	>99	3500	1[b]
Capillary tube discharge	Dry air	350	1246	86	–	–

Therefore, there is a high demand for large flow DBD systems, which are more practical for practical applications. In addition, the design methodology and investigation of the characteristics of DBD systems for VOC degradation at large flow rates are also essential for the DBD-based system as a feasible solution for VOC abatement in the fields of building ventilation, industrial effluents, etc. In this context,

the focus of this dissertation is placed on the development of large-flow DBD systems and the investigation of their characterization at large flow rates.

2.7 Summary

As reported in numerous studies, DBD plasma has proven to be an effective treatment technology for a wide range of VOCs and air pollutants. The degradation in DBD plasma is dominated by four main reactions: electron impact reactions, radical oxidation, excited-molecule reactions, and ion-molecule reactions. However, there are still some drawbacks, such as limited treatment capacity, lack of knowledge on decomposition characteristics at large flow rates, etc., which hinder the practical application of DBD plasma technology for VOC abatement. Therefore, in the study of this dissertation, the attention is focused on the development of large-flow DBD system, acquisition of decomposition characteristics on VOC treatment, and further optimization of these DBD systems based on the experimental results.

Chapter 3 Design and characterization of single- and two-layer large-flow DBD reactors

3.1. Introduction

In Chapter 2, by reviewing the major published works regarding DBD plasma-based VOC abatement, the effectiveness of DBD plasma on various VOC degradation and the degradation pathways for toluene treatment in air/H2O DBD plasma were demonstrated. Consequently, DBD plasma has proven to be an effective technology for the decomposition of VOCs, which is mainly achieved by two types of systems: DBD-alone and catalysis systems, as evidenced by numerous studies. In addition, it has been found these DBD systems were energized by the applied voltages ranging from 50 Hz to a few kHz, namely based on the low frequency properties of DBD. Nevertheless, almost all of these efforts were concentrated at the lab scale at small flow rates, and the processing capability was restricted to low gas flow rates (less than a few L/min); all the characterizations and optimizations were also performed at the lab scale, which is far from practical industrial applications. To address this issue, in the first phase of this study, two scalable DBD reactors (single-layer and two-layer) capable of treating gases at flow rates two orders of magnitude greater than small-flow DBD reactors (typically less than 1 or a few L/min) for VOC abatement are developed and characterized at large flow rates. In addition, the scalability and superiority of the multilayer DBD configuration (two-layer reactor) will be verified by comparing the degradation performance of the two DBD reactors in the treatment of toluene, in terms of several key geometric and processing parameters.

3.2. Design of large-flow DBD reactors and their experimental setup

3.2.1. Concept of the large-flow DBD reactors: scalable single-Layer and two-layer types

Two types of large-flow DBD reactors were designed and fabricated, i.e., the scalable type (single-layer reactor) and the multilayer type (two-layer reactor), which comprise a discharge gap with a thickness of 2 mm. The details of the two reactors are presented in Figure 3.1. The single-layer reactor consists of three components rendered using different colors: gas inlet (blue), gas outlet (blue), and the degradation part in between; the system is 850 mm long and 250 mm wide, as shown in the upper part of Figure 3.1(a).

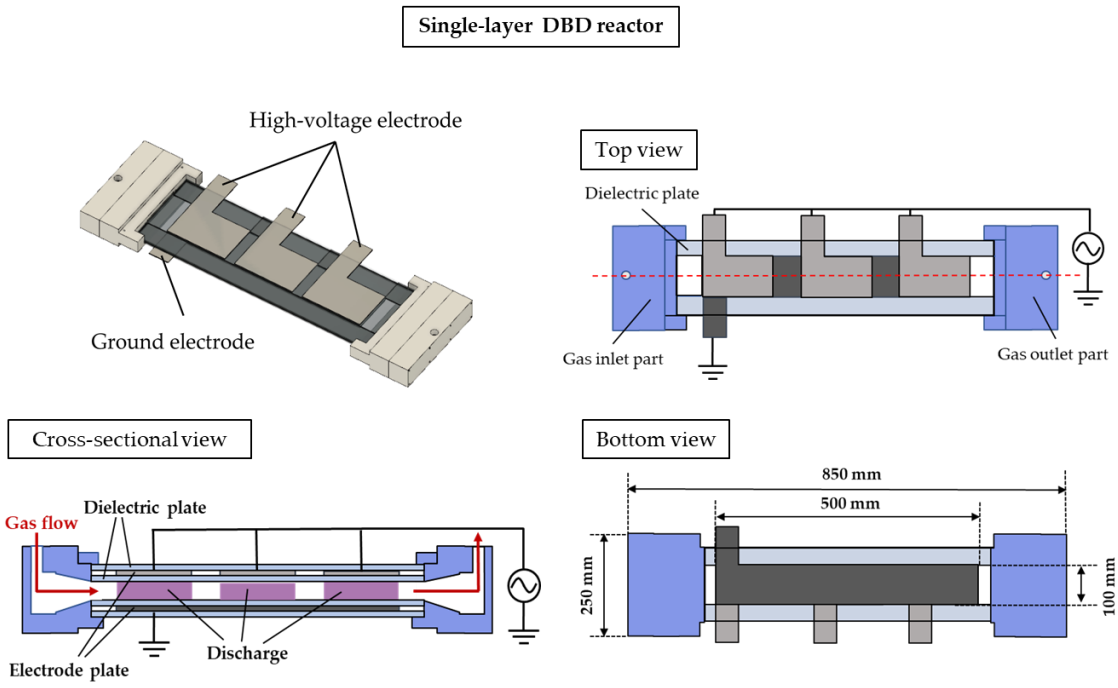

(a)

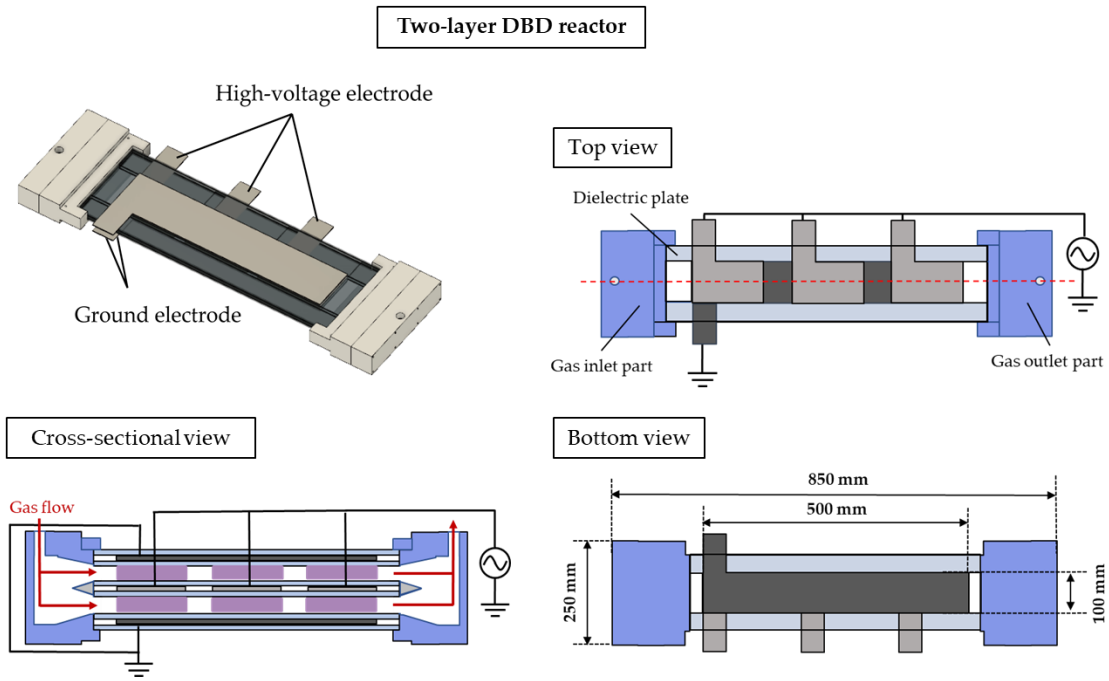

(b)

Figure 3.1. Schematics of large-flow dielectric barrier discharge (DBD) reactors in top, cross-sectional, and bottom views: (**a**) scalable single-layer and (**b**) multilayer (two-layer) DBD reactors.

The gas inlet and outlet part were made of acrylic resin. In addition, the gas inlet and outlet part also serve as buffer channels, thus enabling the passage of the gas through the degradation part uniformly. In the degradation part, i.e., the plasma zone, Al was adopted as the electrode, due to its excellent electrical conductivity (only after Au, Ag, and Cu), low price, low weight, and easy engineering. For example, its electrical conductivity is approximately 60% as much as Cu, but its specific gravity is only 1/3 of that of Cu, so it is possible to conduct approximately twice as much current with the same weight. Utilizing its characteristics, it is used in almost all high-voltage power transmission lines. Accordingly, for the discharge electrodes, one Al plate (length 500 mm, width 100 mm, and thickness 2 mm) and three smaller Al plates (length 150 mm, width 100 mm, thickness 2 mm) serve as the ground and high-voltage electrodes, where the electrodes are covered by four glass plates (length 600 mm, width 200 mm, and thickness 2 mm) on both sides, thus acting as insulating dielectrics (κ= 7–7.5). Between the glass-covered electrodes, polytetrafluoroethylene sheets (length 600 mm, width 50 mm, and thickness 2 mm) are inserted as spacers to form a discharge space of 90 cm^3, as shown in the cross-sectional view in the center of Figure 3.1(a). Based on the single-layer reactor, one more electrode layer is stacked on top to configure a two-layer reactor (multilayer type) with a discharge zone that is twice as large as that of the single-layer reactor, thus realizing a discharge space of 180 cm^3. The cross-sectional view shown in the center of Figure 3.1(b) indicates the formation of two flow paths. When a high AC voltage is applied on the electrodes (e.g., generally several kV), a uniform plasma discharge can be observed in the discharge zone as depicted in the cross-sectional views in Figure 3.1.

3.2.2. Experimental setup

The experimental setup is shown in Figure 3.2. There are four main components: a gas-mixing system, an alternating current (AC) power supply, large-flow DBD reactors, and analytical instruments. The flow of evaporated toluene in the container is achieved by mixing the toluene in water and diluting it using compressed air to emulate humidified toluene-mixed air. A mass-flow controller (MFC, Japan Star Techno, Osaka, Japan) was used to adjust the concentration of the toluene by modifying the ratio of the gas flow rates between the toluene and compressed air. The toluene concentrations before and after the treatment were determined using a gas detector tube (Toluene, No. 122, Gastec Corporation, Ayase, Japan) at the outlet of the large-flow DBD reactor. The large-flow DBD reactor was energized by using a 50 Hz AC power source (rated voltage 0–22 kV). Additionally, an energy meter (TAP-TST8N, Sanwa Supply Inc., Okayama,

Japan) was installed at the power supply plug to monitor the input power. The input power included the power consumed by the plasma discharge (discharge power: power consumed by the reactor), voltage transformer, and associated circuits. The waveforms of the applied voltage as well as current were observed on a digital oscilloscope (DPO4104, Tektronix, Tokyo, Japan) using a 1000:1 high-voltage probe (HPV-39pro, PINTEC, Beijing, China), current probe (TCP303, Tektronix, Tokyo, Japan), and a current probe amplifier (TCPA300, Tektronix). Furthermore, a capacitor [Cm (1 uF)] provided a ground connection, and a low-voltage probe (Tek P5100, Tektronix) was attached to determine the voltage. The results obtained by using the high- and low-voltage probes were displayed on the digital oscilloscope, and the generated Lissajous figures were utilized to derive the discharge power deposited in the reactor [27,76]. All the measurements were conducted at room temperature (24 °C) and atmospheric pressure, and the measured data were repeated more than three times to ensure accuracy.

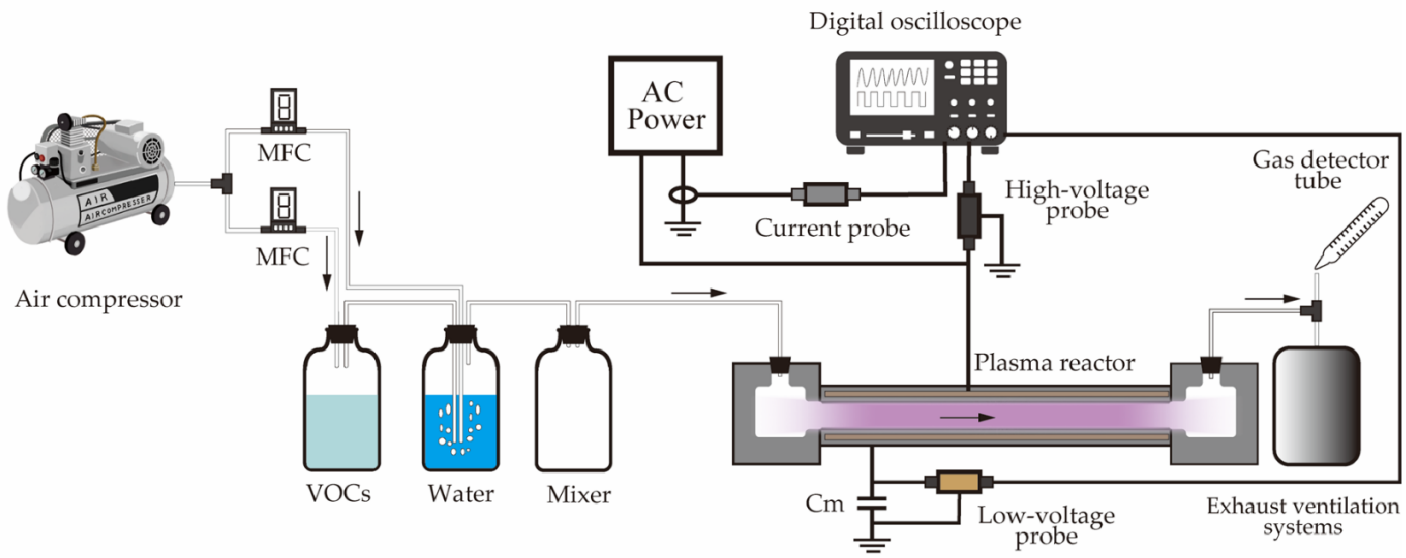

Figure 3.2. Schematic of the experimental setup using the single-layer DBD reactor (AC: alternating current; MFC: mass-flow controller; VOC: volatile organic compound).

The decomposition rate of toluene ($\eta_{toluene}$) was calculated from its initial concentration (C_{init}, parts per million (ppm)) and final concentration (C_{fin}, ppm) at the outlet, according to Equation (3.1) [3,6],

$$\eta_{toluene}\ (\%) = \frac{C_{init} - C_{fin}}{C_{init}} \times 100 \tag{3.1}$$

The toluene decomposition quantity (DQ, mg/min) reflects the decomposed quantity of toluene (mg) per unit time (min) and can be calculated using Equation (3.2) [6].

$$DQ\ (\text{mg/min}) = \frac{M \times C_{init} \times \eta_{toluene} \times \text{Q}}{100 \times 22.4} \times \frac{273.15}{(273.15 + T)} \times 10^{-3} \tag{3.2}$$

where M denotes the relative molecular mass of toluene (92.14), T is the ambient temperature (24 °C), and Q denotes the flow rate (L/min).

Equation (3.3) expresses the energy efficiency (EE, g/kWh); this is the metric used to evaluate the energy efficiency for toluene degradation in the DBD reactors. PE is an indicator that denotes the decomposed quantity of toluene (g) per unit energy consumption (kWh) [6].

$$EE\ (\text{g/kWh}) = \frac{DQ \times 60}{\text{P}} \tag{3.3}$$

where P denotes the discharge power (W) consumed by the DBD reactors, which can be calculated from Lissajous figures as explained in Figure 2.3(a), using Equation (2.9).

3.3. Investigation of the effect of geometric parameters on the properties of the DBD at large flow rates

3.3.1. Optimization of the discharge gap between high-voltage and ground electrodes

The discharge gap is considered to be one of the most crucial parameters in DBD reactor configurations that affects the initial discharge voltage and power density, thereby determining the decomposition characteristics of the DBD reactors for exhaust gases [6,77]. To determine the optimum discharge gap distance for large-flow DBD reactors, part of the single-layer DBD reactor discharge length (equal to 150 mm) was adopted to investigate the effects of discharge gap thickness (for values in the range of 1–3 mm), as shown in Figure 3.3(a). The toluene to be decomposed was diluted with air to a concentration of 100 parts per million (ppm), adjusted by the MFC to a flow rate of 50 L/min, and humidified through a water bath. In this study, the temporary reactor was energized by high voltages at 50 Hz (f) in the range of 15–21.5 kV (zero-to-peak value).

As a function of the applied voltage, Figure 3.3(b) shows how the discharge gap affects the toluene decomposition quantity. When the applied voltages were 15–18.5 kV, the highest toluene decomposition quantity was observed at the discharge gap of 2 mm between electrodes. This result indicates that as the thickness of the discharge gap across the electrodes decreases, the stability of the generated plasma increases at a relatively lower voltage due to the enhanced electric field strength [78]. However, the faster flow velocity of the gas through the plasma zone owing to the thinner discharge gap results

in decreased residence times in the plasma zone and lower decomposition quantities. In contrast, when the discharge gap becomes thicker, a higher applied voltage is required to sustain a stable plasma to achieve an equivalent decomposition quantity [36,43]. Therefore, the discharge gap of 2 mm is optimum for the development of the large-flow DBD reactors in this study in terms of the discharge voltage and residence time in the plasma zone.

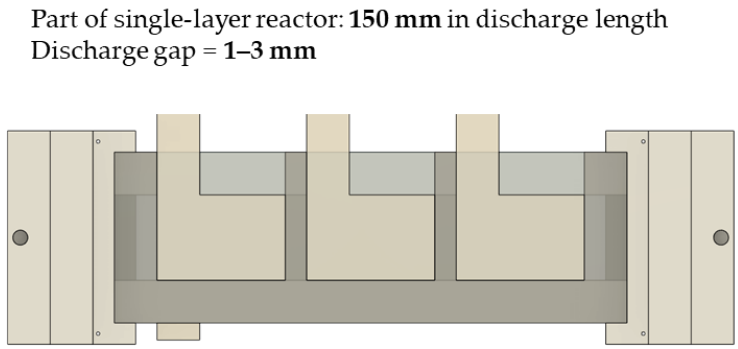

(a)

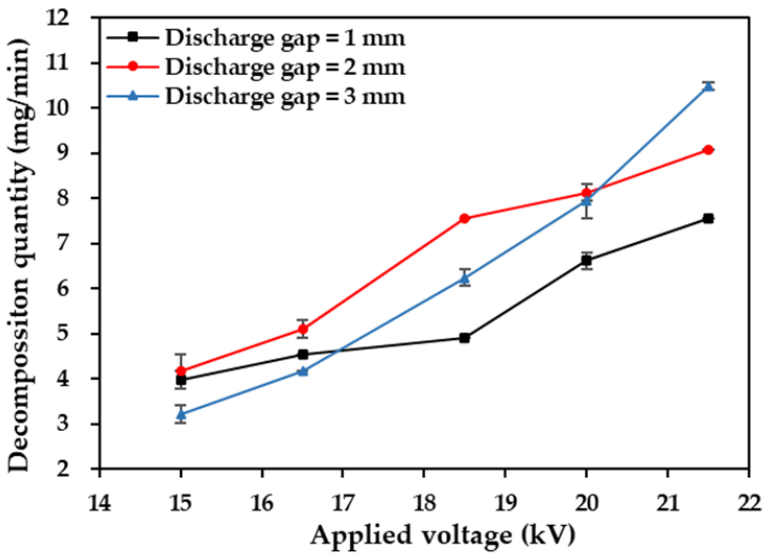

(b)

Figure 3.3. (**a**) Single-layer DBD reactor with a discharge length of 150 mm, and (**b**) effects of discharge gap on toluene decomposition quantity plotted as a function of the applied voltage.

3.3.2. Effects of applied voltage at large flow rates

Figures 3.4(a), (b) depict the typical voltages and currents for discharges in single-layer and two-layer DBD reactors at 50 Hz and 18.5 kV, respectively, in which the initial toluene concentrations and gas flow rates were maintained at 100 ppm and 50 L/min, respectively. The first halves of each semi-period are marked by short, intense pulses. A pulse may consist of one or more microdischarges that occur simultaneously whenever a threshold voltage is exceeded across the interelectrode space (>14 kV in the single-layer DBD reactor). Additionally, a higher voltage was observed at the first half of each semi-period in the two-layer reactor with the same voltage applied; this led to higher discharge power per discharge unit time. This is attributed to the fact that the larger capacitance ratio leads to a higher voltage across the gas gap in the two-layer reactor, as can be observed in the Lissajous figures in Figure 3.4(c) [36]. Furthermore, the two-layer reactor system consumes much higher discharge powers at the given applied voltages (31.20 W at 18.5 kV) compared with the 14.14 W consumed by the single-layer reactor, due to its large discharge space (twice as large) and the higher voltage across the gas gap. This finding suggests that greater power can be transported to the plasma to dissociate molecules in toluene-mixed air by using a multilayer structure with alternating layers of electrodes (based on the single-layer reactor design).

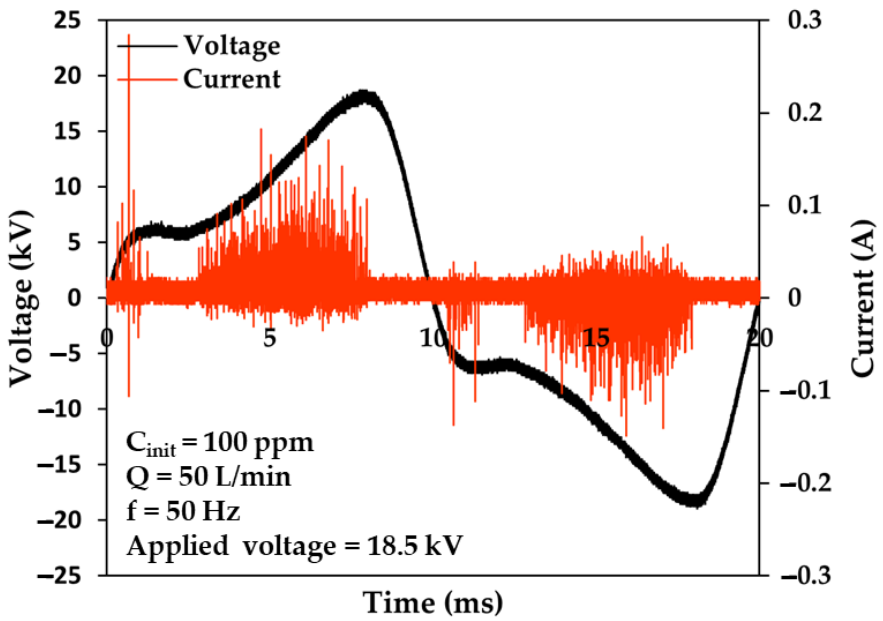

(a)

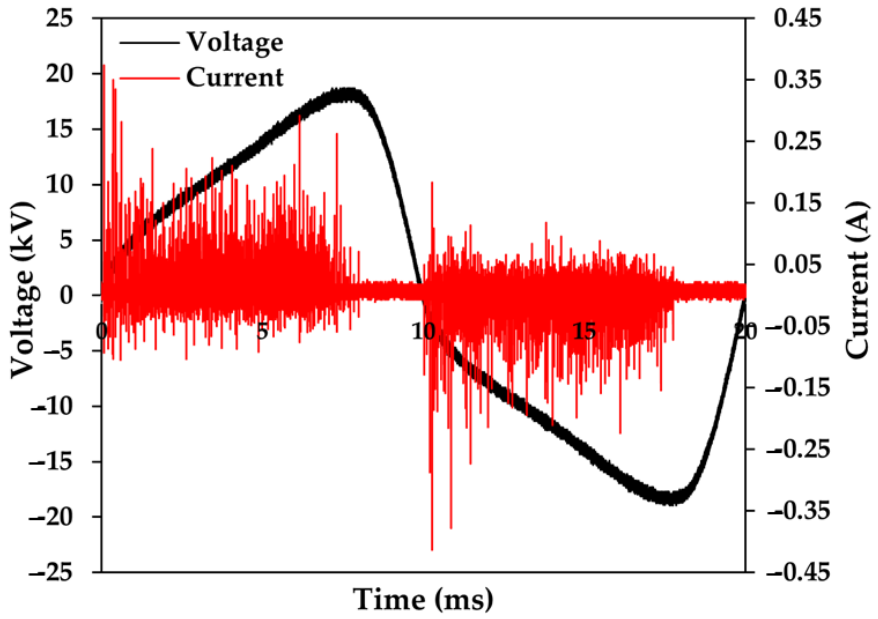

(b)

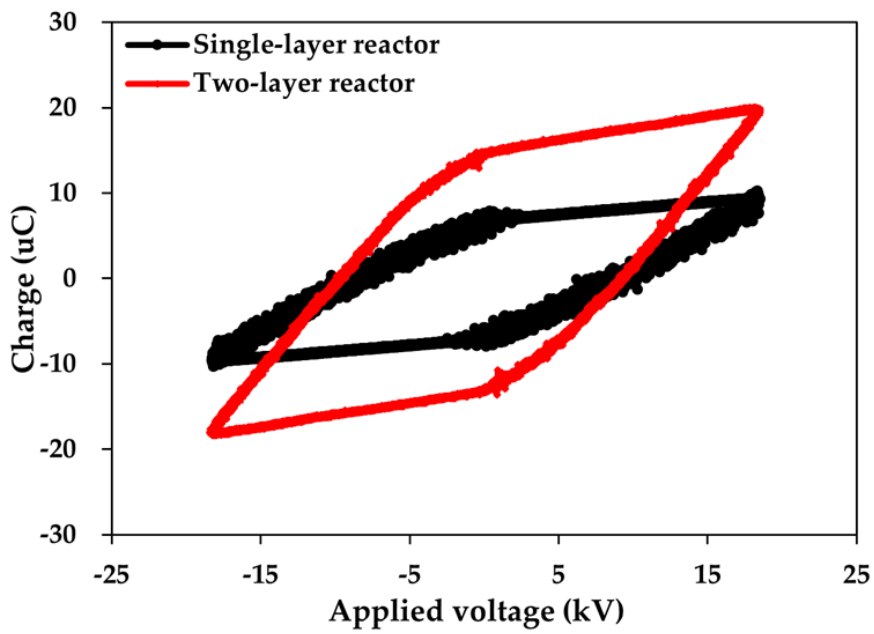

(c)

Figure 3.4. Waveforms of (**a**) typical voltages and currents of discharges in the single-layer DBD reactor, (**b**) two-layer reactor, and (**c**) corresponding Lissajous figures.

The plots of the toluene decomposition rate and energy efficiency versus voltage and discharge power are depicted in Figure 3.5 for single- and two-layer DBD reactors, where the initial toluene concentration of 100 ppm and gas flow rate of 50 L/min of the toluene-mixed air (intended to be treated) are maintained. As shown in Figure 3.5(a), at increased applied voltages, the decomposition rates in the two DBD reactors increase considerably. As the applied voltage increases from 15 kV to 21.5 kV, the decomposition rate increases from 16% to 57% at 21.5 kV in the single-layer reactor and from 47.5% to 79% in the two-layer reactor. It has also been reported that increased applied voltages contribute to larger numbers of energetic electrons, which is conducive to the production of reactive species and the probability of collisions with toluene molecules [36,74]. The increased applied voltage has a positive effect on the toluene decomposition rate. The trend of these results is similar to that of the applied voltage in large-flow DBD reactors at a flow rate of 50 L/min, compared with other low-flow reactors, as reported by Guo et al. [74] (at 0.1 L/min) and Jiang et al. [36,75] (at 1.08 L/min). Moreover, a remarkable difference in the toluene decomposition rate between the two reactors was observed at all applied voltages possibly because the two-layer reactor (0.24 s) was associated with a mean residence time (for individual toluene molecules in the plasma, zone) which was twice as large as that of the single-layer reactor (0.12 s) at 50 L/min. This result suggests the superiority of the multilayer structure of the two-layer reactor regarding the decomposition rate at the same process capacity (50 L/min).

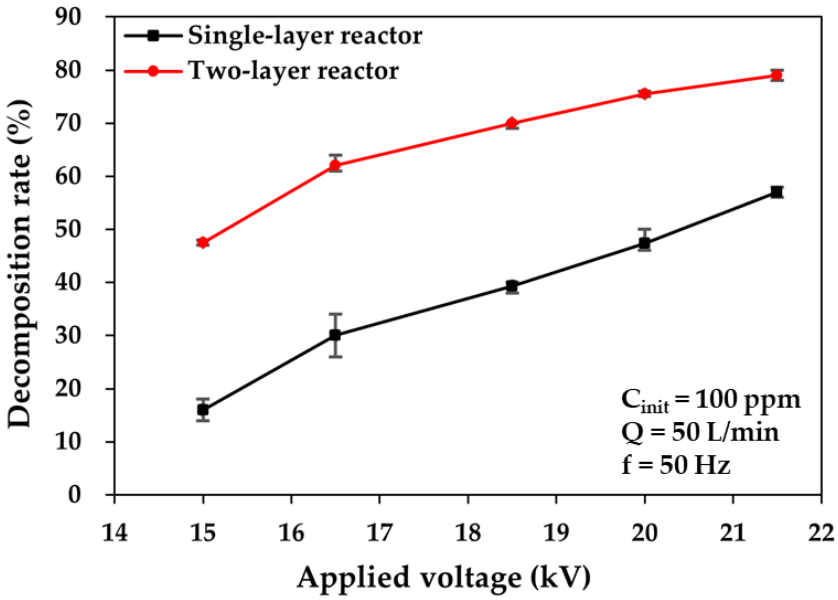

(a)

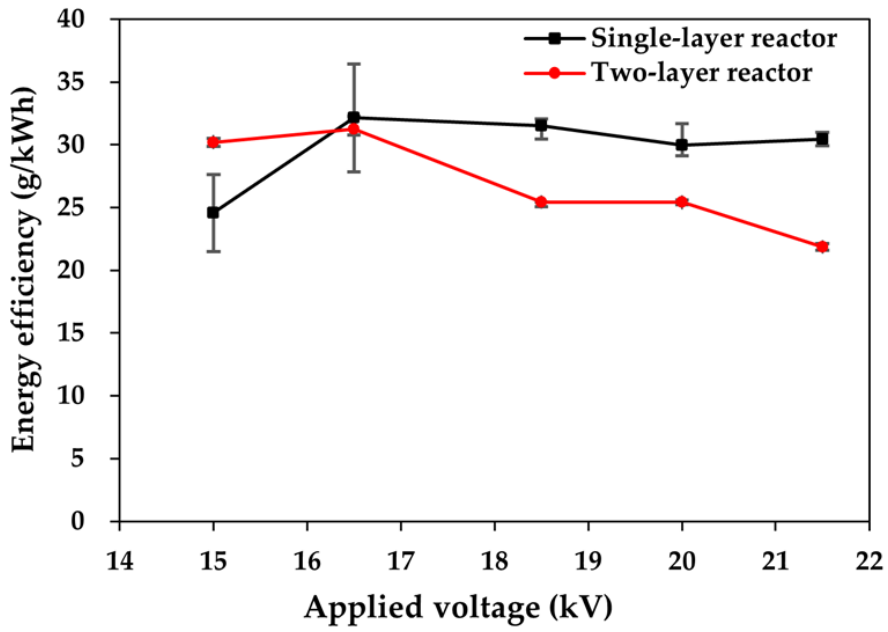
Single-layer reactor
Two-layer reactor
Energy efficiency (g/kWh)
Applied voltage (kV)
0
5
10
15
20
25
30
35
40
14
15
16
17
18
19
20
21
22

(b)

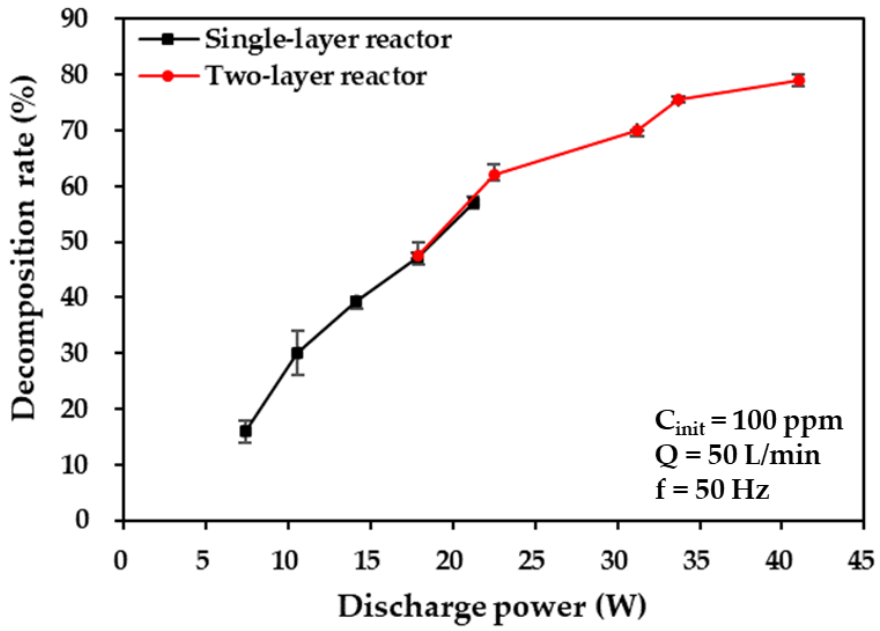
Single-layer reactor
Two-layer reactor
Decomposition rate (%)
Discharge power (W)
C_{init} = 100 ppm
Q = 50 L/min
f = 50 Hz
0
10
20
30
40
50
60
70
80
90
0
5
10
15
20
25
30
35
40
45

(c)

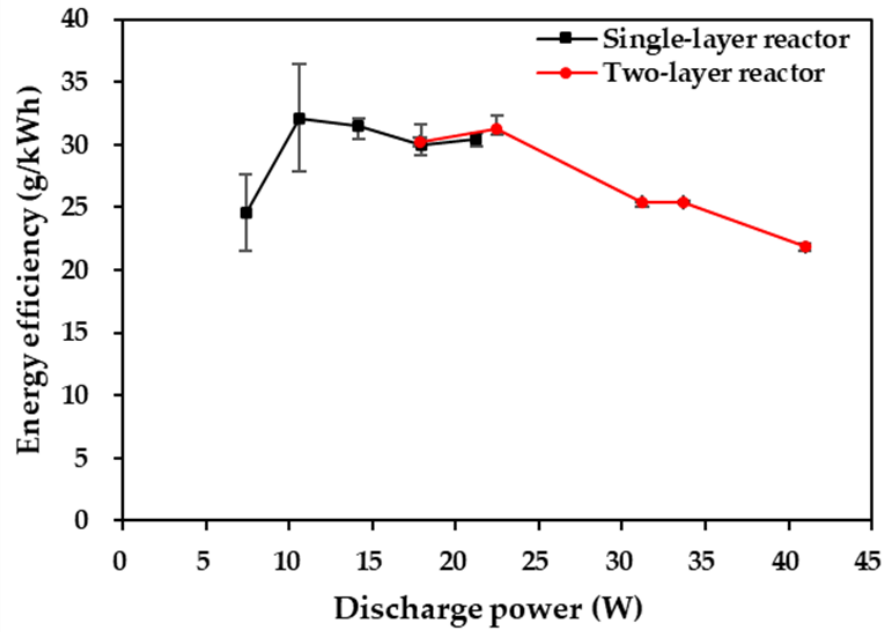

(d)

Figure 3.5. Effects of applied voltage on (**a**,**c**) toluene decomposition rate and (**b**,**d**) energy efficiency plotted as a function of applied voltage in the cases of the single- and two-layer DBD reactors at 50 L/min.

As shown in Figure 3.5(c), the same decomposition rates were observed at the same discharge power in the single- and two-layer reactors, thus exhibiting the same decomposition characteristics per unit discharge power. This implies that the multilayer structure of the two-layer reactor is feasible in terms of the discharge power.

Conversely, the energy efficiency increased initially and then decreased slightly as the applied voltage increased in the single-layer reactor case; the two-layer reactor presented a similar trend, but the response was better than that of the single-layer reactor at the applied voltage of 15 kV and comparable at 16.5 kV. Subsequently, the response decreased considerably, as shown in Figure 3.5(b). The energy efficiency changes from 24.57 g/kWh to 32.14 g/kWh, drops to 30.44 g/kWh at 21.5 kV in the single-layer reactor case, and slightly increases from 30.20 g/kWh to 31.27 g/kWh before decreasing to 21.85 g/kWh in the two-layer reactor case. This finding may be attributed to the fact that a partial discharge occurred at a lower applied voltage range; this produced an insufficient quantity of high-energy electrons and active species that contributed to the decomposition of toluene, and thus resulted in higher energy efficiency [75]. However, the partial discharge gradually changes into a full plasma discharge with an increase in

the applied voltage, thus resulting in the generation of an excessive number of high-energy electrons and active species. This causes a decrease in energy efficiency; this phenomenon was more prominent in the two-layer reactor due to the considerably higher decomposition rates. These findings indicate that the two-layer reactor can process faster flow rates. In addition, when decomposition occurs at the same discharge power, the single- and two-layer reactors yield similar energy efficiency outcomes, as shown in Figure 3.5(d). These results demonstrate the feasibility of the two-layer reactor and its superiority in energy efficiency due to the higher decomposition rate compared to the single-layer reactor.

3.3.3. Effects of flow rate on large-flow dbd reactors

Toluene's discharge characteristics and degradation performance are also affected by the gas flow rate. Figure 3.6 shows graphs of the toluene decomposition rate and energy efficiency versus the gas flow rate for single- and two-layer reactors at the applied voltage of 21.5 kV. The results in Figure 3.6 show that the toluene decomposition rate decreased with increased gas flow rates at the set applied voltage. In contrast, both reactors resulted in increases in their corresponding energy efficiency. The same phenomenon was also observed by Jiang et al. [42,46,75], who used small-flow DBD reactors (0.5–2 L/min). When the gas flow rate rises from 10 to 110 L/min, the toluene decomposition rates decrease from 85% to 51% at 110 L/min in the single-layer reactor case and from 86% to 59.5% in the two-layer reactor case. In the lower range of flow rates (10 to 30 L/min), the single-layer reactor achieved decomposition rates comparable to those of the two-layer reactor, even though the two-layer reactor resulted in a residence time that was twice as long as that of the single-layer reactor. This can be attributed to the adequate residence time of the toluene molecules in the discharge zone of both reactors in the lower flow rate range, ensuring a high probability of collisions for the toluene molecules, energetic electrons, and active species; thus, the decomposition rates of the two reactors were close to each other [36,79]. There was, however, a significant difference between the decomposition rates between the two reactors when the flow rates increased from 50 to 110 L/min. This is attributed to the residence time differences, as these offset the adverse effects observed at increased flow rates in the two-layer reactor. This implies that the two-layer reactor in the multilayer structure exhibits superior decomposition characteristics in terms of the decomposition rate at higher flow rates, indicating a larger processing capacity.

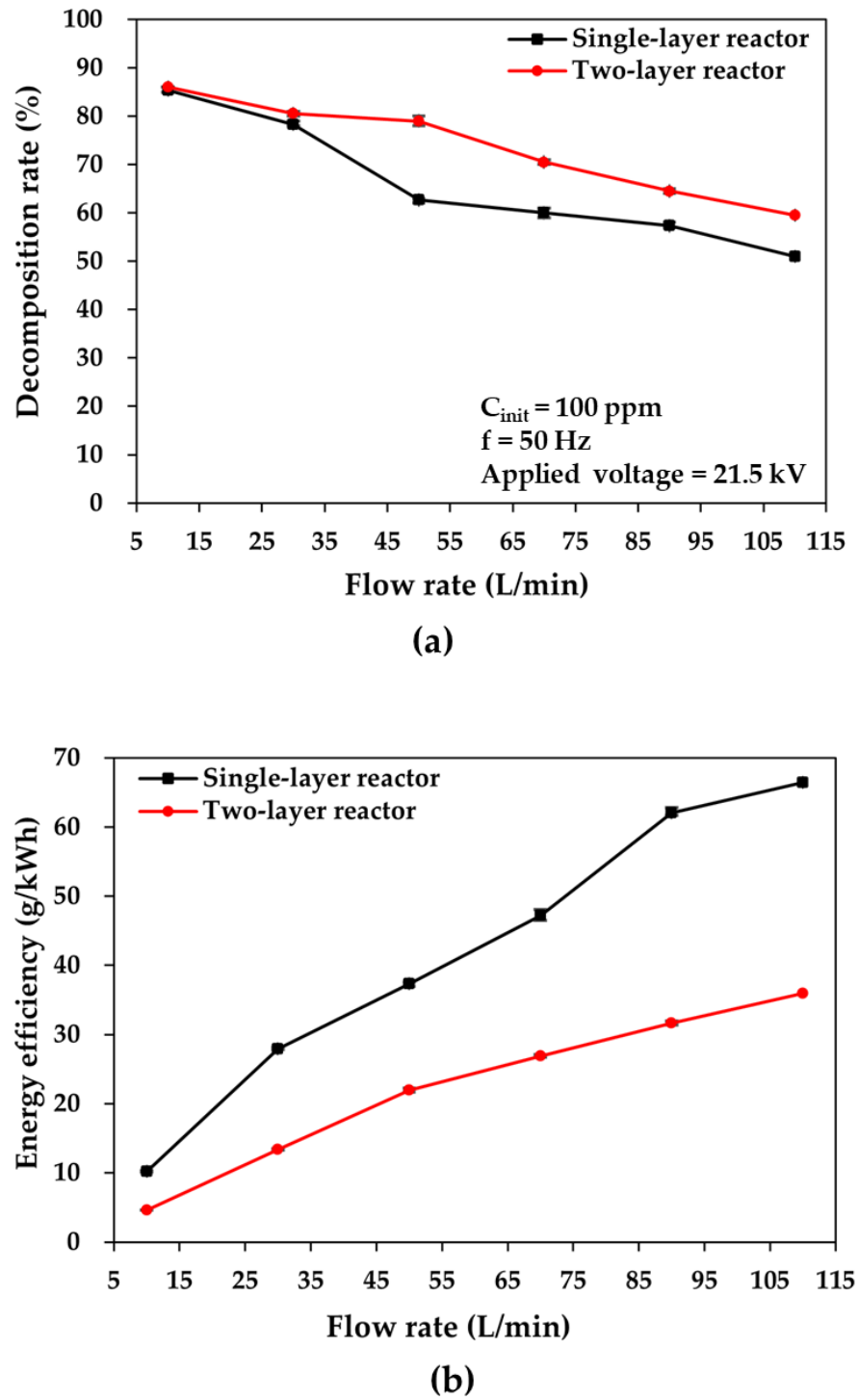

Figure 3.6. Comparisons of (a) toluene decomposition rate and (b) energy efficiency plotted as a function of flow rate in the cases of single- and two-layer DBD reactors.

At the same time, the energy efficiency increased from 10.20 g/kWh to 66.43 g/kWh at 110 L/min in the single-layer reactor and from 4.63 g/kWh to 35.99 g/kWh in the two-layer reactor case. It has been reported that increased flow rates lead to an increased number of toluene molecules (per unit discharge time) dissociated in the plasma zone (which contains an abundance of active species), thereby improving the energy efficiency considerably [79]. In addition, the single-layer reactor yielded higher energy efficiencies at all flow rates, which may be attributed to the fact that the energetic electrons and active species resulting from the discharge power deposited in the single-layer reactor can be fully utilized for toluene dissociation, thus leading to higher energy efficiency, whereas the discharge power deposited in the two-layer reactor is too large to be fully utilized.

In conclusion, the two-layer reactor is superior to the single-layer reactor in terms of the decomposition rate at all flow rates; however, in terms of energy efficiency, the single-layer is more advantageous. This implies that the two-layer reactor may be overqualified for use in the flow-rate range of 10–110 L/min and could be adapted to handle much higher flow rates to achieve comparable or larger energy efficiencies than those of the single-layer reactor.

3.3.4. Effects of flow velocity on large-flow dbd reactors

The two types of DBD reactors were compared at different flow velocities, i.e., different residence times. Furthermore, the flow velocities in the reactors were 1, 2, 3, 4, and 4.583 m/s, which corresponded to residence times of 0.5, 0.25, 0.167, 0.125, and 0.109 s, respectively. Figure 3.7 displays the plots of the toluene decomposition rate and energy efficiency versus flow velocity in the cases of the two reactors, when the applied voltage and toluene concentration were fixed at 21.5 kV and 100 ppm, respectively. In Figure 3.7(a), as the flow velocity increased from 1 to 4.58 m/s, the toluene decomposition rate decreased from 79% to 41% at 4.58 m/s, i.e., at a flow rate of 55 L/min in the single-layer reactor, and from 82% to 59.5% at 4.58 m/s, i.e., at a flow rate of 110 L/min in the two-layer reactor.

The enlarged flow velocity, i.e., the reduced residence time, adversely affects the toluene decomposition rate. The results in the large-flow DBD reactors (for flow rates of up to 110 L/min) concur with the results at smaller flow rates in other DBD reactors, as observed by Chen et al. [42,46,76] at 1 L/min and by Zhu et al. [42,46,76] at 0.36–1 L/min. Furthermore, the decomposition rate in the single-layer reactor exhibited a more abrupt decrease at a fixed applied voltage than that in the two-layer reactor case; this can be attributed to the higher discharge power per discharge unit time in the two-layer reactor,

as explained in Section 3.1, which leads to a higher decomposition rate in the upper flow-velocity range.

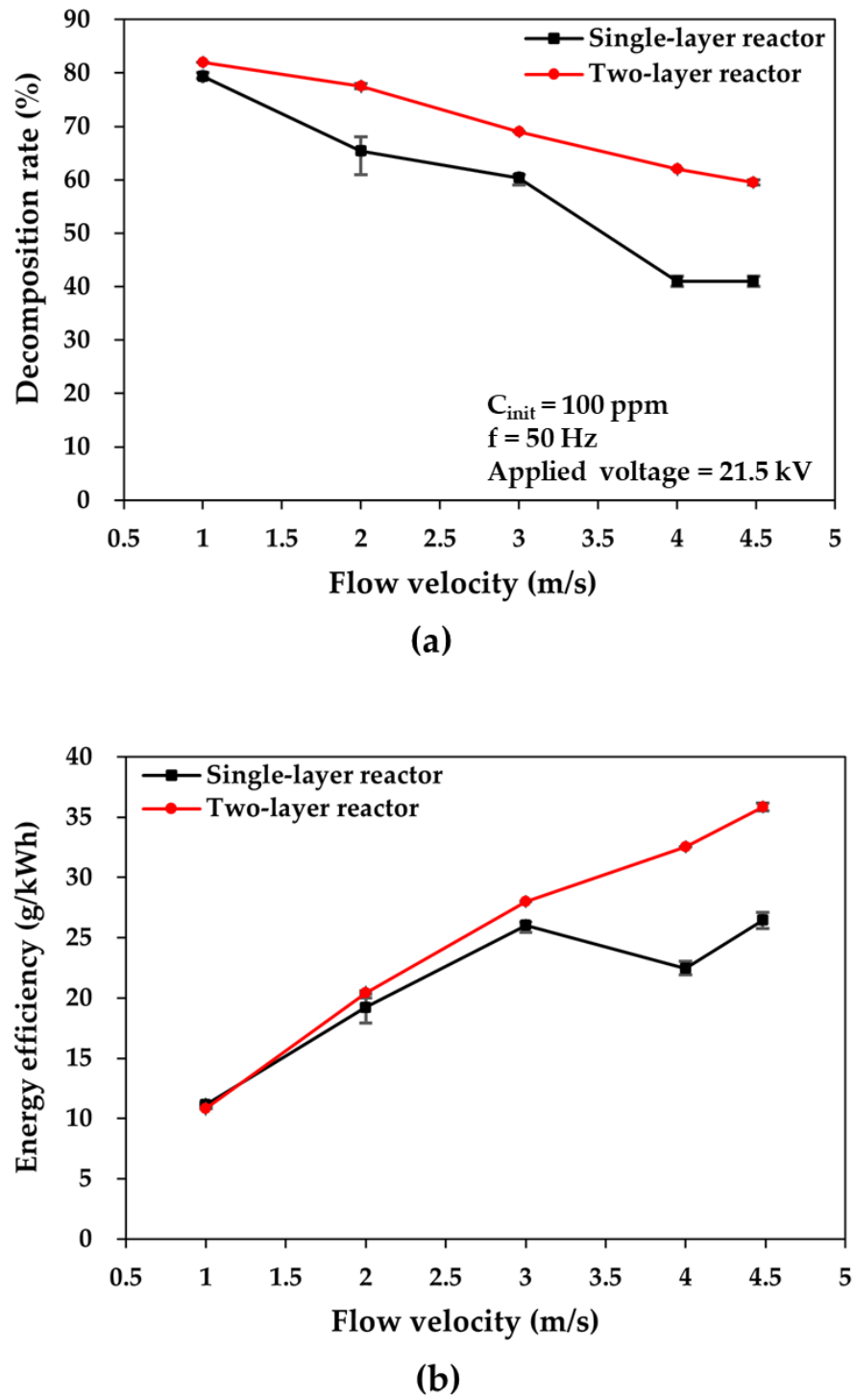

Figure 3.7. Comparisons of (**a**) toluene decomposition rate and (**b**) energy efficiency plotted as a function of flow velocity in the two DBD reactor cases.

As shown in Figure 3.7(b), as the flow velocity increased from 1 to 4.58 m/s, the energy efficiency increased from 11.16 to 26.43 g/kWh in the single-layer reactor case and from 10.80 to 35.85 g/kWh in the two-layer reactor case. The energy efficiency in both reactors increased at increased flow velocities; this can be attributed to the increased number of toluene molecules per unit discharge time. It was also found that the difference in energy efficiency between the two reactors increased as the flow velocity increased. This is because the toluene decomposition quantity was lower in the single-layer reactor case due to the more abrupt decrease in the decomposition rate. Therefore, regarding the decomposition rate and the higher level of energy efficiency, the decomposition performance of the two-layer reactor is superior to that of the single-layer reactor in terms of flow velocity. Additionally, the processing capability of the two-layer reactor is double that of one-layer reactor at the same flow velocity.

3.3.5. Effects of discharge length on large-flow dbd reactors

Figure 3.8 shows plots of the toluene decomposition rate and energy efficiency versus discharge length for the two DBD reactors at an applied voltage of 21.5 kV and a flow rate of 50 L/min. The high-voltage electrodes of the two DBD reactors were designed to comprise three parts with discharge lengths of 150, 300, and 450 mm from the gas inlet.

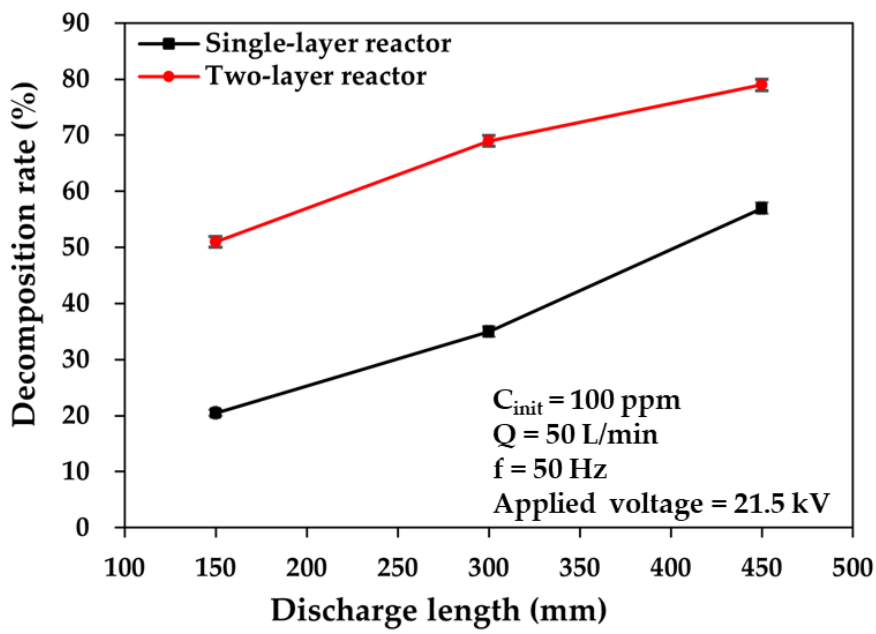

(a)

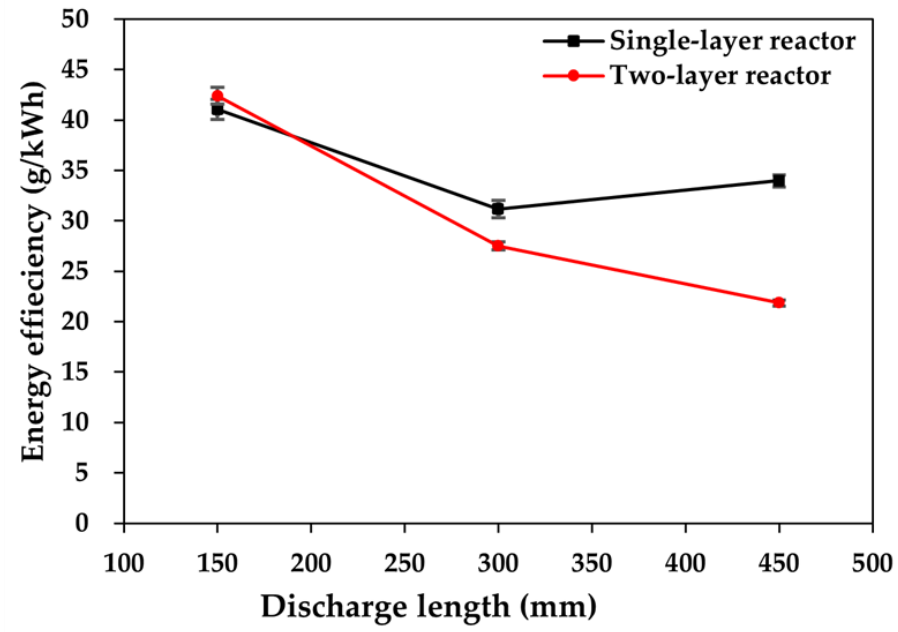

(b)

Figure 3.8. Comparisons of (a) toluene decomposition rate and (b) energy efficiency plotted as a function of discharge length in the two DBD reactor cases.

In both reactors, as the discharge length increases, the decomposition rate of toluene increases, as illustrated in Figure 3.8(a). As the discharge length increases from 150 mm to 450 mm, the toluene decomposition rate increases from 21% to 57% and from 57% to 79% in the single- and two-layer reactors, respectively. This is because the extended discharge length creates a larger plasma zone, which can help increase both the average energetic electron density and the number of microdischarges, thus contributing to the toluene decomposition quantity per unit discharge time at the set flow rate of 50 L/min. The occurrence of this phenomenon in large-flow DBD reactors (at the flow rate of 50 L/min) compared with the results at smaller flow rates in other DBD reactors was also reported by Zhang et al. [42,46,80] at 0.5 L/min, Ashford et al. [42,46,80] at 0.0419 L/min, and Chang et al. [42,46,80] at 0.5 L/min.

However, the corresponding energy efficiency in the single-layer reactor decreased from 41.08 to 33.98 g/kWh as the discharge length increased (Figure 3.8(b)). It was also reported that the increased discharge length caused an increase in power consumption for the generation of an enlarged plasma zone [6,7,11,21,78,79], which led to a higher decomposition quantity per discharge time in the single-layer reactor case; in turn, this finally improved energy efficiency. Conversely, the two-layer reactor exhibited the same

trend (from 42.39 to 21.85 g/kWh), but the decrease in energy efficiency was considerably higher. In the two-layer reactor, however, the excessive energy input caused by the increased discharge length caused a more abrupt decrease in energy efficiency compared with the single-layer reactor, given that the larger discharge space can yield a relatively greater decomposition quantity per discharge time at shorter discharge lengths. Nevertheless, it still exhibited comparable energy efficiency for a broad range of discharge lengths. These findings prove the superiority of the multilayer structure of the two-layer reactor in terms of the discharge length and provide directive data for the future configuration design of large-flow DBD reactors.

3.4. Summary

In summary, a scalable large-flow DBD reactor (single-layer reactor) was proposed and fabricated for VOC abatement. Based on the single-layer reactor, another large-flow DBD reactor with a multilayer structure (two-layer reactor) was developed. The effects of applied voltage, gas flow velocity, gas flow rate, and discharge length on degradation performances, including the decomposition rate and energy efficiency in large-flow DBD reactors, were also investigated. Moreover, by comparing the decomposition performances between the two types of DBD reactors, the feasibility and superiority of multilayer structures in large-flow DBD reactor configurations were demonstrated. The experimental results revealed that the performances of large-flow DBD in toluene decomposition displayed characteristics similar to those of small-flow DBD reactors on the lab scale, as demonstrated in Section 3. For example, increasing the gas flow velocity and rate has a negative effect on the decomposition rate; however, it is favorable for energy efficiency. These findings indicate the feasibility of large-flow plasma generation, which has not been reported in other previous studies.

In addition, in the single-layer reactor, the best decomposition rate of 85% was achieved at a flow rate of 10 L/min, and the corresponding energy efficiency was 10.20 g/kWh. When the flow rate increased to 110 L/min, a decomposition rate of 51% and energy efficiency of 66.43 g/kWh were observed. Conversely, in the two-layer reactor, the best decomposition rate of 86% was also achieved at 10 L/min, with the corresponding energy efficiency of 4.63 g/kWh. Moreover, a decomposition rate of 59.5% and energy efficiency of 35.99 g/kWh were achieved at a faster flow rate of 110 L/min. Therefore, large-flow DBD reactors turned out to be effective and efficient for toluene abatement. Additionally, the higher decomposition performances of the two-layer reactor at faster flow rates confirm that the processing capability can be enhanced by

employing a multilayer structure, providing a viable scheme for the configuration of DBD systems for practical use.

Nevertheless, there are still issues that need to be overcome for practical applications in industry. First, despite the effectiveness of large-flow DBD reactors in the decomposition of toluene, the environmental risk of their by-products needs an in-depth investigation and evaluation. Second, only the degradation performances using toluene were demonstrated in this study. Accordingly, additional investigations are required to understand the chemical reactions involved as well as the degradation mechanism for multiple VOC mixtures in large-flow DBD systems. Finally, despite the achievement of a toluene decomposition rate of 59.5% at a fast flow rate of 110 L/min, further processing capabilities (e.g., 1000 L/min or faster) are still required. Accordingly, an upscaled, large-flow DBD reactor in a multilayer structure (ten layers), which can cope with gas degradation up to 1000 L/min for VOC abatement, is being developed, and will be discussed in the next chapters.

Chapter 4 Design and characterization of ten-layer upgraded large-flow DBD reactors

4.1 Introduction

In chapter 3, two types of large-flow DBD reactors, specifically single- and two-layer DBD reactors have been developed [81]. These reactors can treat exhaust gases at flow rates that are two orders of magnitude greater (up to 110 L/min) compared to those of small-flow DBD reactors, which are typically limited to a few L/min or lower. Additionally, they achieved a high decomposition rate of 59.5% on toluene with an initial concentration of 100 ppm when a power of 41.23 W was applied in the two-layer case. Decomposition characteristics were also obtained at different applied voltages, flow rates, flow velocities, and discharge lengths. The results indicated the feasibility and superiority of the multilayer configuration scheme for upscaling DBD reactors with high throughput. It has been shown that the appropriate discharge gap and length for the DBD reactors in this study are 2 mm and 200 mm, respectively, in terms of energy efficiency. Nevertheless, further processing capabilities (e.g., 1000 L/min or higher) are still required to realize practical applications with high efficiency.

Based on the results above, in Chapter 4, an upscaled, large-flow, ten-layer DBD reactor with a processing capacity of up to 1000 L/min is designed and fabricated, which serves as an upgraded version of the previously reported single- and two-layer DBD reactors in Chapter 3 [81]. This development is novel and has not been previously reported, serving as an upgraded version of the previously reported single- and two-layer DBD reactors [6,7,11,21,82,83]. The flow path design of the ten-layer DBD reactor was validated via computational fluid dynamics (CFD) simulations and empirical measurements. In addition, the fundamental characterization including multi-gas ignition involving various gases such as Air, Ar, He, N_2, O_2, and CO_2, as well as electrical and spectroscopic characterizations at large flow rates (50−1000 L/min), were conducted. Thus, the proposed design methodology is expected to lay the foundation for developing practical DBD reactor systems aimed at VOC control.

4.2. Design of large-flow DBD reactor and its experimental setup

4.2.1. Rationales of the upscaled large-flow DBD reactor: ten-layer DBD reactor

The design and fabrication of an upgraded, large-flow, ten-layer DBD reactor were completed. The design schemes of the ten-layer DBD reactor are depicted in Figure 4.1, which is composed of ten identical single-layer DBD units; Each unit can generate one layer of plasma, which is accomplished by two Al plates (200 mm×100 mm×1 mm) serving as electrodes; Each Al plate was attached with two glass plates (250 mm × 200 mm × 2 mm) on both sides, acting as insulating dielectrics (relative permittivity: κ = 7–7.5); In addtion, the two glass-covered Al plated were partitioned by two polytetrafluoroethylene sheets (250 mm×50 mm×2 mm) at edges to form a discharge space of 40 cm^3 per DBD unit. A ten-layer DBD cascade with a 400 cm^3 discharge space was constructed by stacking ten DBD units with alternating high-voltage and ground electrodes, as shown in Figure 4.1(a). With the ten-layer DBD cascade as the gas treatment part, a large-flow, ten-layer DBD reactor was established with a gas inlet, a gas flow equalizing part (including an airflow diffuser plate and two perforated metal plates with 3 and 5-mm holes), and a gas outlet, as rendered in the overall view (upper), as well as in the cross-sectional view (lower) in Figure 4.1(b). Thus, the design scheme enabled a small-footprint and easily scalable large-flow DBD reactor with a height of only 75 mm and ten DBD units (12 mm in height) that could also be modulated in the vertical direction.

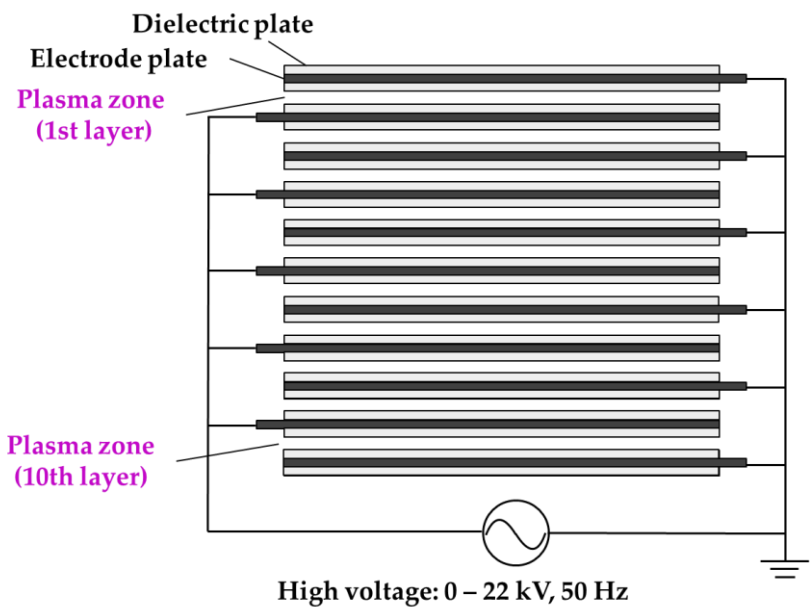

(a)

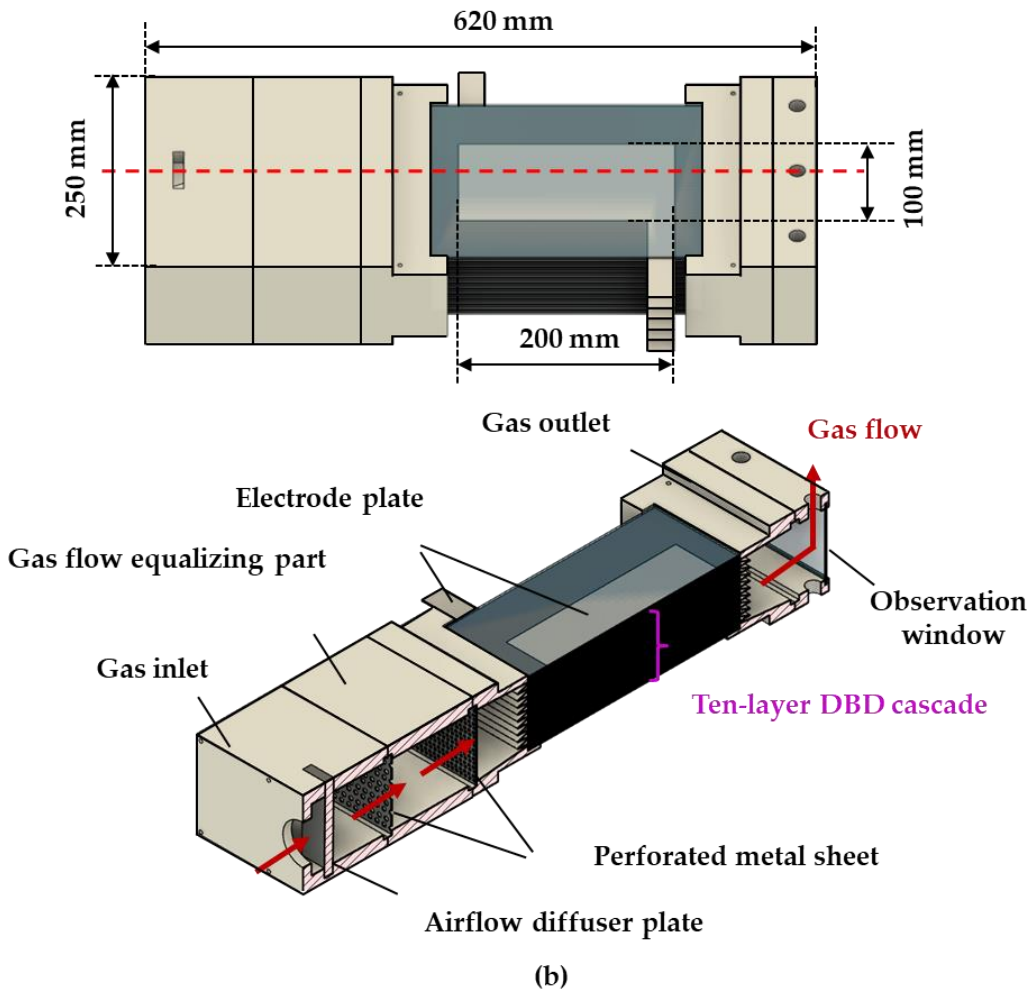

Figure 4.1. Design schemes of the ten-layer DBD reactor: (a) Schematic of the ten-layered gas treatment part (ten-layer DBD cascade); (b) overall and cross-sectional views of the complete configuration of the ten-layer DBD reactor.

4.2.2. CFD simulation-assisted flow path design

Ensuring uniform airflow in each flow channel of the ten-layer DBD reactor is indispensable for achieving stable and homogeneous plasma generation in each layer, thereby maximizing the optimum performance. Therefore, fluid dynamics simulations were conducted during the process of designing a ten-layer, large-flow DBD reactor to gain insight into the fluid dynamics of the flow path [15,84,85]. Autodesk CFD simulation software (Autodesk Inc., San Rafael, CA, USA) was used. To verify the velocity field of the ten channels in the ten-layer DBD reactor, the governing equations describing the conservation of mass and momentum are as follows; The continuity and Navier-Stokes equations for an incompressible flow were discretized and solved using

the finite element method (FEM). Because the fluid flow introduced to the ten-layer DBD reactor was treated as turbulent incompressible flow in this study , and the continuity equation can be written as follows [15,85,86]:

$$\frac{\partial \boldsymbol{\rho}}{\partial t} + \rho \nabla \cdot \boldsymbol{u} = 0 \tag{4.1}$$

where **u** represents the flow velocity vector, ρ and t are fluid density and time. the Navier-Stokes equation is given by Equation (2) [15,86,87].

$$\rho \frac{\partial \boldsymbol{u}}{\partial t} + \rho(\nabla \cdot \boldsymbol{u})\boldsymbol{u} = \rho g - \nabla P + \mu \nabla^2 \boldsymbol{u} \tag{4.2}$$

therein, the components of g, P, and μ denote the gravitational acceleration vector, pressure, and dynamic viscosity, respectively.

Three models, without an airflow diffuser plate or a perforated metal plate (Model 1: none), with an airflow diffuser plate alone (Model 2: airflow diffuser), and with both (Model 3: airflow diffuser + perforated metal), were established to investigate the flow velocity per channel of the ten-layer DBD reactor during the design phase. For all models, air was set as the working fluid, whose boundary conditions, including the flow rate at the inlet surface and the pressure at the outlet surface of the flow volume, were set to 1000 L/min and 0 psi (pounds per square inch), respectively, with no heat transfer. Moreover, the mesh size of all models was implemented with the Automatic Meshing function, where the following parameters (i.e., Resolution factor = 1.000, Edge growth rate = 1.100, Minimum points on edge = 2, Points on longest edge = 10, Surface limiting aspect ratio = 20, and Volume growth rate = 1.35) were prescribed. Thus, the configurations of the mesh distribution for the three models were defined. Table 4.1 provides the analytical information with which the simulations were performed. Notably, the temperature transfer and plasma ignition were not considered in the CFD simulations in this study.

Table 4.1. Information on the meshing of the three models.

Model	Mesh element	Fluid node	Solid node	Total node
None	Tetrahedral	126865	81699	208564
Airflow diffuser	Tetrahedral	127756	82275	210031
Airflow diffuser + perforated metal	Tetrahedral	216881	85611	302492

In addition to CFD simulation verification, practical velocity measurements were performed for each channel using a hot-wire anemometer (TSI 9565-A, TSI Incorporated, Shoreview, USA) at a temperature of 24 °C and atmospheric pressure, and the results were in agreement with those obtained by the simulation. Furthermore, optical emission spectroscopy (OES) using a spectrometer (Maya2000Pro, Ocean Photonics, Tokyo, Japan) and an optical fiber (P600-1-SR, Ocean Insight, Orlando, USA) with wavelengths between 200 and 1100 nm was performed to verify the uniformity of plasma generation in each channel of the ten-layer DBD reactor through the optical emission intensity. To ensure fidelity, all measurements were repeated at least three times at three measurement points and averaged.

4.2.3. Experimental setup

Figure 4.2 shows the experimental setup. It has four basic parts: a gas flow control section, an AC power source, a ten-layer DBD reactor, and electrical and spectroscopic measurement instruments. The gas flow of air introduced into the ten-layer DBD reactor was induced by a vortex blower (VB-003S-E2, Hitachi Industrial Equipment Systems Co., Tokyo, Japan), and the flow rates of the airflow to be treated were adjusted using a gate valve and hot-wire anemometer (TSI 9565-A). To power the ten-layer DBD reactor, a 50 Hz AC power supply (voltage range:0-22 kV, zero-to-peak value) was chosen. The waveforms of the applied voltage and current were analyzed using a digital oscilloscope (DPO4104, Tektronix, Tokyo, Japan) with a current monitor (4100, PEARSON ELECTRONICS, Inc., CA, USA) and a 1000:1 high-voltage probe (HPV-39pro, PINTEC, Beijing, China). Moreover, the power consumption of the entire setup and the ten-layer DBD reactor (i.e., discharge power: the power deposited to the plasma discharge) was monitored using a watt meter (TAP-TST8N, Sanwa Supply Inc., Okayama, Japan) and calculated using Lissajous figures observed through a capacitor (C_m = 1 ◎F). The average dissipated power in the plasma discharge is the product of the Lissajous figure area and power supply frequency (i.e., 50 Hz) [27,76,77]. The capacitance of the ten-layer DBD reactor during plasma discharge was also calculated from the Lissajous figures. The spectroscopic properties were investigated using a spectrometer (Maya2000Pro), whereas the gas temperature of the plasma was determined using a fiber-optic temperature transmitter (FTX-300-LUX+, OSENSA Innovations Corp., BC, Canada) outfitted with a fiber-optic temperature probe (PRB-G40-2.0M-ST-C, OSENSA Innovations Corp., BC, Canada), with measurement points located at the fifth layer of the ten-layer DBD reactor. All the measurements were implemented under conditions at

a temperature of 24 °C and atmospheric pressure. For fidelity, all the measurements were repeated at least three times, and averaged data were obtained.

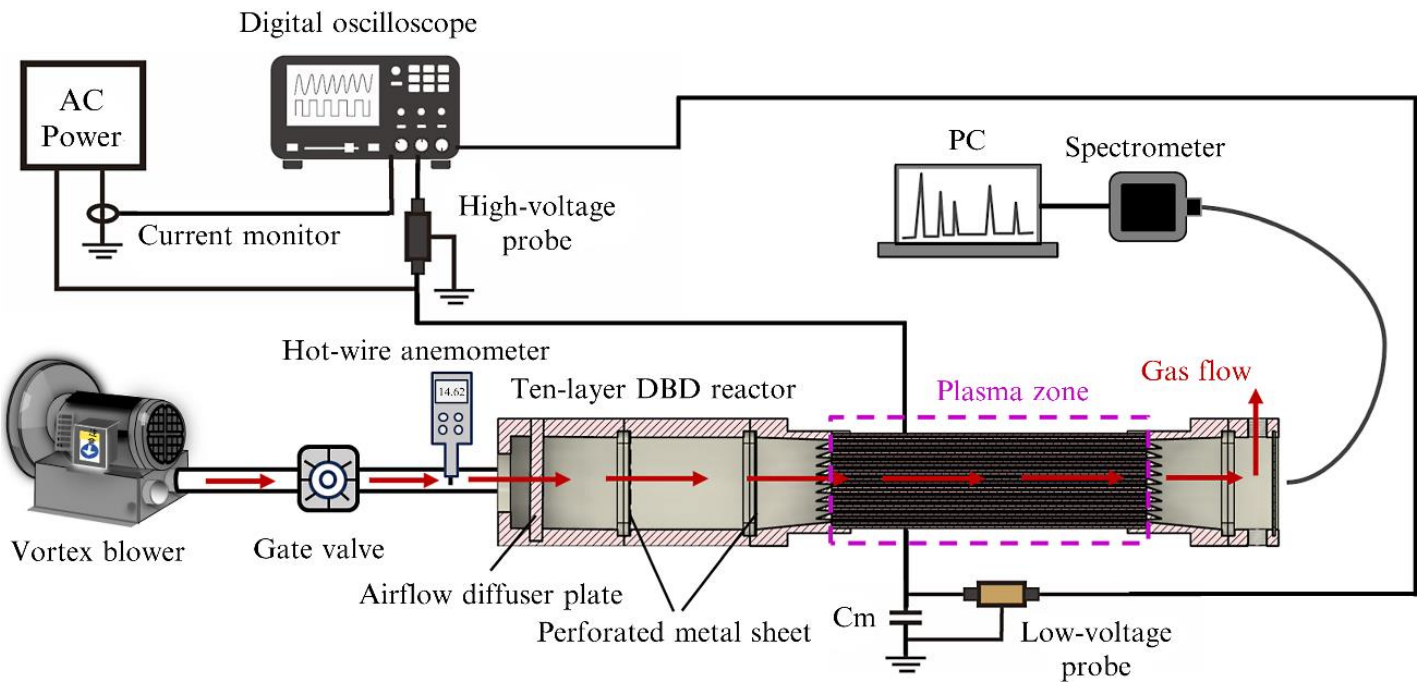

Figure 4.2. Schematic of the experimental setup used for the electrical and spectroscopic characterizations.

4.3. Fundamental characterization of the ten-layer DBD reactor

4.3.1. Optimization of the flow path

CFD simulations of the three models in Subsection 2.2 were carried out to optimize the flow path of the ten-layer DBD reactor. The initial gas flow rate of the boundary conditions was set to 1000 L/min and the flow velocity per flow channel at the measurement points was computed, as shown in the upper right panel in Figure 4.3(a). The maximum velocity of each flow channel was used to determine velocity uniformity. As shown in Figure 4.3(b)(1), at an initial gas flow rate of 1000 L/min at the inlet surface, a concentrated airflow was initiated and extended to the flow channels. As a result, a localized high velocity field was formed in the central flow channels, resulting in a maximum velocity difference of 0.93 m/s between the max- and mini-velocity flow channels, with the standard deviation of the ten layers being 0.35 m/s, 3.39% of the average velocity (10.20 m/s).

However, the nonuniformity of the flow velocity among the flow channels was significantly reduced by the introduction of an airflow diffuser plate, which decentralized the concentrated airflow, as shown in Figure 4.3(c)(1). Accordingly, the uniformity of the velocity field of each flow channel was improved to a significantly reduced velocity difference of 0.24 m/s between the max- and mini-velocity flow channels, with a standard deviation of 0.08 m/s, 0.79% of the average velocity (10.34 m/s). In addition, the combination of the airflow diffuser and the perforated metal plates further refined the uniformity, bringing the velocity difference down to 0.13 m/s, with a standard deviation of 0.04 m/s, 0.41% of the average velocity (10.40 m/s), as observed in Figure 4.3(d)(2). This finding suggests that introducing an airflow diffuser and perforated metal plates is a practical and effective tactic for improving nonuniformity without major modifications to the DBD reactor configuration.

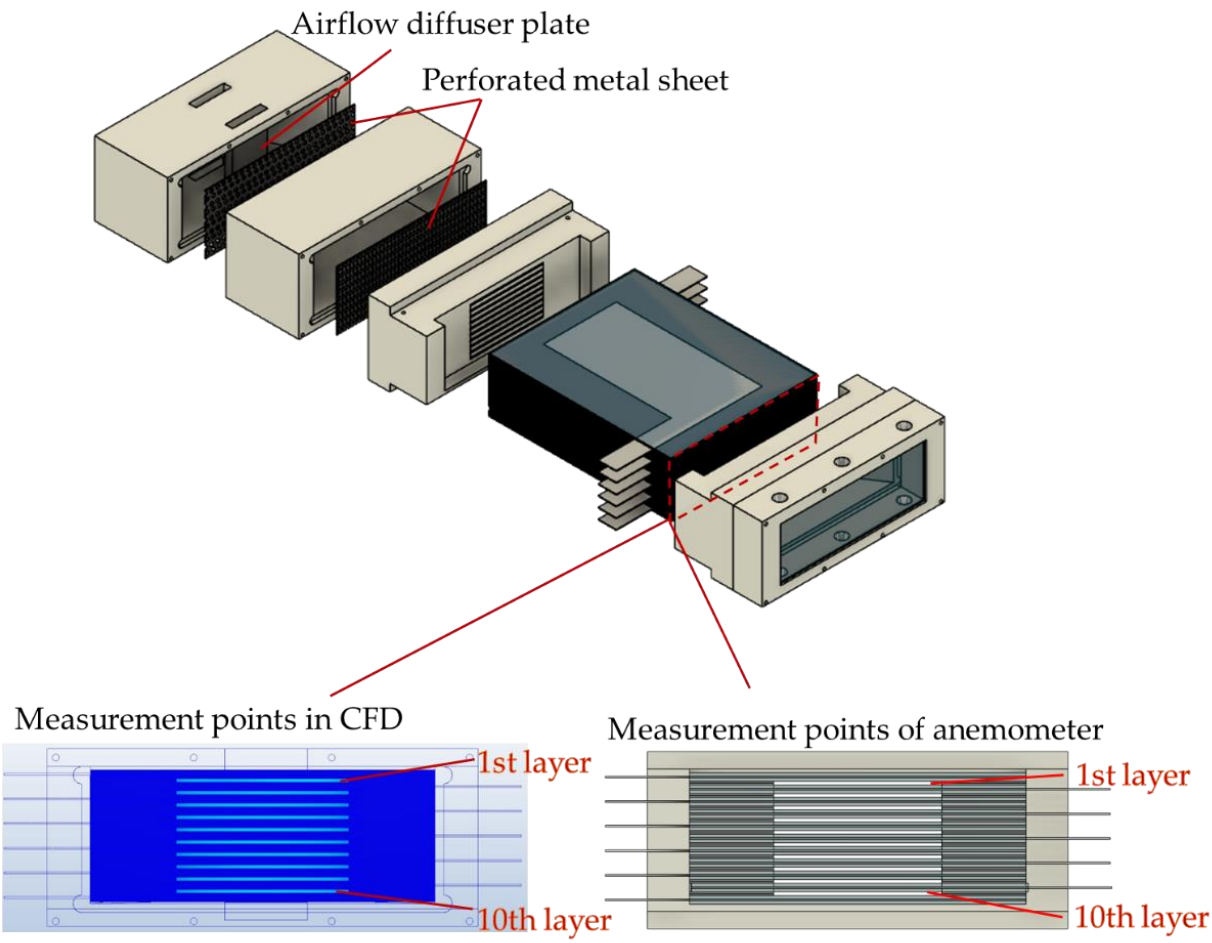

(a)

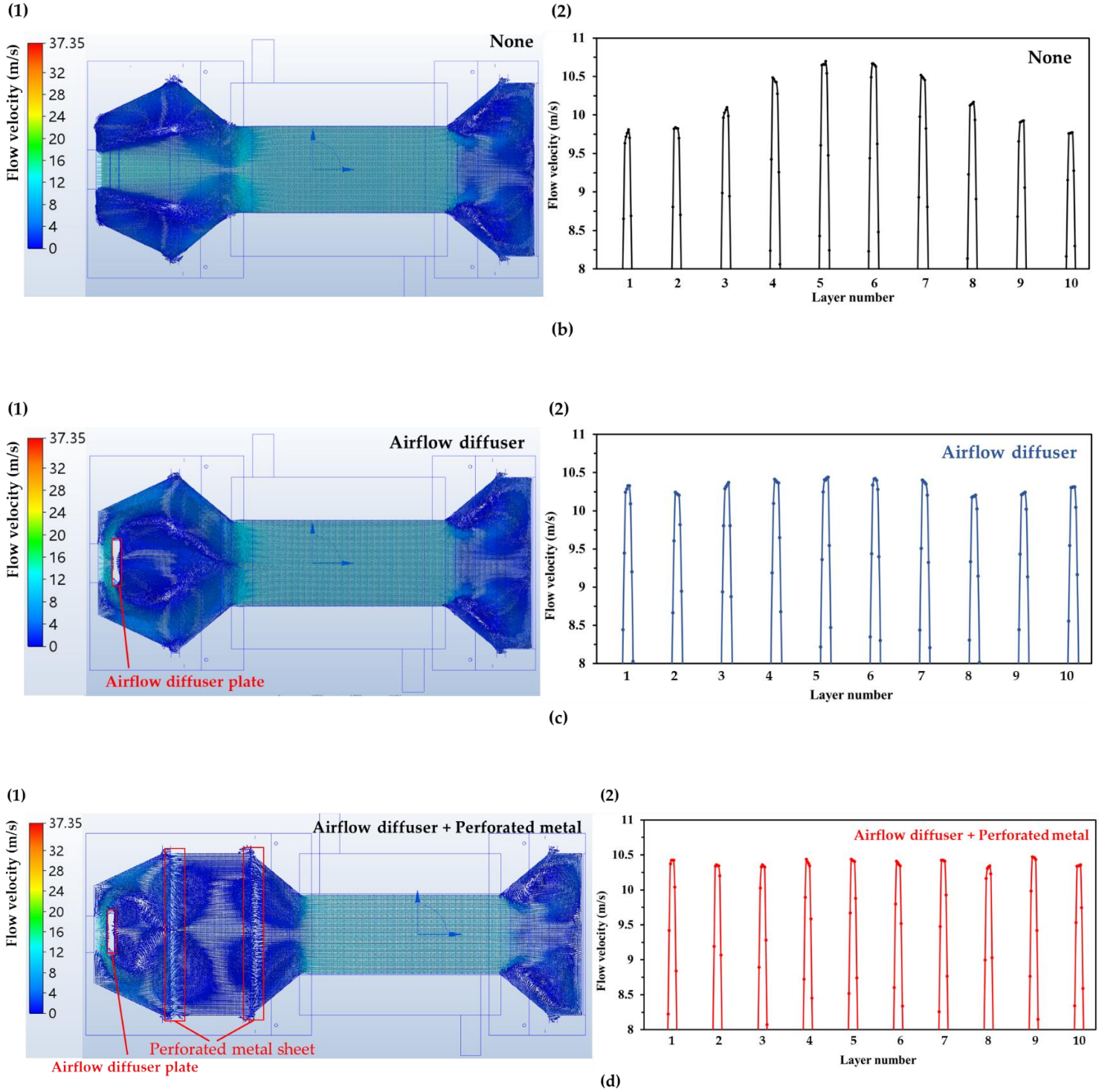

Figure 4.3. (a) Measurement points in CFD (upper right) and for practical velocity measurements (lower right); the flow vector profiles at the fifth layer (left) and flow velocity per channel (right) of the three simulation models of the ten-layer DBD reactor: (b) None, (c) airflow diffuser, and (d) airflow diffuser + perforated metal.

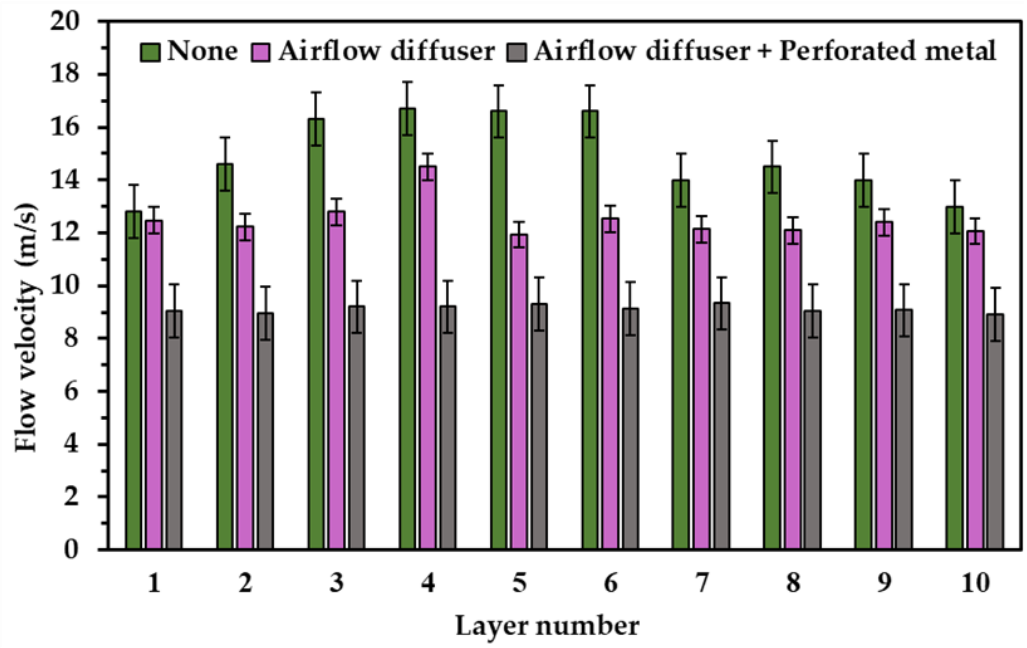

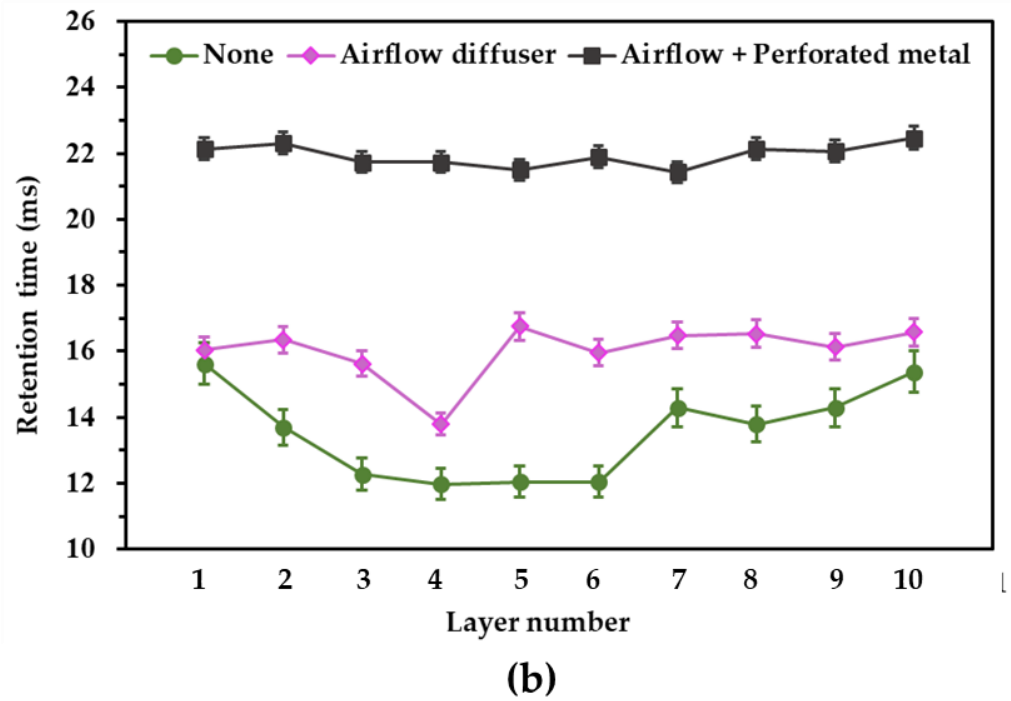

Figure 4.4. (a) Flow velocity and (b) retention time per channel of the three patterns (None, airflow diffuser, airflow diffuser + perforated metal).

According to the results derived from the CFD simulations, the ten-layer DBD reactor was successfully fabricated. Subsequently, practical measurements of the flow velocity per channel were implemented. Benefitting from the modular design, the flow velocities of three patterns (None, Airflow diffuser, and airflow diffuser + perforated metal) corresponding to the three models analyzed in the CFD simulations were measured using a hot-wire anemometer at the measurement points, as shown in the lower right of Figure 4.3(a), where the gas flow rate induced by the vortex blower was adjusted and fixed at 1000 L/min with the third pattern (airflow diffuser + perforated metal). The three patterns exhibited trends similar to those of the CFD-computed results with excellent agreement. Obviously, the pattern: Airflow diffuser + Perforated metal outperformed other patterns (None: average velocity of 14.91 m/s, velocity difference of 3.9 m/s, standard deviation of 1.38 m/s; Airflow diffuser: average velocity of 12.52 m/s, velocity difference of 0.87 m/s, standard deviation of 0.71 m/s) with the minimum velocity difference of 0.37 m/s between the max- and min-velocity flow channels, and the standard deviation of the ten layers is 0.13 m/s, 1.47% of the average velocity (9.12 m/s), as shown in Figure 4.4(a). This result was also evidenced by the retention time per channel of the three patterns, where the third pattern presented the lowest standard deviation of the retention time of 0.32 ms compared to the other two patterns (None: 1.26 ms, Airflow diffuser: 0.77 ms), as rendered in Figure 4.4(b). However, a significant decrease in the average velocity from 14.91 m/s to 9.12 m/s (i.e., increase in the average retention time from 13.41 ms to 21.94 ms) was observed after the introduction of the airflow diffuser and perforated metal plates, unlike the cases in the CFD simulations, in which the rate remained at the same level of 10.20 m/s. This result may be attributed to the vortex blower (static wind pressure at 50 Hz: 3.4 kPa) used in this study, which cannot provide a sufficient wind pressure, resulting in a significantly reduced average velocity, i.e., a lowered gas flow rate. Despite slight deviations between the CFD simulations and practical measurements, these results indicate that the incorporation of the airflow diffuser and perforated metal plates improved the uniformity of the flow velocity per channel in the ten-layer DBD reactor.

4.3.2. Multi-gas plasma ignition

Based on the above results, a ten-layer DBD reactor, which includes a combination of an airflow diffuser and perforated metal plates, was fabricated and examined for plasma generation, which is one of the primary metrics that should be satisfied. The ten-layer DBD reactor was powered by a sinusoidal 50 Hz AC power source ranging between 0 and 22 kV. Figure 4.5(a) shows the plasmas successfully generated in the ten-layer DBD

reactor using multiple gases (air, argon, helium, nitrogen, oxygen, and carbon dioxide) under the corresponding experimental conditions. Notably, the applied voltages for excitation and ionization varied widely between the different source gases. This can be attributed to the large difference in the dielectric strengths of the source gases [88,89]. This result suggests multiple potential applications for the ten-layer DBD reactor because the reactive species produced in the plasma vary with the ignited gas source [21,89]. Plasma generation at a high targeted flow rate (1000 L/min) was also investigated. As shown in Figure 4.5(b), stable air-induced plasma ignition was observed in each flow channel of the ten-layer DBD reactor, confirming the rationality of the flow path design using CFD simulations and the effectiveness of the ten-layer DBD reactor at large flow rates for large-area plasma generation.

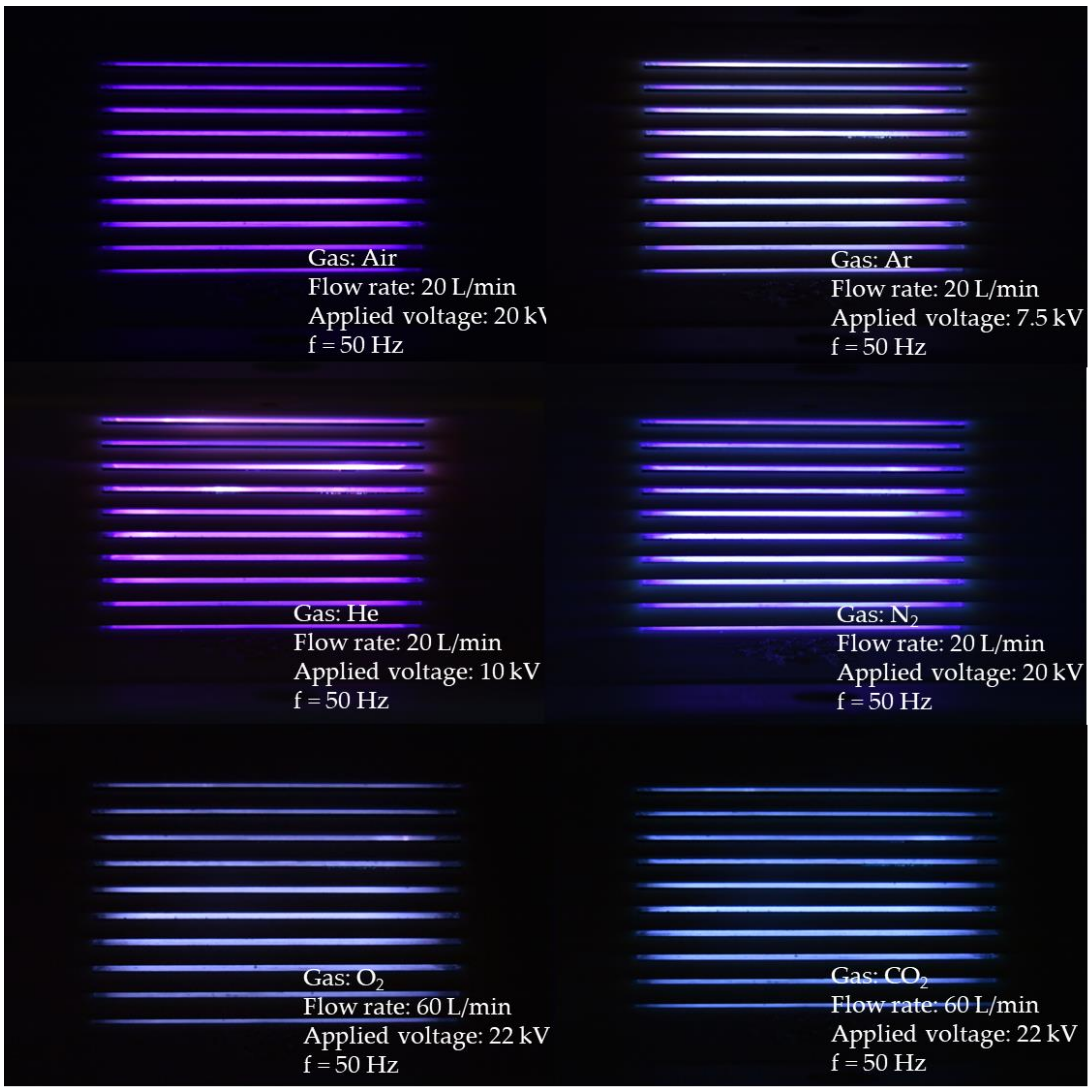

(a)

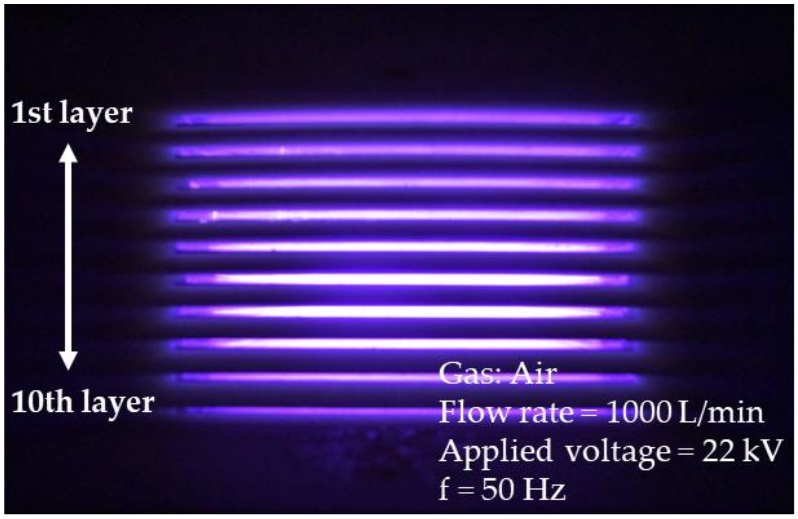

(b)

Figure 4.5. (a) Generation of plasma with multiple gases (Air, Ar, He, N_2, O_2, and CO_2); (b) air plasma ignited at a large flow rate of 1000 L/min.

4.3.3. Electrical characteristics at large flow rates

In addition to the evaluation of multi-gas plasma generation, the electrical characteristics of the ten-layer DBD plasma were also investigated because energy consumption is a critical consideration in industrial applications. Figure 4.6(a) and (b) show the typical voltage and current waveforms and the Lissajous figure (i.e., Q–U characteristics) in the ten-layer DBD reactor during plasma discharge, where the applied voltage and working gas were set to 22 kV and air, respectively. As shown in Figure 4.6(a), pulse current lines occur simultaneously with the ionization of the working gas when the applied voltage rises above a threshold (>16 kV in the ten-layer DBD reactor). The discharge frequency was dominated by that of the applied voltage, which was 50 Hz. Figure 4.6(b) presents the Q-U characteristics of the ten-layer DBD reactor, through which the power dissipated in the discharge was calculated. For example, when the applied voltage was fixed at 22 kV, the discharge powers were 97.60 W at 50 L/min, 95.50 W at 110 L/min, and 85.12 W at 1000 L/min, respectively. In addition, the discharge power of the ten-layer DBD reactor (95.50 W at 110 L/min, 22 kV) is approximately 2.32 times larger than that of the two-layer DBD reactor (41.23 W at 110 L/min, 21.5 kV) as studied previously, which can be attributed to the larger discharge space of the ten-layer case (400 cm^3), which is 2.22 times larger than that of the two-layer case (180 cm^3); This is in good agreement with the power characteristics of two previously reported large-flow DBD reactors [81], and

therefore, a comparable decomposition rate for toluene (e.g., 59.5% at 245 L/min, 22 kV) can be expected.

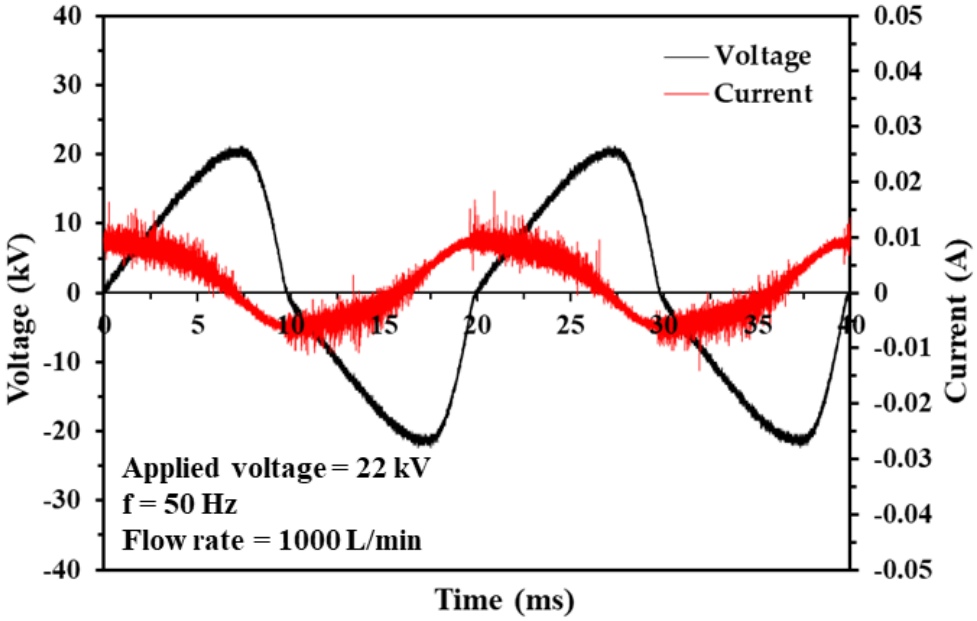

(a)

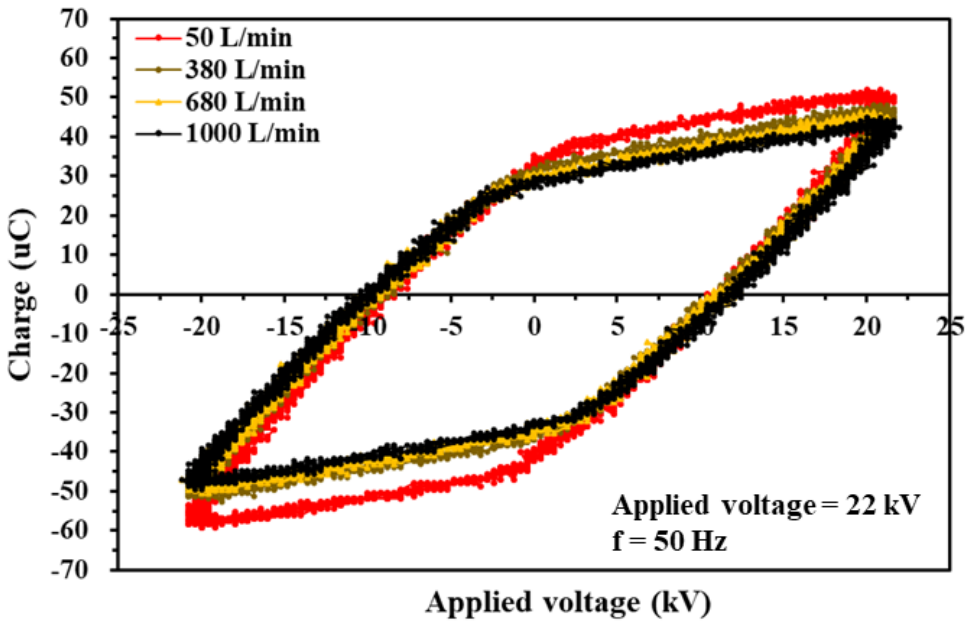

(b)

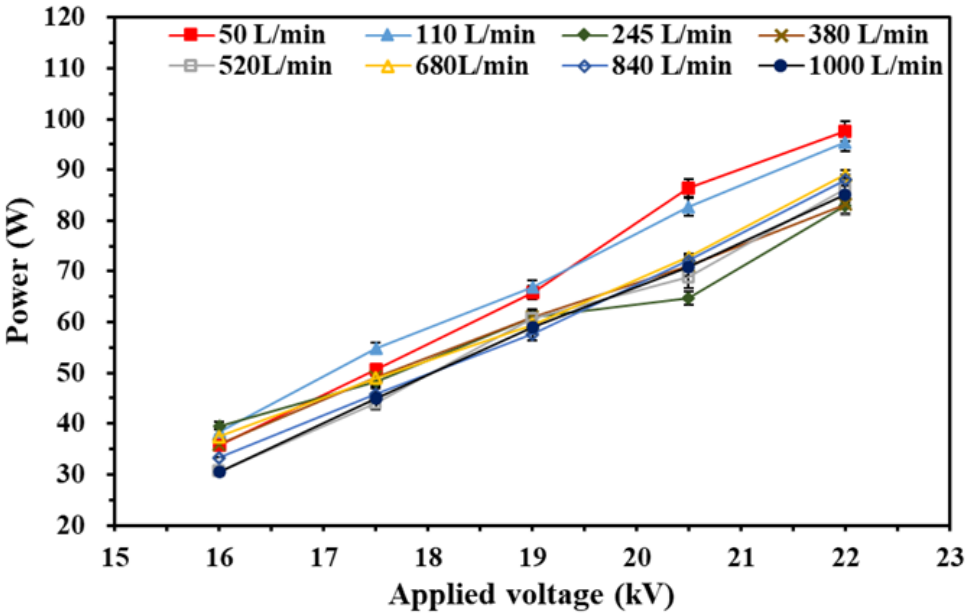

(c)

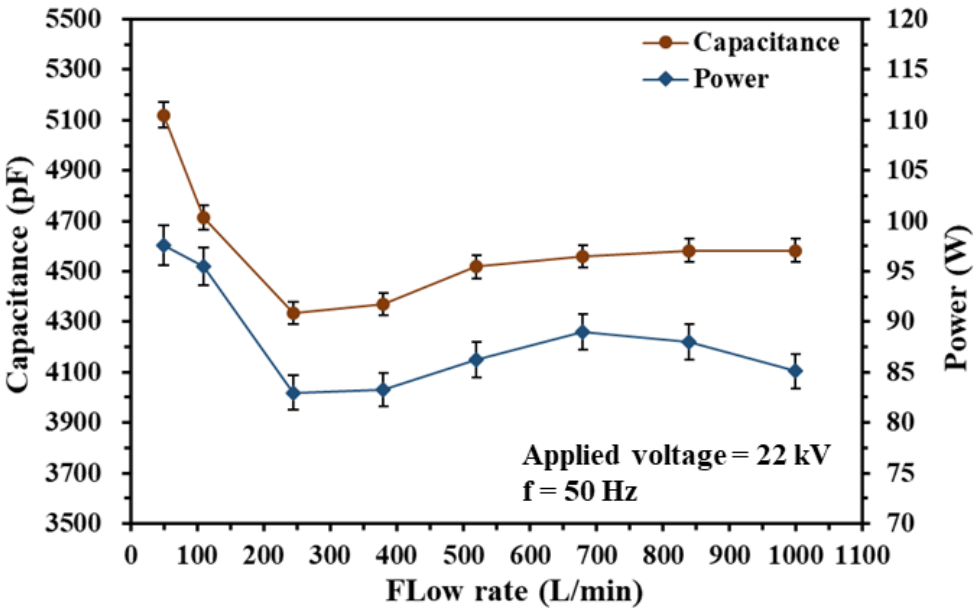

(d)

Figure 4.6. (a) Typical voltage and current waveforms and (b) Q–U Lissajous figures of the ten-layer DBD reactor at 22 kV; (c) power consumption as a function of applied voltage at different gas flow rates (air) and (d) plot of capacitances during plasma discharge versus flow rate for the ten-layer DBD reactor.

A plot of the discharge power versus applied voltage is depicted in Figure 4.6(c) for the ten-layer DBD reactor, where the working gas was set to air, and the gas flow rate was varied from 50 to 1000 L/min. The discharge power of the ten-layer DBD reactor increased as the applied voltage increased, irrespective of changes in the gas flow rate. For example, at a flow rate of 1000 L/min, as the applied voltage increased from 16 kV to 22 kV, the discharge power rose from 31 W to 85 W. This indicated that the applied voltage played a beneficial role in determining the discharge power (P), since the discharge power is proportional to the maximum charge (q_{max}) transferred through and the effective breakdown voltage (V_b) across the discharge gap (i.e., $P = 2 \times V_b \times q_{max} \times f$, where f denotes the frequency of the AC power source; $q_{max} = 2C_d(V_{max} - V_b) - 2C_gV_b$, where C_d, C_g and V_{max} represent the total dielectric capacitance, the gap capacitance and the maximum of the applied voltage, respectively) [21,90]. On the other hand, a decrease of discharge power was observed at higher gas flow rates (245–1000 L/min), as shown in Figure 4.6(c). This result can be ascribed to the increased airflow, which minimizes the thermal effect caused by the plasma discharge, resulting in a lower relative permittivity of the dielectrics (C_d) used in the ten-layer DBD reactor. The lower the relative permittivity of the dielectrics, the lower the maximum charge (q_{max}) transferred through the discharge gap for the same applied voltage, resulting in a low discharge power [36,77]. This can also be observed in Figure 4.6(b) and (d), where the relative permittivity of the dielectrics of the ten-layer DBD reactor first drops significantly from 5120 pF to 4333 pF as the gas flow rate increases from 50 L/min to 245 L/min, and then (>380 L/min) begins to fluctuate around a similar level of 4583 pF at an applied voltage of 22 kV.

4.3.4. Spectroscopic characteristics and gas temperature measurement of the air plasma

As a powerful tool, OES is widely used to determine plasma properties, especially for studying excited and active species and excitation, vibrational, and rotational temperatures. In this study, OES was used to validate the uniformity of plasma generation in each channel of a ten-layer DBD reactor at a targeted large flow rate of 1000 L/min, and to confirm the optimum operating flow rate. Figure 4.7(a) presents the optical emission spectrum in the range of 200–900 nm for the air discharge in the fifth flow channel of the DBD reactor, where the applied voltage and gas flow rate were fixed at 19 kV and 1000 L/min, respectively. It can be seen that the typical peak lines of the air plasma which mainly result from the excited N_2 (i.e., N_2 second positive band: N_2 ($C^3\Pi_u$–$B^3\Pi_g$), N_2^+ first negative band: N_2^+ ($B^2\Sigma^+_u$ –$X^2\Sigma^+_g$), and N_2 fist positive band:

$N_2(B^3\Pi_g–A^3\Pi_u)$) were observed, as the main constituents of air are N_2 (78.08%) and O_2 (20.95%); Moreover, atomic nitrogen (N) at 747.55 nm and 868.55 nm were also determined; In contrast, only NO($A^2\Sigma$ –$X^2\Pi$) was detected in the O_2-related lines, which may be due to the extremely strong emission intensity of the excited nitrogen species. These peak lines were identified by comparison with references [70,90–93]. Moreover, the optical emission spectrum of each channel during the plasma discharge at 1000 L/min exhibited an extremely similar emission intensity under the same ignition conditions, with a standard deviation of the emission intensities in the ten layers of 646, 2.22% of the average emission intensity (29048). This confirms the uniformity of plasma generation in each layer, which is consistent with the results presented in Subsection 3.1, as depicted in Figure 4.7(b).

The spectroscopic characteristics of the ten-layer DBD reactor were investigated with relation to the applied voltage and gas flow rate, with the integration time and average number of times set to be 3 seconds and 5, respectively. As shown in Figure 4.7(c), for all gas flow rate cases, the increased voltage leads to a remarkably increased emission intensity at the 337.93 nm line of the fifth layer of the DBD reactor, which is due to the power deposited to discharge being enhanced by the increased voltage. In contrast, the emission intensity varied significantly from 26602 to 62073 at 22 kV as the gas flow rate increased from 50 to 1000 L/min. The 50 L/min case showed the lowest emission intensity at all applied voltages because the gas flowing with this low rate could not deliver sufficient atoms and molecules per unit time for ionization, resulting in the lowest emission intensity of 28602 at 22 kV. However, as the gas flow rate increased from 110 to 380 L/min, the insufficiency of molecular delivery was slightly alleviated, leading to a relatively high emission intensity at 22 kV (49164 at 110 L/min, 47987 at 245 L/min, and 45673 at 380 L/min). In contrast, at 520 and 680 L/min, the insufficiency of the molecular supply was further alleviated, resulting in an emission intensity peak at 62073 at 680 L/min and 22 kV. This suggests that there is an optimum operating flow rate for the ten-layer DBD reactor. However, as the gas flow rate increased above 840 L/min, the emission intensity decreased because the excess molecule supply and rapidly decreasing transit time caused partial discharge in the plasma zone, resulting in a decrease in the emission intensity at 840 and 1000 L/min.

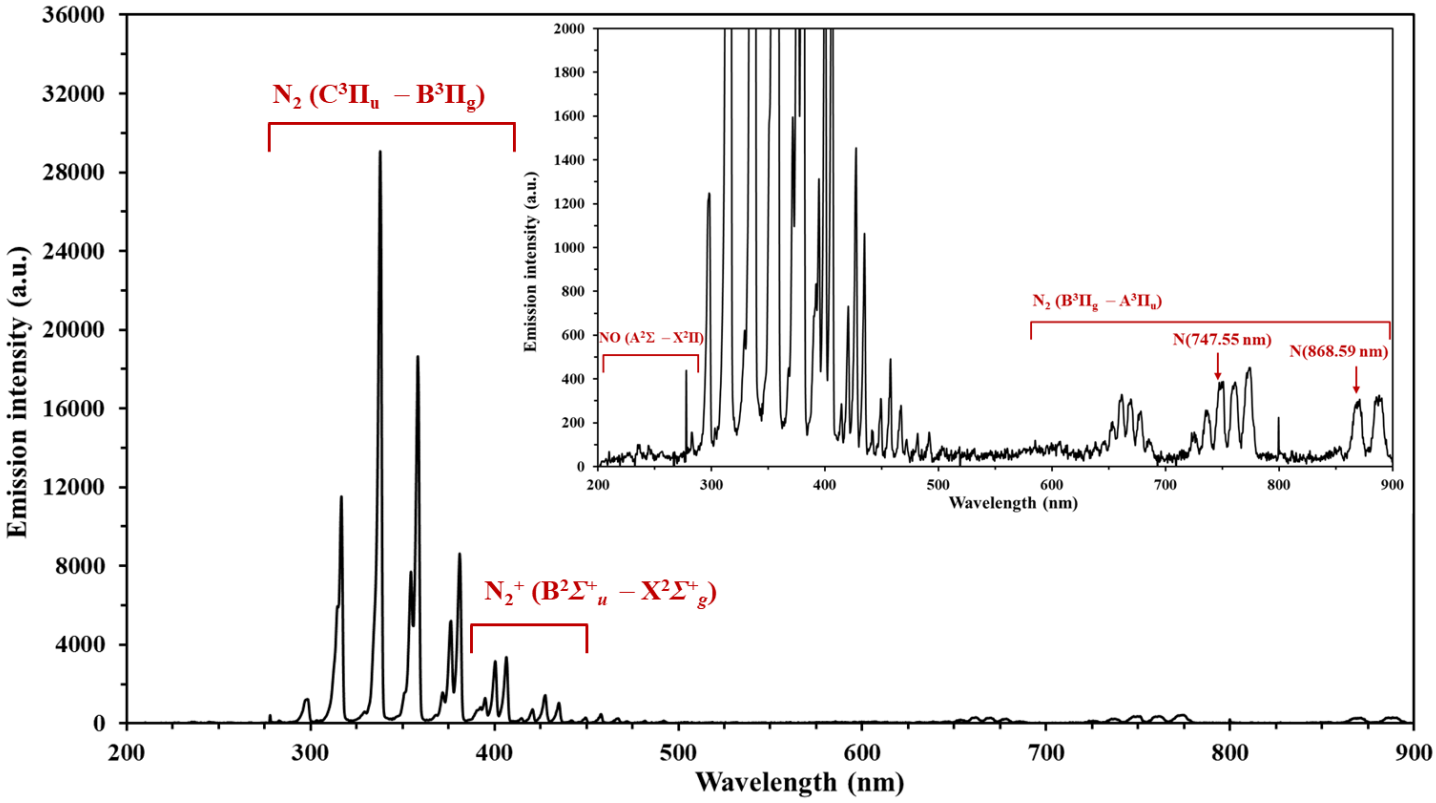
Emission intensity (a.u.)
Wavelength (nm)
N2 (C3Πu – B3Πg)
N2+ (B2Σ+u – X2Σ+g)
NO (A2Σ – X2Π)
N2 (B3Πg – A3Πu)
N(747.55 nm)
N(868.59 nm)

(a)

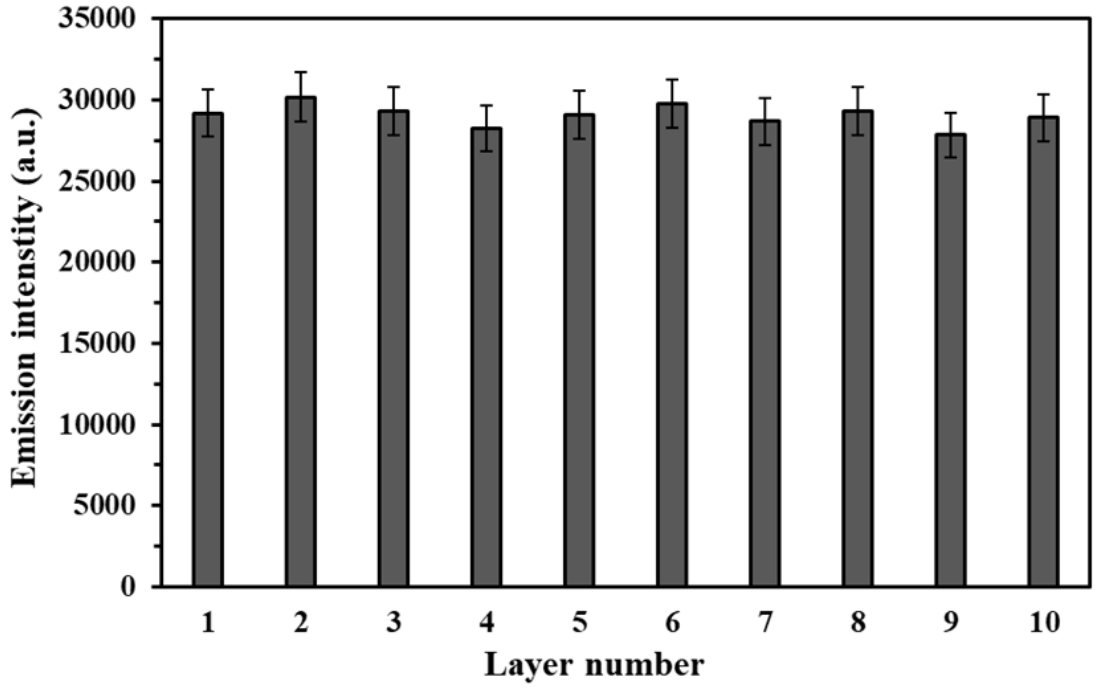
Emission intenstity (a.u.)
Layer number

(b)

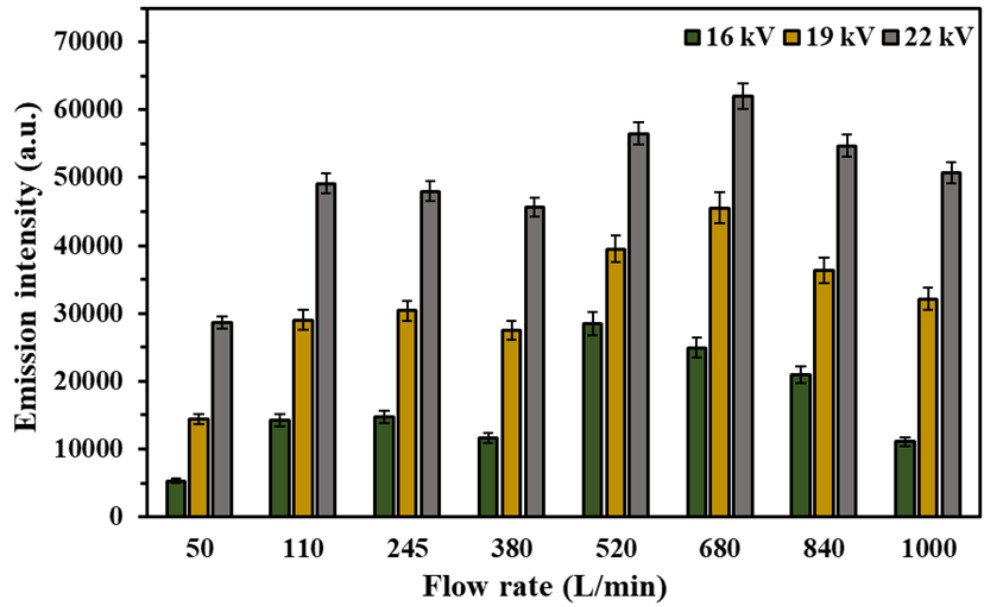

(c)

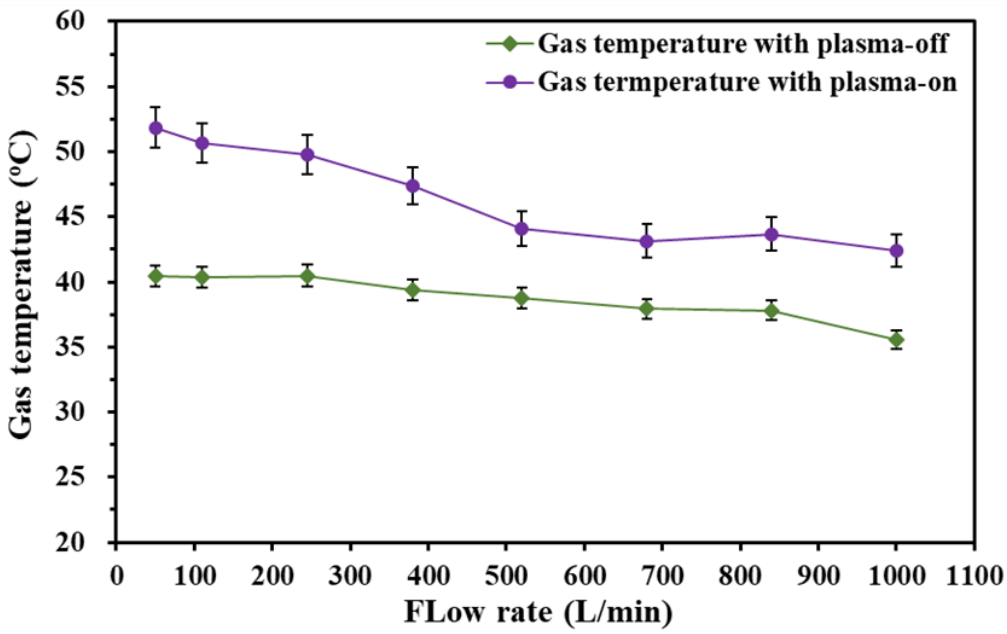

(d)

Figure 4.7. (a) Optical emission spectrum of the air plasma discharge at the fifth layer and (b) emission intensities at the 337.93 nm line in each flow channel of the ten-layer DBD reactor, ignited at 19 kV and 1000 L/min; (c) emission intensities at the 337.93 nm line of the air plasma discharge in the fifth channel at different gas flow rates; (d) gas temperature of the air plasma as a function of gas flow rate at 22 kV.

The gas temperature of the air plasma was evaluated with respect to the gas flow rate. The fiber optic temperature probe was placed at the fifth layer of the ten-layer DBD reactor, and the gas temperatures of the plasma-off were recorded when the temperature reached a plateau (approximately 30 min after gas injection), while those of the plasma-on were recorded 10 min after plasma ignition. Figure 4.7(d) shows the gas temperature of the air plasma generated in the ten-layer DBD reactor as a function of the gas flow rate, where the applied voltage was fixed at 22 kV, and the initial gas temperature before plasma-on (i.e., gas temperature with plasma-off) varied from 35.5 °C at 1000 L/min to 40.43 °C at 50 L/min. The increase in the gas temperature after plasma-on ranged from a maximum of 11.42 °C at 50 L/min to a minimum of 5.23 °C at 680 L/min. As can be observed, all the gas temperatures of the plasma generated in the ten-layer DBD reactor irrespective of the change in the gas flow rates, were maintained at a low temperature (42.41–51.85 °C), corroborating the generation of LTP. Moreover, the plasma gas temperature significantly dropped from 51.85 °C at 50 L/min to 44.12 °C at 520 L/min, and then gradually declined to 42.41 °C at 1000 L/min. This phenomenon can be attributed to the increased heating effect at lower flow rates, which is caused by the heated gate valve due to the collision of large flow rate wind induced on the primary side; And the increasing cooling effect at higher flow rates can alleviate the heating effect resulting from both the heated gate valve and the plasma discharge, as demonstrated in Subsection 3.3 [21,94]. This result is also in excellent agreement with the finding that higher temperatures at lower gas flow rates increase the relative permittivity of the dielectrics of the ten-layer DBD reactor.

4.4. Summary

In Chapter 4, an upscaled, large-flow, ten-layer DBD reactor, capable of treating gas at a flow rate of 1000 L/min, was designed and fabricated for large-flow gas treatment, especially for controlling VOCs. The design methodology for developing large-flow DBD reactors, including CFD simulations, flow path optimization via practical and OES measurements, and electrical and spectroscopic characterizations, provided fundamental knowledge for real-life application of DBD technologies, especially for environmental protection (exhaust purification, outdoor and indoor air pollution mitigation, wastewater treatment, CO_2 reduction, etc.). Notably, both CFD simulations and practical velocity measurements confirmed remarkable improvement in airflow uniformity in the multilayer DBD configuration owing to the incorporated airflow diffuser and perforated plates. The velocity uniformity in the ten-layer DBD reactor was

significantly improved from 1.38 m/s to 0.13 m/s, considering the standard deviation of the ten flow channels in the practical measurements. Moreover, multi-gas (Air, Ar, He, N_2, O_2, and CO_2) plasma ignition and large-flow plasma generation of up to 1000 L/min were achieved with the upscaled ten-layer DBD reactor, and this observation validated its effectiveness under multi-gas conditions and at large flow rates. Furthermore, spectroscopic characterization and gas temperature evaluation of the air plasma at large flow rates were also carried out, which confirmed that the optimum working flow rate was 680 L/min (in terms of emission intensity), and the gas temperature at the plasma-on condition was maintained at (low values) 51.85 and 42.41 °C at 50 and 1000 L/min, respectively.

However, the treatment characteristics and performance of the ten-layer DBD reactor for indoor air pollutants, such as VOCs, were not investigated at this stage. Next-step investigations will be focused on the characterization of VOC degradation and are presented in Chapter 5.

Chapter 5 Decomposition characterization of the ten-layer upgraded large-flow DBD reactor on toluene

5.1 Introduction

In Chapter 4, an upscaled large flow ten-layer DBD reactor capable of treating gas up to a flow rate of 1000 L/min was designed and fabricated for large flow gas treatment as an upgrade to the previously developed single- and two-layer DBD reactors discussed in Chapter 4. Best of all, the flow path design of the ten-layer DBD reactor was validated via computational fluid dynamics (CFD) simulations and empirical measurements. In addition to flow path optimization, stable plasma generation was achieved with multiple gases, as well as air at a targeted high flow rate of 1000 L/min in the ten-layer DBD reactor, proving the feasibility of the multilayer configuration (i.e., ten layers in this case) for the development of large-flow DBD reactors aimed at large-flow gas processing. The proposed design methodology is expected to lay the foundation for developing practical DBD reactor systems. Nevertheless, the treatment characteristics and performance of the ten-layer DBD reactor for indoor air pollutants, such as VOCs, were not investigated.

Therefore, here in Chapter 5, the degradation performance of the developed ten-layer DBD reactor on representative VOCs (e.g., toluene) will be tested and the decomposition characteristics at large flow rates will be investigated. Moreover, the plasma generation and decomposition characteristics with a high-frequency intermittent-pulse power supply will also be examined. Finally, based on the above results, prospective optimization strategies for the further improvement of large flow DBD reactors will also be discussed.

5.2. Experimental setup

The experimental setup is shown in Figure 5.1, four main components composed the setup: toluene concentration adjustment part, gas flow adjustment part, a ten-layer DBD reactor, and measurement instruments. The flow of evaporated toluene in the container was achieved by mixing the toluene in water and then was carried into the reactor using compressed air. Simultaneously, another airflow induced by a vortex blower (VB-003S-E2, Hitachi Industrial Equipment Systems Co., Tokyo, Japan) was introduced to dilute the evaporated toluene airflow, emulating humidified toluene-mixed air. A mass-flow controller (MFC, Japan Star Techno, Osaka, Japan) and gate vale were used to adjust the concentration of the toluene and flow rates to be treated. The toluene concentrations before and after the treatment were determined at the outlet of the ten-layer DBD reactor,

meanwhile, the ozone concentration as an indicator of reactive species production was also determined by a gas detector tube (182SA OZONE, KOMYO RIKAGAKU KOGYO K.K., Kawasaki, Japan).The power consumption of the ten-layer DBD reactor and the whole setup were monitored by Lissajous figures observed by a digital oscilloscope and an energy meter, respectively. The decomposition characteristics of toluene including decomposition rate and energy efficiency were investigated. The equations for calculating the toluene decomposition rate, energy efficiency, and power consumption of the DBD reactor can be referred to in several studies reported by Xu et al. and Jiang et al. [36,81], or in Eqs. (3.1-3.3) and (2.9), as presented in Chapter 4. All the measurements were implemented under conditions at room temperature (24 ◦C), atmospheric pressure. For fidelity, all measurements were repeated at least three times, and the averaged data were obtained.

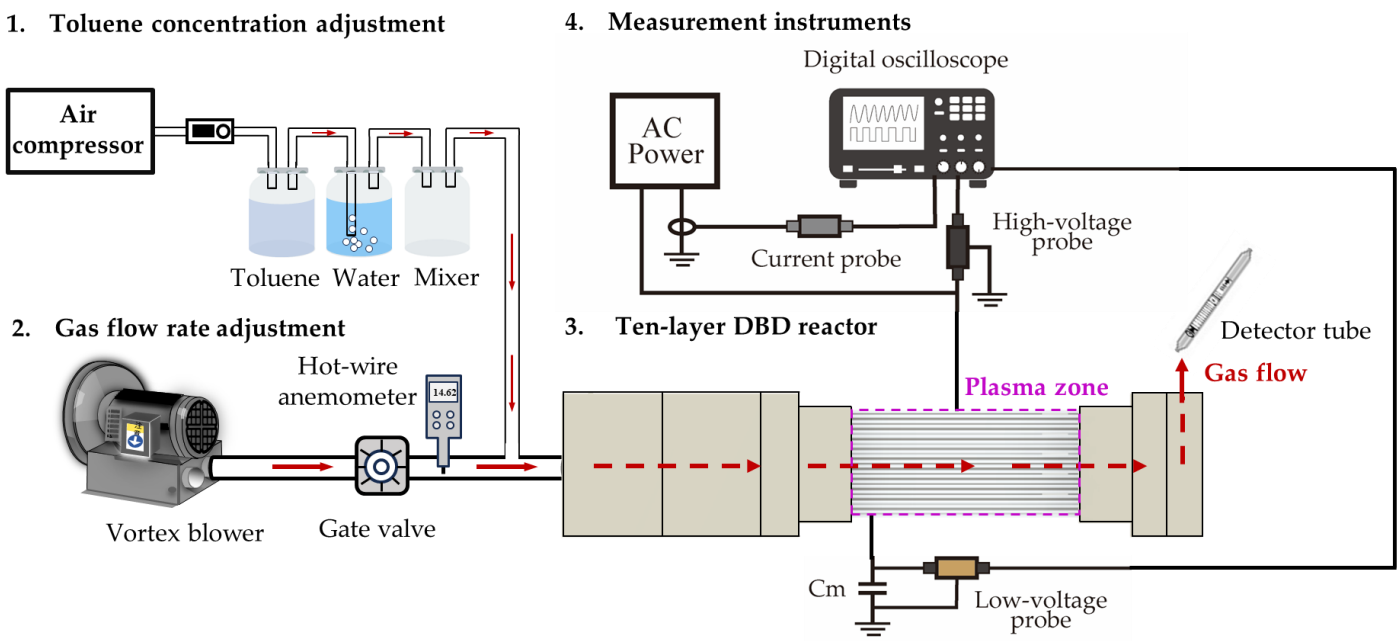

Figure 5.1. Schematic depiction of the experimental setup for toluene degradation evaluation.

5.3. Decomposition characteristics of the ten-layer DBD reactor on toluene

5.3.1. Effects of applied voltage at large flow rates

In order to evaluate the degradation performance at large flow rates up to 1000 L/min (50−1000 L/min), decomposition characterizations were performed on toluene, including decomposition rate and energy efficiency. Figure 5.2 shows the plots of the toluene

decomposition rate and energy efficiency versus applied voltage for ten-layer DBD reactor, where the initial toluene concentration of 100 ppm was maintained, gas flow rates of the toluene-mixed air (intended to be treated) and applied voltage varied from 50–1000 L/min and 16–22 kV, respectively.

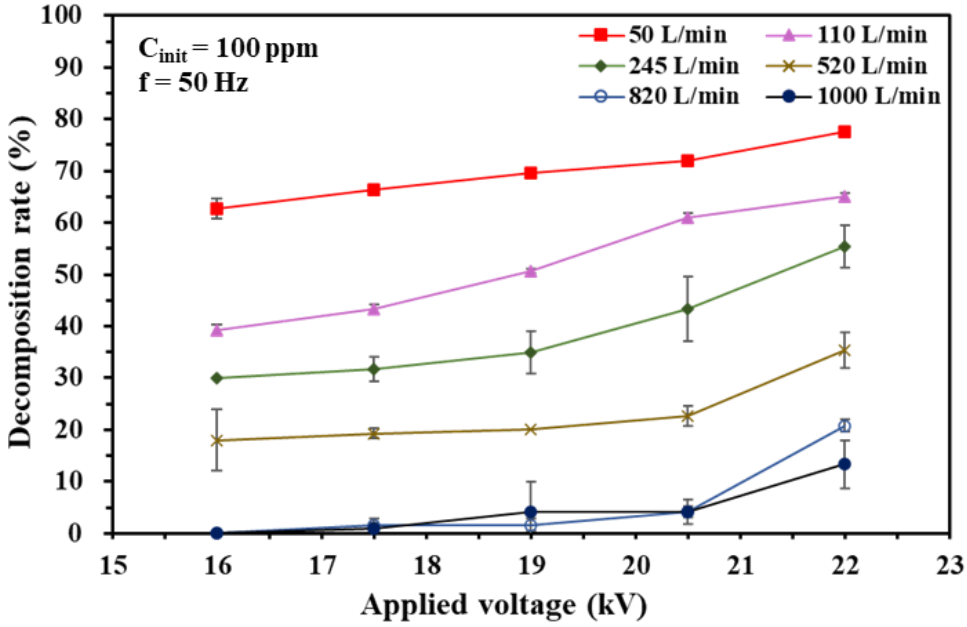

(a)

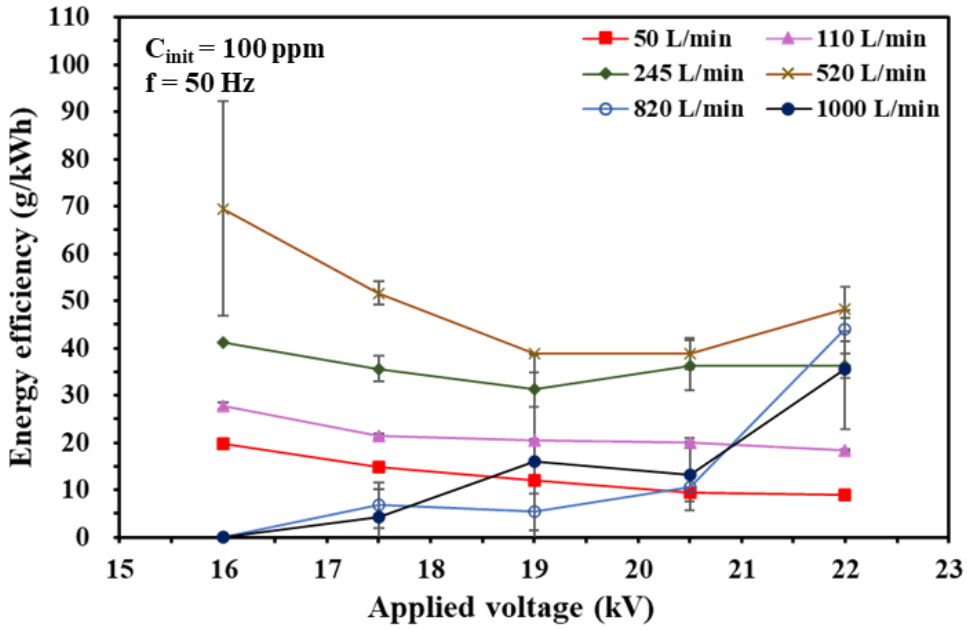

(b)

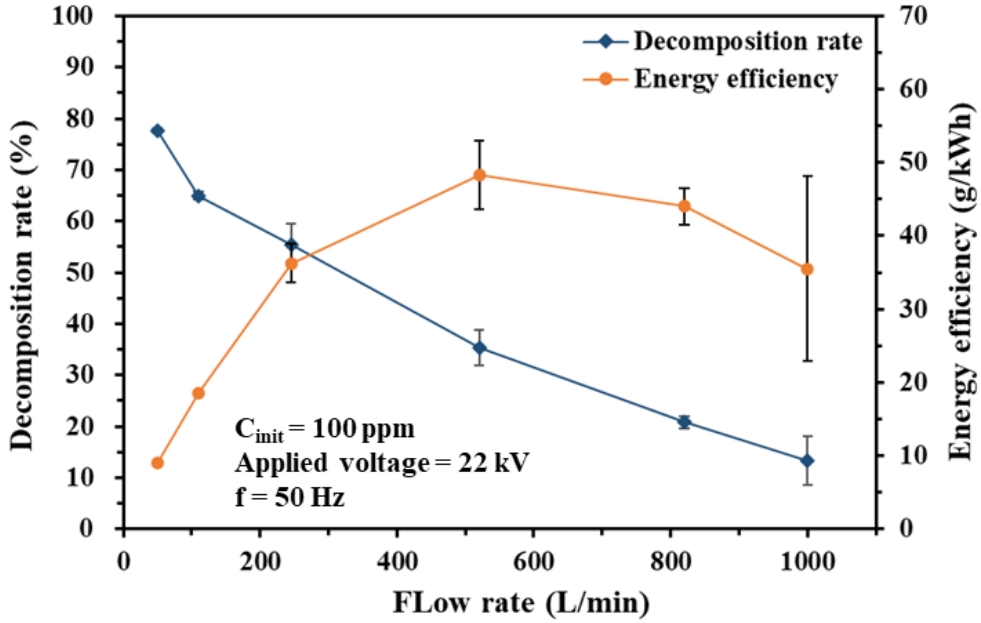

(c)

Figure 5.2. (a) Toluene decomposition rate and (b) energy efficiency plotted as a function of applied voltage; And (c) these characteristics at 22 kV plotted as a function of flow rate in the ten-layer DBD reactor.

It can be observed in Figure 5.2 that the applied voltage played an inducive role in the toluene degradation, exhibiting a similar phenomenon as reported in our previous study [81] as well as demonstrated by Guo et al. [76] (at 0.1 L/min), Jiang et al. [24,72] (at 1.08 L/min) and Wang et al. [77] (at 1–3 L/min). This can be ascribed to the fact that increased applied voltages boost more significant numbers of highly energetic electrons, promoting the production of reactive species and the probability of collisions with toluene molecules, thereby contributing to the decomposition rate [36,75]; In other words, the following reactions were fostered as the deposited power increased in the H_2O-containing air plasma [6,8,33,70,95].

Electron impact reactions:

$$e^- + C_6H_5CH_3 \rightarrow \text{Intermediate byproducts} + e^- \quad \text{R5.1}$$

Oxidation by radicals:

$$e^- + O_2 \rightarrow 2O + e^- \quad \text{R5.2}$$

$$O + O_2 \rightarrow O_3 \quad \text{R5.3}$$

$$e^- + H_2O \rightarrow H + OH + e^- \quad \text{R5.4}$$

$$e^- + O_2 \rightarrow O(^1D) + O(^3P) + e^- \quad \text{R5.5}$$

$$O(^1D) + H_2O \rightarrow 2OH \quad \text{R5.6}$$

$$O_3 + H_2O \rightarrow 2OH + O_2 \quad \text{R5.7}$$

$$OH + C_6H_5CH_3 \rightarrow \text{Intermediate byproducts} + H_2O \quad \text{R5.8}$$

$$O + C_6H_5CH_3 \rightarrow \text{Intermediate byproducts} \quad \text{R5.9}$$

Excited-molecule reactions:

$$N_2(A) + C_6H_5CH_3 \rightarrow \text{Intermediate byproducts} + N_2 \quad \text{R5.10}$$

Ion-molecule reactions:

$$O_2^+ + C_6H_5CH_3 \rightarrow \text{Intermediate byproducts} + O_2 \quad \text{R5.11}$$

$$N_4^+ + C_6H_5CH_3 \rightarrow \text{Intermediate byproducts} + 2N_2 \quad \text{R5.12}$$

On the contrary, the toluene decomposition rate dropped considerably with increasing gas flow rates at all set applied voltages, from 78% at 50 L/min down to 13% at 1000 L/min at the set applied voltage of 22 kV, as plotted in Figure 5.2(a) and (c). This can be ascribed to the rapidly decreasing residence time from 0.48s at 50 L/min down to 0.0238s at 1000 L/min, resulting in a lowered probability of collisions between the toluene molecules, energetic electrons, and reactive species in the plasma zone, as presented in Figure 5.3(a); In addition, the number of discharge cycles (i.e., the number of plasma discharges that occur during the residence time in the discharge zone) decreased significantly as the flow rate increased, from 24 at 50 L/min down to 1.19 at 1000 L/min, suggesting a partial plasma discharge occurring at each layer; This resulted in an extremely insufficient production of energetic electrons and active species for the decomposition of toluene molecules per unit volume in the discharge zone, as indicated by the rapidly decreasing ozone concentration in Figure 5.3(b) [24,76]. Here, it is noteworthy that a decomposition rate of 55.3% at 245 L/min, 22 kV was achieved in the ten-layer DBD reactor (400 cm^3), which is comparable to that of 59.5% at 110 L/min, 21.5 kV in the two-layer reactor case (180 cm^3), as the former possessed approximately twice as large discharge space, as reported in our previous study [81]; This finding further validated the rationality and effectiveness of the design scheme based on the results of the large-flow DBD reactors studied in our previous study. Furthermore, these findings may largely explain the poor toluene degradation performance in the larger range of gas flow rates and also suggest that a high-frequency power supply is required to ensure

sufficient discharge cycles per second per unit volume, thereby facilitating a full plasma discharge in the discharge zone.

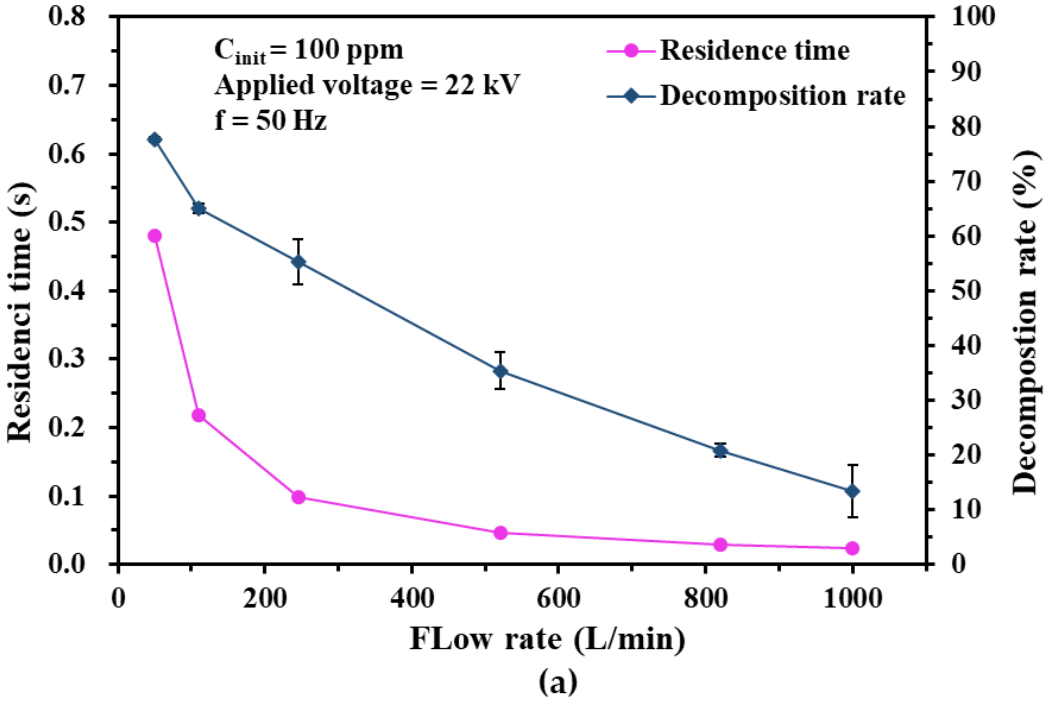

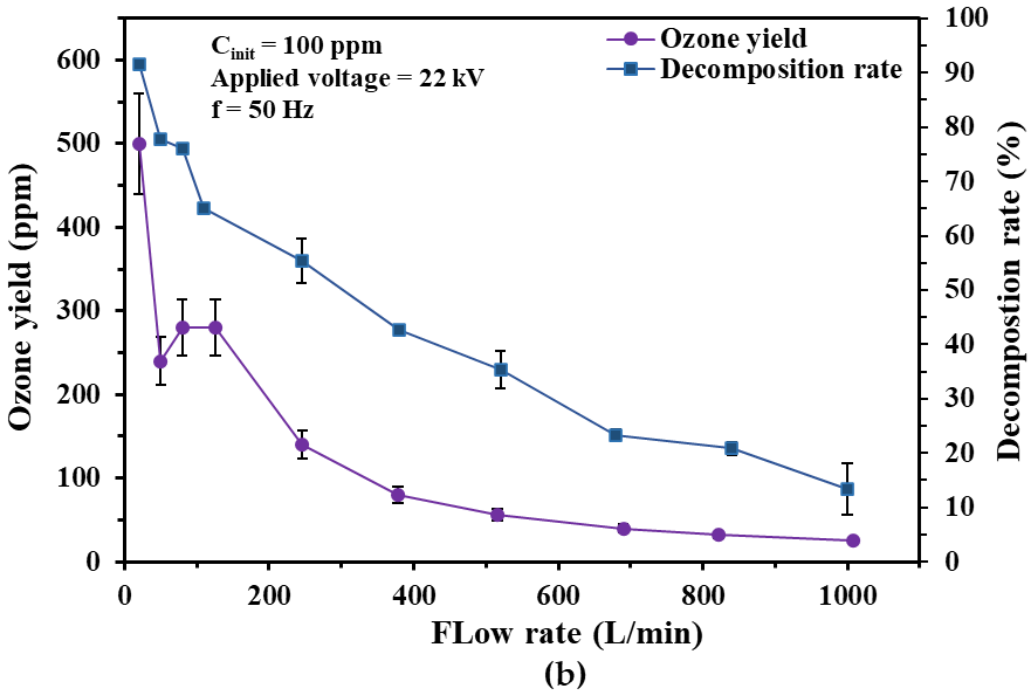

Figure 5.3. (a) Residence time and decomposition rate, (b) ozone yield and decomposition rate plotted as a function of flow rate in the ten -layer DBD reactor at 22 kV.

However, as the applied voltage increased, the corresponding energy efficiency exhibited completely opposite behavior in the lower and higher range of gas flow rates. In the lower range of flow rates (50 to 110 L/min), the corresponding energy efficiency declined from 19.9 g/kWh to 9.0 g/kWh and 27.9 g/kWh to 18.5 g/kWh, at 50 L/min, 110 L/min, respectively, as presented in Figure 5.2(b). This is probably due to the fact that full plasma discharge was ensured with sufficient discharge cycles (24 at 50 L/min, 10.91 at 110 L/min) at lower flow rates, at 16 kV; thus, excess energy deposited into the ten-layer DBD reactor caused by the increased applied voltage was not fully utilized for toluene degradation, resulting in decreased energy efficiency.

Whereas, in the mid-range of flow rates (245 to 520 L/min), the corresponding energy efficiency first decreased from 41.2 g/kWh to 31.3 g/kWh, then increased to about 36.3 g/kWh for the 245 L/min case, while it decreased from 69.5 g/kWh to 38.8 g/kWh, then increased to 48.3 for the 520 L/min case, with the applied voltage increasing from 16 kV to 22 kV. This may be due to the fact that full plasma discharge was also ensured with sufficient discharge cycles (4.9 at 245 L/min, 2.31 at 520 L/min) at mid-range flow rates, excess power deposition could not contribute to a significantly higher decomposition rate at 16-19 kV. However, as the applied voltage continued to increase, a higher decomposition rate was achieved, thereby mitigating the adverse effects of excess power decomposition caused by increased voltage. In the meanwhile, the corresponding energy efficiency increased from 9.0 g/kWh to 48.3 g/kWh at 22 kV, as the gas flow rate climbed from 50 L/min to 520 L/min, as shown in Figure 5.2(c). It has been reported that the larger the flow rate, the more toluene molecules (per unit discharge time) can be delivered to the plasma zone for dissociation, which in turn enhance the energy efficiency [36,79].

In contrast, in the further higher range of flow rates (up to 1000 L/min), the corresponding energy efficiency increased from 0.0 g/kWh to 44.0 g/kWh for the 840 L/min case, from 0.0 g/kWh to 35.5 g/kWh for the 1000 L/min case, with increasing the applied voltage from 16 kV to 22 kV. This phenomenon can be attributed to the fact that the adverse effect of partial discharge caused by the insufficient number of discharge cycles at larger flow rates (1.46 at 820 L/min, 1.20 at 1000 L/min) was gradually improved with the increase of applied voltage, which promoted the toluene decomposition rate and thus contributed to the increase of the corresponding energy efficiency [94,96].

On the other hand, although an increased flow rate (50 to 520 L/min) led to enhanced energy efficiency due to the increased delivery of toluene molecules to the ten-layer DBD reactor, an opposite trend was observed in the larger flow rate range (820 to 1000 L/min), with the corresponding energy efficiency decreasing from 44.0 g/kWh at 840 L/min to

35.5 g/kWh at 1000 L/min, at an applied voltage of 22 KV, as presented in Figure 5.2(c). This phenomenon may be due to the detrimental effect of the rapidly lowering decomposition rate caused by reduced residence time and discharge cycles at higher flow rates not being offset by the beneficial effect of increased toluene molecule delivery, resulting in decreased energy efficiency. This indicates that there is an upper limit to the gas flow rate at which the corresponding efficiency peaks, and for the ten-layer DBD reactor case, the upper limit was approximately at around a gas flow rate of 520 L/min. Moreover, the compromise point for balancing decomposition rate and energy efficiency was confirmed to be at 520 L/min for all metrics, with a decomposition rate of 35% and a corresponding energy efficiency of 48.3 g/kWh at 22 kV, as exhibited in Figure 5.2. In conclusion, these results provide a reasonable methodology to determine the upper processing bound of the gas flow rate for large-flow DBD reactors, enabling them to operate in the most energy-efficient manner, as energy efficiency is a key metric in industrial applications.

5.3.2. Effects of high-frequency intermittent-pulse power supply at large flow rates

In order to improve the deteriorating decomposition rate of the ten-layer DBD reactor in the higher flow rate range (i.e., ~ 1000 L/min), a high-frequency intermittent-pulse power supply (PCT-MBS-50, Plasma Concept Tokyo Inc., Tokyo, Japan) was introduced into the experimental setup described in Section 5.2 to investigate the effects of the high-frequency power supply on the degradation performance of toluene.

Table 5.1. Operational parameters of the high-frequency intermittent power supply and the pulse voltage

Operational parameter	
Mode	Successional/Intermittent
Voltage	0 ~ 20 kV
Output power	0 ~ 20 kW
Successional frequency	1 ~ 50 kHz
Intermittent frequency	100 ~ 3000 Hz
Duty cycle	0 ~ 100%
Pulse voltage	
Period	11 μs
Rise/fall time	~ 3 us

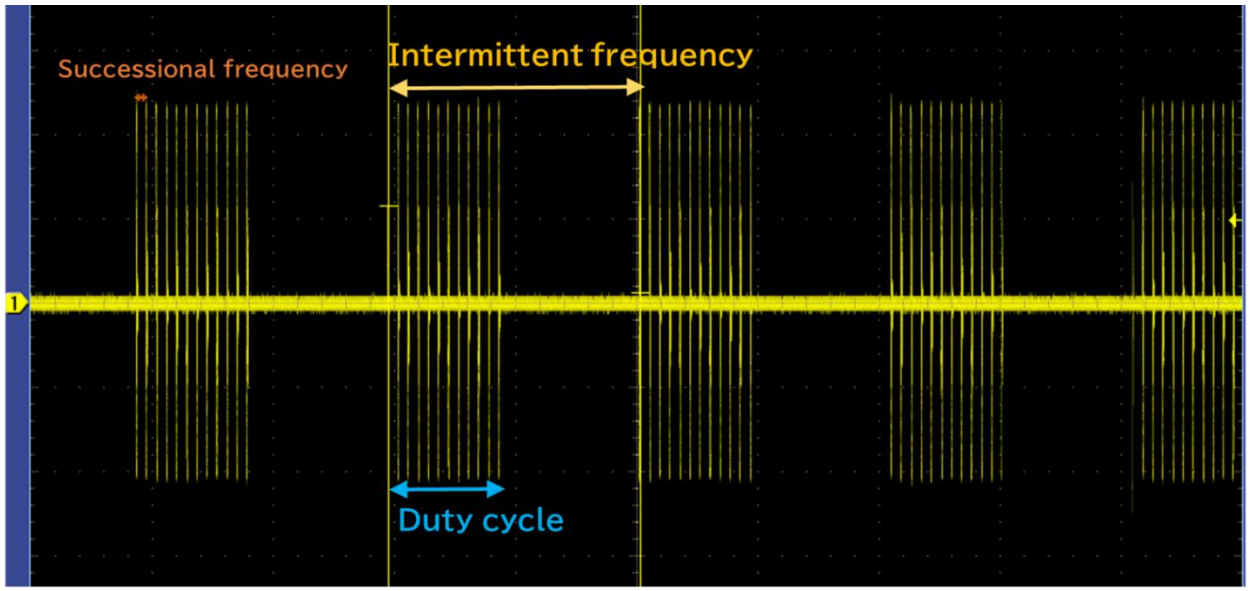

(a)

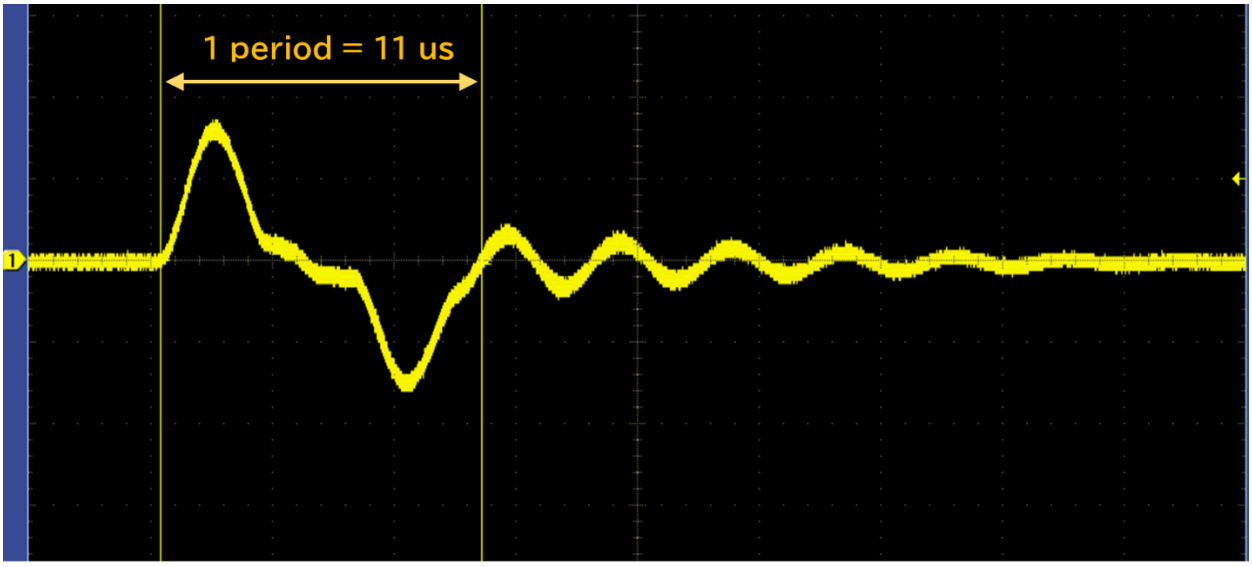

(b)

Figure 5.4. (a) Key parameters of the intermittent pulse power supply: duty cycle, successional and intermittent frequency; and (b) Typical waveform of a pulse voltage.

The operating information and the characteristics of the pulse voltage of the high-frequency power supply are presented in Table 5.1, which has two working modes: successional and intermittent mode. The first mode is determined by the successional frequency alone, while the second is dominated by 3 parameters (successional frequency, intermittent frequency, duty cycle). Figure 5.4 shows the typical waveform of the pulse

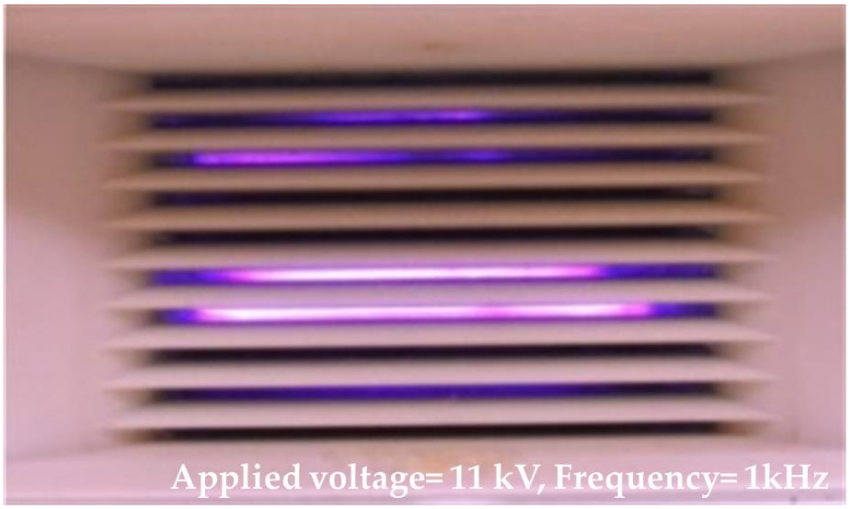
Applied voltage= 11 kV, Frequency= 1kHz

(a)

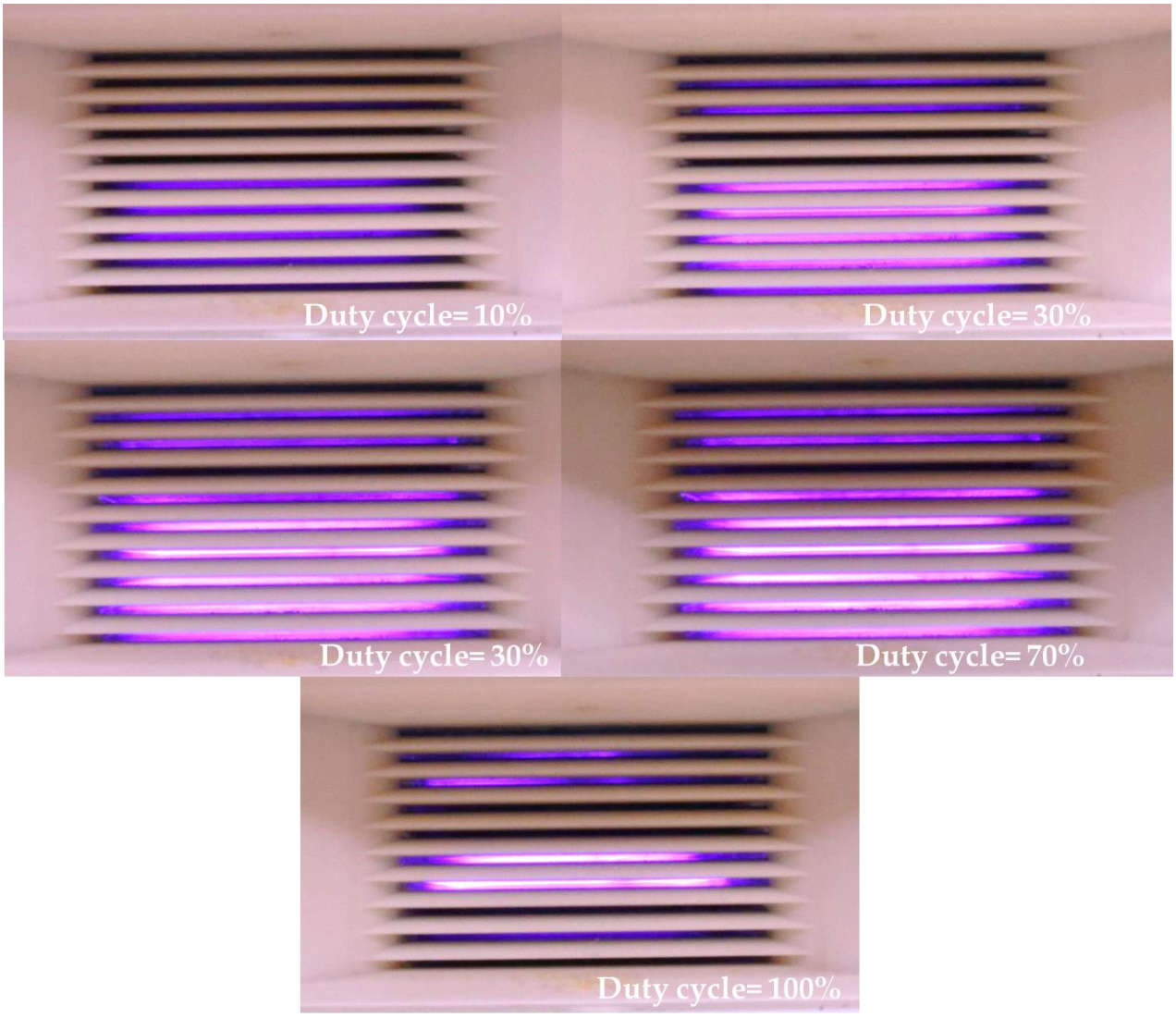
Duty cycle= 10%
Duty cycle= 30%
Duty cycle= 30%
Duty cycle= 70%
Duty cycle= 100%

(b)

Figure 5.5. (a) Plasma discharges at 1000 L/min at 11 kV and 1 kHz of successional frequency in successional mode; and (b) at 11 kV, 1 kHz of successional mode, 0.1 kHz of intermittent frequency, and duty cycle of 10 ~ 100% in intermittent mode.

voltage generated by the high-frequency power supply, whose behavior can be adjusted by the different combinations of the three parameters, while each pulse has a period of 11 us with a rise time of less than 3 us. Accordingly, the successional mode can be regarded as the intermittent mode when the duty cycle is set to 100%.

Using the high-frequency power supply, the plasma generations of the ten-layer DBD reactor were performed with the applied voltage and the gas flow rate set at 11 kV and 1000 L/min, respectively. Figure 5.5(a) exhibits the plasma generation at a successional frequency of 1 kHz in the successional mode. Obviously, only four layers at most were ignited in of the ten-layer DBD reactor, and some of the ignited layers could not even fill the whole zone of one layer. In addition, the plasma generation was also not stable, and instantaneous disappearance was observed. The same phenomenon was observed when the increased successional frequency was increased up to 10 kHz, while the number of plasma layers was maintained. These results indicate that plasma cannot be generated stably in the ten-layer reactor even at the lowest frequency of the pulse voltage power supply. This can be attributed to the extremely high capacitance of the ten-layer DBD reactor (0.699 nF), which requires a longer charge time, and was unable to follow the rapidly changing pulse voltage. Furthermore, the plasma generation was also examined in the intermittent mode at a successional frequency of 1 kHz and an intermittent frequency of 0.1 kHz, with the duty cycle ranging from 10% to 100%, where the applied voltage and air flow rate were fixed at 11 kV and 1000 L/min, respectively. As shown in Figure 5.5(b), at a duty cycle of 100%, i.e. a successional frequency of 1 kHz, only four layers partially filled with plasma were observed, whereas at a duty cycle of 10%, four layers of plasma were also generated, but fuller in each layer. In contrast, up to seven layers were generated in the 30% case. On the other hand, in the 50% and 70% cases, the plasma generation was extended to the largest number of layers, up to 8 layers. These results show that the plasma can be generated more stably with more layers in the ten-layer DBD reactor by adjusting the duty cycle compared to the successional frequency operation. It is noteworthy here that, the plasma generation displayed a random plasma generation in layers even under the totally the same experimental conditions. For example, it can be seen four layers of plasma are ignited at 2 to 5th layer from the bottom, however, the four plasma layers may change to 1-4th layer next time or other layers, less layers.

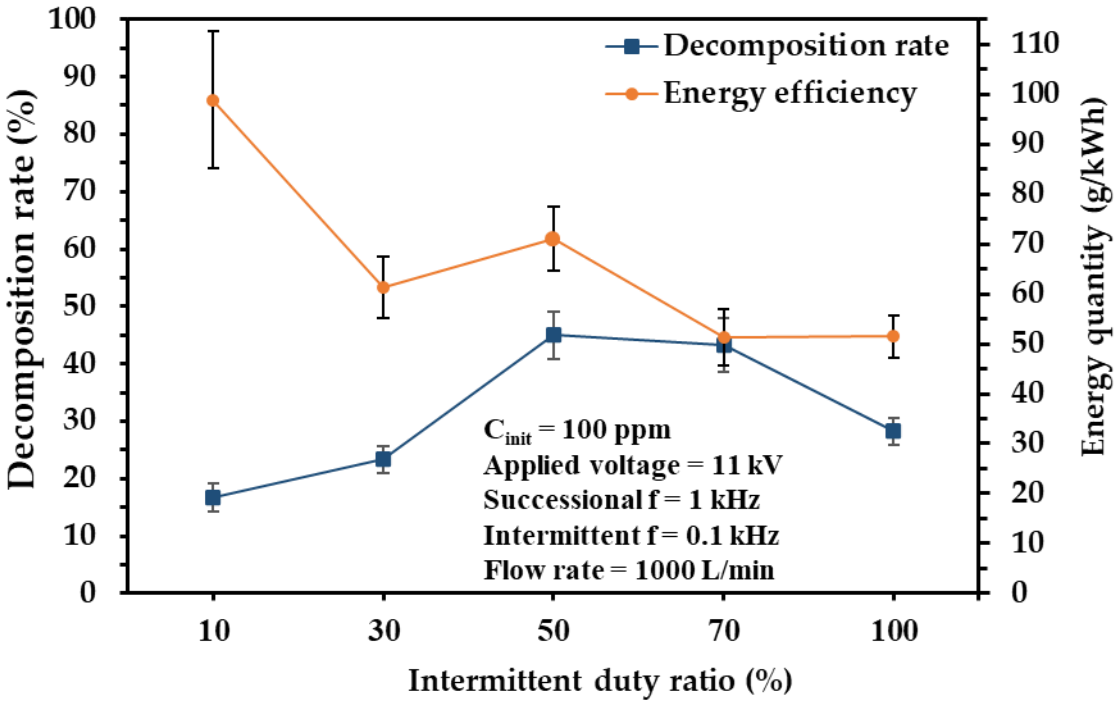
Decomposition rate
Energy efficiency
Decomposition rate (%)
Energy quantity (g/kWh)
Intermittent duty ratio (%)
C_{init} = 100 ppm
Applied voltage = 11 kV
Successional f = 1 kHz
Intermittent f = 0.1 kHz
Flow rate = 1000 L/min
0
10
20
30
40
50
60
70
80
90
100
110
10
30
50
70
100

(a)

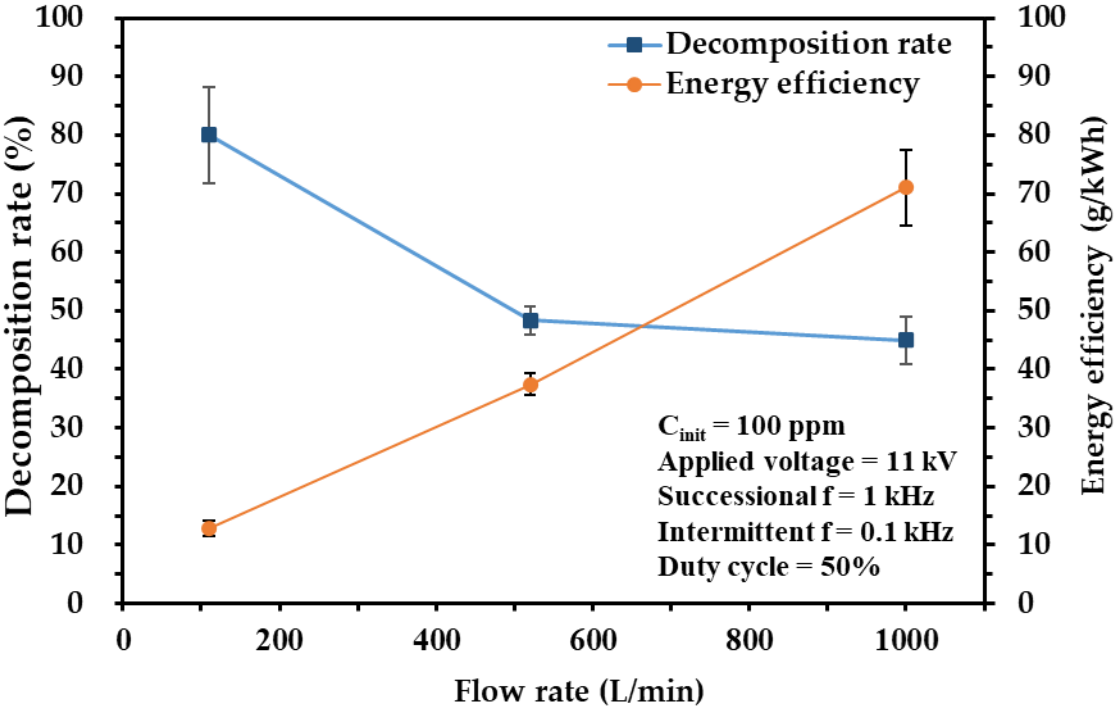
Decomposition rate
Energy efficiency
Decomposition rate (%)
Energy efficiency (g/kWh)
Flow rate (L/min)
C_{init} = 100 ppm
Applied voltage = 11 kV
Successional f = 1 kHz
Intermittent f = 0.1 kHz
Duty cycle = 50%
0
10
20
30
40
50
60
70
80
90
100
0
200
400
600
800
1000

(b)

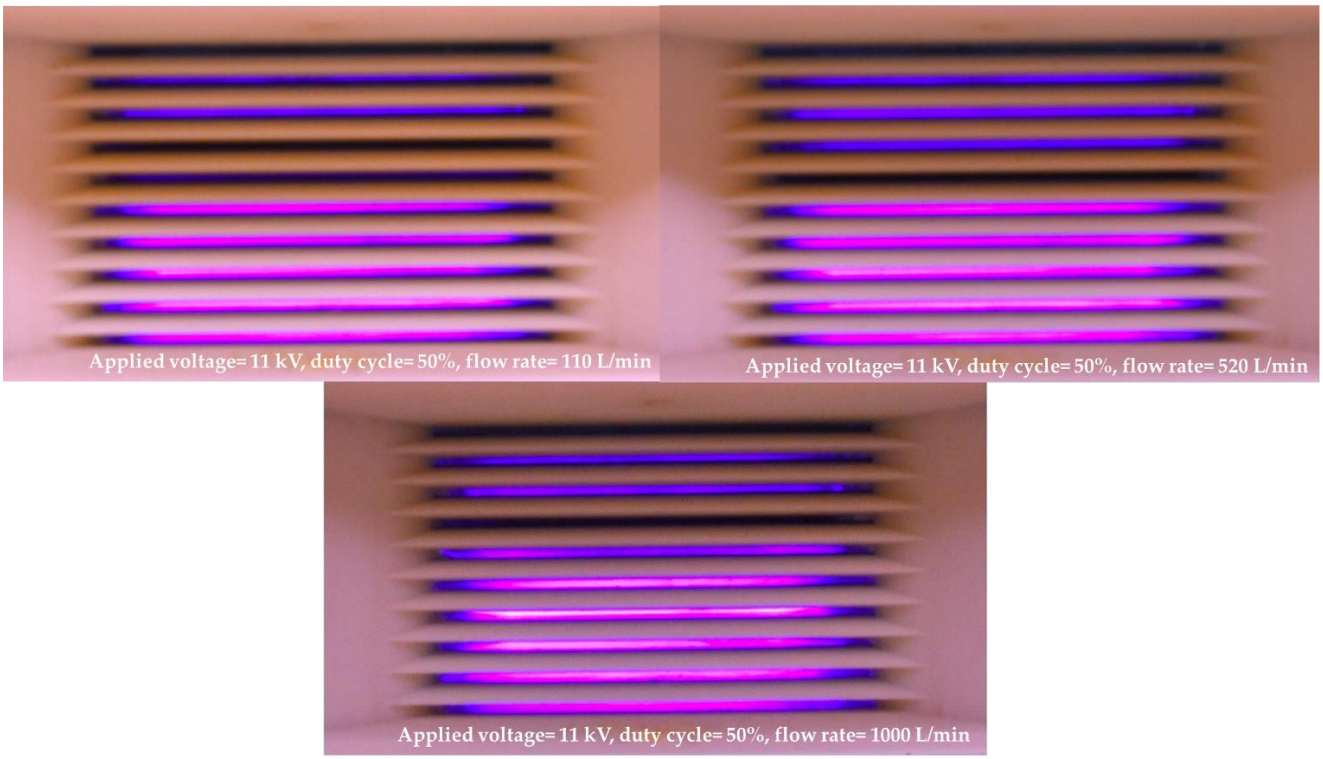

(c)

Figure 5.6. (a) Toluene decomposition rate and energy efficiency plotted as a function of flow rate; and as a function of duty cycle; (c) Plasma discharges at 11 kV, 1 kHz of successional frequency, 0.1 kHz of intermittent frequency, at flow rates of 110 ~ 1000 L/min.

In addition, degradation performance with the high-frequency power supply at large flow rates up to 1000 L/min (110−1000 L/min), decomposition characterizations were also performed on toluene-containing humidified air with an initial concentration of 100 ppm, including decomposition rate and energy efficiency. Figure 5.6 (a) shows the decomposition rate and energy efficiency plotted as a function of the duty cycle, when the applied voltage, the successional and intermittent frequency are fixed at 11 kV, 1 and 0.1 kHz, respectively. It is clear that the toluene decomposition rate increases with the increase of the duty cycle at a fixed voltage, but the energy efficiency in terms of toluene decomposition shows an opposite trend. However, the decomposition rate at the duty cycle of 50% and the energy efficiency at the 100% case deviated from the trends, which can be attributed to the extremely unstable plasma generation caused by the pulse voltage, which resulted in a large fluctuation. Nevertheless, a significant improvement in the decomposition rate (45% at 11 kV, 1 kHz successional frequency, 0.1 kHz

intermittent frequency, 50% duty cycle) was achieved compared with that when the ten-layer DBD reactor is energized by the 50 Hz sinusoidal power supply (13% at 22 kV, 50 Hz). At an applied voltage of 11 kV, the toluene decomposition increases from 17 % to 45 % as the duty cycle rises from 10 % to 50 %, but then decreases to 28% at the 100% duty cycle. Whereas the corresponding energy efficiency decreases from 98.8 to 51.5 g/kWh at the duty cycle of 100%. When the applied voltage and frequency are kept constant, a discharge at a higher duty cycle is conducive to the production of more reactive species during the pulse-on stage, including radicals and ions. During the pulse-off stage, a portion of the reactive species remains and can be used to ignite the future discharge event [97].

Figure 5.6 (b) exhibits the decomposition rate and energy efficiency plotted as a function of the gas flow rate, when the applied voltage, the successional frequency, intermittent frequency, and duty cycle are fixed at 11 kV, 1 kHz, 0.1 kHz, and 50% respectively. It can be seen that the decomposition rate decreases from 80% to 45% while the corresponding energy efficiency increases from 12.9 to 71.0 g/kWh as the flow rate increases from 110 to 1000 L/min. This is a similar phenomenon to that discussed in subsection 4.3.3. However, a different phenomenon was observed, which may be the reason why there was a significant decrease in decomposition between the flow rates of 110 and 520 L/min. As shown in Figure 5.6(c), compared to seven layers of plasma generation in the 110 L/min case, eight layers of plasma were generated in the 520 and 1000 L/min cases. This indicates that both the pulse voltage frequency and the flow rate can affect the plasma generation in the ten-layer DBD reactor, thereby changing the degradation performance in toluene decomposition.

5.4. Summary

In summary, based on the results of our previous study, an upscaled, large-flow, ten-layer DBD reactor capable of processing hundreds of L/min of gas was designed and fabricated for VOC abatement. In addition, a decomposition rate of 55% at 245 L/min and 22 kV with a corresponding energy efficiency of 36.3 g/kWh was achieved in the ten-layer DBD reactor, which was in good agreement with the single- and two-layer DBD cases, as reported in our previous study, corroborating the rationality and effectiveness of the design scheme of multilayer for DBD reactor configurations [81]. Moreover, a decomposition rate of 35% at 22 kV with a corresponding energy efficiency of 48.3 g/kWh was achieved at a significantly high flow rate of 520 L/min, which meets the Acute Exposure Guideline Level (AEGL 1: 67 ppm) for toluene established by the National Institute of Health Sciences (NIHS) in Japan [98].

In addition, the plasma generation and degradation performance in toluene decomposition were also investigated using the ten-layer DBD reactor energized by a high-frequency power supply. In particular, a decomposition rate of 80% at 110 L/min and 45% at 1000 L/min was achieved, even though only seven or eight layers of plasma were ignited, at 11 kV applied voltage, 1 kHz continuous frequency, 0.1 kHz intermittent frequency, and 50% duty cycle. This is much higher than the 13% at 22 kHz and 1000 L/min, when energized by the 50 Hz sinusoidal power supply. Nevertheless, the partial and unstable plasma generation caused by the high-frequency intermittent-pulse power supply is still a major problem that requires further investigation and optimization.

Whereas, at the targeted flow rate of 1000 L/min, only a decomposition rate of 13 % was observed. Nevertheless, there are still promising tactics that can be taken to realize practical applications in industry. First, as mentioned above, high-frequency power supply has great potential to ensure sufficient discharge cycles, thereby improving the decomposition rate at the thousand-level flow rates. Moreover, the introduction of catalysts into the plasma zones to facilitate the synergistic effect (e.g., SMF, Cu, Ag/ TiO_2, Fe_2O_3/MnO, etc.) is another effective approach to increase the decomposition rate, as reported in numerous studies [40,67,69]. Therefore, these two approaches as such are planned actions to refine the performance of the ten-layer DBD reactors in the future. Further on, post-treatment product analysis for environmental risk assessment, degradation studies on several VOCs and their mixtures, studies and improvements on CO_2 mineralization after toluene treatment, etc. are still issues to be addressed for further refinement of large flow DBD reactors, which are also planned for future works.

Chapter 6 Overall summary

6.1. Overall summary of this dissertation

Volatile organic compounds (VOCs), which comprise a staple of air pollutants, are emitted in various industrial sectors. To counteract this, non-thermal plasma (NTP) technology, especially dielectric barrier discharge (DBD) plasma-based systems, has emerged as a promising option for the abatement due to its effective degradation of air pollutants through reactions with abundant high energy electrons and reactive species (e.g., in humidified air-driven plasma, reactive oxygen species: O, O_2^-, O_3 and OH, and reactive nitrogen species including NO and NO_2) at temperatures as low as room temperature, and simple configuration, which also makes it a cost-effective solution compared to other conventional technologies. However, as reviewed in the first part of the dissertation (Chapters 1 and 3), almost all these efforts have been concentrated at the laboratory scale with small flow rates, and the processing capacity has been limited to low gas flow rates (less than a few L/min). Moreover, all the characterizations and optimizations (e.g., configuration, geometric features, catalyst incorporation, etc.) have also been performed at the laboratory scale, which is far from practical industrial applications. Therefore, there is a high demand for large flow DBD systems and investigations of their fundamental properties for VOC degradation at large flow rates, which are more practical in the real-world applications such as building ventilation, industrial effluents, etc.

To address this issue, this dissertation was focused on the development of large-flow plasma sources based on DBD. Three types of large-flow, scalable DBD reactors (i.e., single- and two-layer DBD reactors in the first phase; and ten-layer DBD reactor in the second phase of this dissertation) have been successfully developed to investigate the fundamental properties and decomposition characteristics of VOCs at large flow rates. Meanwhile, the feasibility and superiority of the multilayer configuration for the large-flow DBD reactors (intended for use in VOC abatement) were verified by comparing the degradation performance of the single-layer and two-layer reactors. In addition, in the development of the ten-layer DBD reactor, the flow path was optimized using a simulation tool and empirical measurements, and uniform, stable plasma generation was achieved in each layer at large flow rates. This provides an effective methodology for the development of upscaled DBD reactors with processing capacities of up to 1000 L/min. As a result of these efforts, the following major accomplishments have been achieved:

In the first phase (Chapter 3):

Two types of large-flow DBD reactors, specifically single- and two-layer DBD reactors have been developed. These reactors can treat exhaust gases at flow rates that are two orders of magnitude greater (up to 110 L/min) compared to those of small-flow DBD reactors, which are typically limited to 1 L/min or lower. Additionally, they achieved a high decomposition rate of 59.5% on toluene with an initial concentration of 100 ppm when a power of 41 W was applied in the two-layer case.

Using the two reactors, the degradation performance of toluene treatment was analyzed in large-flow scales (10-110 L/min), including the decomposition rate and energy efficiency at different processing parameters. By comparing the degradation performances of the two reactors, the feasibility and superiority of the multilayer configuration in the large-flow DBD reactors (intended for use in VOC abatement) have been verified.

Furthermore, the experimental results revealed that the performances of large-flow DBD in toluene degradation displayed characteristics similar to those of small-flow DBD reactors on the lab scale. For example, increasing the gas flow velocity and rate has a negative effect on the decomposition rate; however, while it is favorable for energy efficiency. These findings indicate the feasibility of large-flow plasma generation, which has not been reported in other previous studies.

Further on in the second phase (Chapters 4 and 5):

Based on the above findings, an upscaled multilayer reactor, namely large-flow, ten-layer DBD reactor with a processing capacity of up to 1000 L/min was designed and fabricated, serving as an upgraded version of the single- and two-layer DBD reactors in the first phase.

The flow path design of the ten-layer DBD reactor has been validated and optimized via CFD simulations and empirical measurements. This has realized stable and uniform plasma generation in each layer at large flow rates (up to 1000 L/min). Moreover, multi-gas plasma generation involving various gases such as Air, Ar, He, N_2, O_2, and CO_2 has also been achieved with the ten-layer DBD reactor, which is expected to inspire various potential applications.

Following the fundamental characterizations, the decomposition characteristics of toluene treatment at large flow rates (50–1000 L/min), a decomposition rate of 55% at 245 L/min and 22 kV with a corresponding energy efficiency of 36.3 g/kWh was achieved in the ten-layer DBD reactor, which was in good agreement with the single- and two-layer DBD cases, corroborating the rationality and effectiveness of the design scheme of multilayer for DBD reactor configurations.

Moreover, a decomposition rate of 35% at 22 kV with a corresponding energy efficiency of 48.3 g/kWh was achieved at a significantly high flow rate of 520 L/min, which meets the Acute Exposure Guideline Level (AEGL 1: 67 ppm) for toluene established by the National Institute of Health Sciences (NIHS) in Japan.

Thus, these findings and the proposed design methodology for developing large-flow DBD reactors, including CFD simulations, flow path optimization via practical and OES measurements, and electrical, spectroscopic, and VOC decomposition characterizations, provide fundamental data and present guidelines for the implementation of the DBD plasma-based system as a solution for volatile organic compound abatement.

6.2. Future works

Although the main objective of this study: the development of an upscaled large flow DBD reactor aimed at 1000 L/min-class gas flow treatment for VOC abatement has been achieved to a large extent, it's still far from practical applications due to multiple technical issues to be solved and investigated. Notably, although high decomposition rates of 55% at 245 L/min and 35% were observed for toluene with an initial concentration of 100 ppm at an applied voltage of 22 kV, only a decomposition rate of 13% was observed at the target flow rate of 1000 L/min. Furthermore, CO_2 selectivity is another key metric describing the degree of mineralization, which has not been investigated in this dissertation, to evaluate the performance of DBD reactors in terms of environmental risk assessment. Therefore, a few further investigation areas are recommended, in view of the main findings of this study, including:

Most of all, a high-frequency power supply has great potential to ensure sufficient discharge cycles, thereby improving the decomposition rate at the thousand-level flow rates.

Moreover, the introduction of catalysts into the plasma zones to facilitate the synergistic effect (e.g., Cu, Ag/ TiO_2, Fe_2O_3/MnO, etc.) is another effective approach to increase the decomposition rate as well as CO_2 selectivity, as reported in numerous studies [40,67,69]. For this purpose, many configurations are suitable for this purpose, including catalyst-coated electrodes, packed-bed configurations, and catalytic monoliths.

On the other hand, in order to deal with the wide spectrum of VOCs or air pollutants, whose occurrence and concentration depend on many factors and rapidly change over time, more attention should be paid to the investigations for understanding the chemical reactions and mechanism of the decomposition for multiple VOC mixtures in a DBD system. Although numerous research has been carried out to establish decomposition processes of VOC compounds, most deal with single compound only, including the case

in this study.

Further on, post-treatment product analysis (by e.g., FTIR, chromatography, gas chromatography-mass spectrometry) of gaseous and solid emissions for environmental risk assessment to avoid secondary harmful pollutants is also required to ensure sufficient safety for human health and the environment to meet the increasingly stringent environmental regulations.

Therefore, these approaches as such are planned to further refine the performance of the large-flow DBD-based systems in the future.

Acknowledgements

First of all, I would like to thank my advisor, Prof. Akitoshi Okino, who has shared with me these 3 years of graduate school, the good and the not so good moments. I sincerely thank him for the countless great discussions we had over the years, for always having faith in my abilities and knowledge, and for instilling in all of his students his ever-present enthusiasm for atmospheric low-temperature plasma science and engineering. In addition, his guidance, encouragement, and vibrant, excellent lab have been invaluable in helping me to move forward in this field and eventually complete my studies during my Ph.D. program.

I would also like to thank Prof. Tianzhuo Zhan, who welcomed me into his group at Toyo University for a long time. I will always be grateful for his generosity and mentorship and for giving me the opportunity to work in such a great research environment related to thermal management in ICs. At the same time, I would also like to thank Prof. Kentaro Nakamura, Prof. Marie Tabaru, Prof. Takashi Tokuda, and Prof. Takeharu Tsuge for taking the time to review my dissertation, attending my dissertation defense, and providing valuable feedback.

Next, I would like to thank my co-workers in or out of our lab: Mr. Zhizhi Liu, Yohei Fukuyama, Yuki Sumiya, Motoaki Yamauchi, affiliated with Tokyo Tech, and Zhi Cao affiliated with Toyo University, for all the help and support along the way in our various research projects. Much of the work associated with the projects would not have been possible without the generous assistance of these excellent members.

Our elegant lab secretary, Mrs. Natsuko Murakami, has always graciously helped me with the paperwork related to a variety of lab events, such as travel to academic conferences, expense reimbursements, and so on to make the student's lives so much easier. I would like to thank her for all her kind and immeasurable assistance. Of course, my thanks also go to the other members of our laboratory; Asst. Prof. Akane Yaida and Mr. Kenichi Yamazaki have given me many constructive suggestions not only for my research but also for my career; Lab leaders: Mr. Taiki Osawa and Mr. Yuya Shimizu have been very kind to help me with lab affairs and equipment operation. Not only that, Mr. Fang Yuan, Sho Yoshida, Kai Fukuchi and other fellow students of the master's and bachelor's program have been so kind to me and gave me so many happy memories.

There are many other people who have contributed to my development at Tokyo Tech. I am grateful for the many psychological and physical supports that they've given to me, which made me feel very fortunate to be there. Last but not least, I would like to thank

my family and my Goddess, who have always been my greatest psychological and emotional anchors and whose warm words continue to warm my heart.

Finally, I am grateful to all the people who deserve my appreciation and without whom around me I could not imagine that this whole experience during my graduate school could move forward so well over the years. Thank you all.

This study was supported in part by JST SPRING, grant number JPMJSP2106, and by the Cooperative Research Project of the Research Center for Biomedical Engineering.

Bibliography

1. Ibrahim, J.; Al-Bataineh, S. A.; Michelmore, A.; Whittle, J. D., Atmospheric Pressure Dielectric Barrier Discharges for the Deposition of Organic Plasma Polymer Coatings for Biomedical Application. *Plasma Chem. Plasma Process.* **2021**, *41*, DOI: 10.1007/s11090-020-10135-6.
2. Nonthermal Plasma, DOI: 10.1016/B978-0-12-815004-7.00003-2https://www.sciencedirect.com/topics/agricultural-and-biological-sciences/nonthermal-plasma (last time accessed: November 26, 2023).
3. Holubová, Ľ.; Kyzek, S.; Ďurovcová, I.; Fabová, J.; Horváthová, E.; Ševčovičová, A.; Gálová, E., Non-Thermal Plasma-A New Green Priming Agent for Plants? *Int. J. Mol. Sci.* **2020**, *21*, DOI: 10.3390/ijms21249466.
4. Song, M. Y.; Chun, H., Species and characteristics of volatile organic compounds emitted from an auto-repair painting workshop. *Sci. Rep.* **2021**, *11*, 16586.
5. Stockwell, C. E.; Coggon, M. M.; Gkatzelis, G. I.; Ortega, J.; McDonald, B. C.; Peischl, J.; Aikin, K.; Gilman, J. B.; Trainer, M.; Warneke, C., Volatile organic compound emissions from solvent- and water-borne coatings – compositional differences and tracer compound identifications. *Atmos. Chem. Phys.* **2021**, *21*, 6005–6022.
6. Lu, W.; Abbas, Y.; Mustafa, M. F.; Pan, C.; Wang, H., A review on application of dielectric barrier discharge plasma technology on the abatement of volatile organic compounds. *Front. Environ. Sci. Eng. China* **2019**, *13*, 30.
7. Guo, Y.; Ye, D.; Chen, K.; He, J., Toluene removal by a DBD-type plasma combined with metal oxides catalysts supported by nickel foam. *Catal. Today* **2007**, *126*, 328–337.
8. Abdelaziz, A. A.; Ishijima, T.; Seto, T., Humidity effects on surface dielectric barrier discharge for gaseous naphthalene decomposition. *Phys. Plasmas* **2018**, *25*, 043512.
9. Liang, P.; Jiang, W.; Zhang, L.; Wu, J.; Zhang, J.; Yang, D., Experimental studies of removing typical VOCs by dielectric barrier discharge reactor of different sizes. *Process Saf. Environ. Prot.* **2015**, *94*, 380–384.
10. Blin-Simiand, N.; Jorand, F.; Magne, L.; Pasquiers, S.; Postel, C.; Vacher, J.-R., Plasma Reactivity and Plasma-Surface Interactions During Treatment of Toluene by a Dielectric Barrier Discharge. *Plasma Chem. Plasma Process.* **2008**, *28*, 429–466.
11. Saleem, F.; Rehman, A.; Ahmad, F.; Khoja, A. H.; Javed, F.; Zhang, K.; Harvey, A., Removal of toluene as a toxic VOC from methane gas using a non-thermal plasma dielectric barrier discharge reactor. *RSC Adv.* **2021**, *11*, 27583–27588.
12. Iwai, T.; Inoue, H.; Kakegawa, K.; Ohrui, Y.; Nagoya, T.; Nagashima, H.; Miyahara, H.; Chiba, K.; Seto, Y.; Okino, A., Development of a High-Efficiency Decomposition Technology for Volatile Chemical Warfare Agent Sarin Using Dielectric Barrier Discharge. *Plasma Chem. Plasma Process.* **2020**, *40*, 907–920.
13. Lu, X.; Naidis, G. V.; Laroussi, M.; Reuter, S.; Graves, D. B.; Ostrikov, K., Reactive species in non-equilibrium atmospheric-pressure plasmas: Generation, transport, and biological effects. *Phys. Rep.* **2016**, *630*, 1–84.

14. Laroussi, M., Low temperature plasma-based sterilization: Overview and state-of-the-art. *Plasma Process. Polym.* **2005**, *2*, 391–400.
15. Suenaga, Y.; Takamatsu, T.; Aizawa, T.; Moriya, S.; Matsumura, Y.; Iwasawa, A.; Okino, A., Plasma Gas Temperature Control Performance of Metal 3D-Printed Multi-Gas Temperature-Controllable Plasma Jet. *NATO Adv. Sci. Inst. Ser. E Appl. Sci.* **2021**, *11*, 11686.
16. Suenaga, Y.; Kawano, H.; Takamatsu, T.; Matsumura, Y.; Ito, N.; Iwasawa, A.; Okino, A., Ultrasonic-Combined Plasma Bubbling for Adherent Bacteria Disinfection on Medical Equipment. *Plasma Chem. Plasma Process.* **2022**, *42*, 575–586.
17. Aida, M.; Iwai, T.; Okamoto, Y.; Miyahara, H.; Seto, Y.; Okino, A., Development of an ionization method using hydrogenated plasma for mass analysis of surface adhesive compounds. *J. Anal. At. Spectrom.* **2018**, *33*, 578–584.
18. Černáková, L.; Kováčik, D.; Zahoranová, A.; Černák, M.; Mazúr, M., Surface Modification of Polypropylene Non-Woven Fabrics by Atmospheric-Pressure Plasma Activation Followed by Acrylic Acid Grafting. *Plasma Chem. Plasma Process.* **2005**, *25*, 427–437.
19. Suenaga, Y.; Takamatsu, T.; Aizawa, T.; Moriya, S.; Matsumura, Y.; Iwasawa, A.; Okino, A., Influence of Controlling Plasma Gas Species and Temperature on Reactive Species and Bactericidal Effect of the Plasma. *NATO Adv. Sci. Inst. Ser. E Appl. Sci.* **2021**, *11*, 11674.
20. Montero-Montoya, R.; López-Vargas, R.; Arellano-Aguilar, O., Volatile Organic Compounds in Air: Sources, Distribution, Exposure and Associated Illnesses in Children. *Ann Glob Health* **2018**, *84*, 225–238.
21. Wang, J.; Cheng, S.; Liu, N.; Lu, N.; Shang, K.; Jiang, N.; Li, J.; Wu, Y., Degradation of toluene by tube-tube coaxial dielectric barrier discharge: power characteristics and power factor optimization. *Environ. Technol.* **2021**, 1–14.
22. Kogelschatz, U., Dielectric-barrier discharges: their history, discharge physics, and industrial applications. *Plasma Chem. Plasma Process.* **2003**, *23*, 1–46.
23. Pemen, A. J. M.; Chirumamilla, V. R.; Beckers, F. J. C. M.; Hoeben, W. F. L. M.; Huiskamp, T., An SDBD Plasma-Catalytic System for On-Demand Air Purification. *IEEE Trans. Plasma Sci. IEEE Nucl. Plasma Sci. Soc.* **2018**, *46*, 4078–4090.
24. Schiavon, M.; Torretta, V.; Casazza, A.; Ragazzi, M., Non-thermal Plasma as an Innovative Option for the Abatement of Volatile Organic Compounds: a Review. *Water Air Soil Pollut. Focus* **2017**, *228*, 388.
25. Manley, T. C., The Electric Characteristics of the Ozonator Discharge. *Trans. Electrochem. Soc.* **1943**, *84*, 83.
26. Francke, K.-P.; Rudolph, R.; Miessner, H., Design and Operating Characteristics of a Simple and Reliable DBD Reactor for Use with Atmospheric Air. *Plasma Chem. Plasma Process.* **2003**, *23*, 47–57.
27. Tu, X.; Gallon, H. J.; Twigg, M. V.; Gorry, P. A.; Christopher Whitehead, J., Dry reforming of methane over a Ni/Al2O3 catalyst in a coaxial dielectric barrier discharge reactor. *J. Phys. D Appl. Phys.* **2011**, *44*, 274007.

28. Pipa, A. V.; Koskulics, J.; Brandenburg, R.; Hoder, T., The simplest equivalent circuit of a pulsed dielectric barrier discharge and the determination of the gas gap charge transfer. *Rev. Sci. Instrum.* **2012**, *83*, 115112.
29. Pipa, A. V.; Hoder, T.; Koskulics, J.; Schmidt, M.; Brandenburg, R., Experimental determination of dielectric barrier discharge capacitance. *Rev. Sci. Instrum.* **2012**, *83*, 075111.
30. Wagner, H.-E.; Brandenburg, R.; Kozlov, K. V.; Sonnenfeld, A.; Michel, P.; Behnke, J. F., The barrier discharge: basic properties and applications to surface treatment. *Vacuum* **2003**, *71*, 417–436.
31. Atkinson, R., Atmospheric chemistry of VOCs and NOx. *Atmos. Environ.* **2000**, *34*, 2063–2101.
32. Leung, D. Y. C., Outdoor-indoor air pollution in urban environment: challenges and opportunity. *Front. Environ. Sci. Eng. China* **2015**, *2*, DOI: 10.3389/fenvs.2014.00069.
33. Vandenbroucke, A. M.; Morent, R.; De Geyter, N.; Leys, C., Non-thermal plasmas for non-catalytic and catalytic VOC abatement. *J. Hazard. Mater.* **2011**, *195*, 30–54.
34. González-Martín, J.; Kraakman, N. J. R.; Pérez, C.; Lebrero, R.; Muñoz, R., A state-of-the-art review on indoor air pollution and strategies for indoor air pollution control. *Chemosphere* **2021**, *262*, 128376.
35. Khan, F. I.; Kr. Ghoshal, A., Removal of Volatile Organic Compounds from polluted air. *J. Loss Prev. Process Indust.* **2000**, *13*, 527–545.
36. Jiang, N.; Zhao, Y.; Shang, K.; Lu, N.; Li, J.; Wu, Y., Degradation of toluene by pulse-modulated multistage DBD plasma: Key parameters optimization through response surface methodology (RSM) and degradation pathway analysis. *J. Hazard. Mater.* **2020**, *393*, 122365.
37. Magureanu, M.; Mandache, N. B.; Parvulescu, V. I.; Subrahmanyam, C.; Renken, A.; Kiwi-Minsker, L., Improved performance of non-thermal plasma reactor during decomposition of trichloroethylene: Optimization of the reactor geometry and introduction of catalytic electrode. *Appl. Catal. B* **2007**, *74*, 270–277.
38. Zhang, H.; Li, K.; Sun, T.; Jia, J.; Wang, G., The combination effect of dielectric barrier discharge (DBD) and TiO2 catalytic process on styrene removal and the analysis of the by-products and intermediates. *Res. Chem. Intermed.* **2013**, *41*, DOI: 10.1007/s11164-013-1180-6.
39. Guo, Y.; Liao, X.; He, J.; Ou, W.; Ye, D., Effect of manganese oxide catalyst on the dielectric barrier discharge decomposition of toluene. *Catal. Today* **2010**, *153*, 176–183.
40. Subrahmanyam, C.; Renken, A.; Kiwi-Minsker, L., Catalytic non-thermal plasma reactor for abatement of toluene. *Chem. Eng. J.* **2010**, *160*, 677–682.
41. Raju, B. R.; Reddy, E. L.; Karuppiah, J.; Reddy, P. M. K.; Subrahmanyam, C., Catalytic non-thermal plasma reactor for the decomposition of a mixture of volatile organic compounds. *J. Chem. Sci.* **2013**, *125*, 673–678.
42. Zhang, H.; Li, K.; Sun, T.; Jia, J.; Lou, Z.; Feng, L., Removal of styrene using dielectric barrier discharge plasmas combined with sol–gel prepared TiO2 coated γ-Al2O3. *Chem. Eng. J.* **2014**, *Complete*, 92–102.

43. Mei, D.; Tu, X., Conversion of CO2 in a cylindrical dielectric barrier discharge reactor: Effects of plasma processing parameters and reactor design. *Journal of CO2 Utilization* **2017**, *19*, 68–78.
44. Karuppiah, J.; Manoj Kumar Reddy, P.; Linga Reddy, E.; Subrahmanyam, C., Catalytic non-thermal plasma reactor for decomposition of dilute chlorobenzene. *Plasma Process. Polym.* **2013**, *10*, 1074–1080.
45. Ma, T. J.; Lan, W. S., Ethylene decomposition with a wire-plate dielectric barrier discharge reactor: parameters and kinetic study. *Int. J. Environ. Sci. Technol.* **2015**, *12*, 3951–3956.
46. Ashford, B.; Tu, X., Non-thermal plasma technology for the conversion of CO2. *Current Opinion in Green and Sustainable Chemistry* **2017**, *3*, 45–49.
47. Wang, C.; Zhang, G.; Wang, X., Comparisons of discharge characteristics of a dielectric barrier discharge with different electrode structures. *Vacuum* **2012**, *86*, 960–964.
48. Byeon, J. H.; Park, J. H.; Jo, Y. S.; Yoon, K. Y.; Hwang, J., Removal of gaseous toluene and submicron aerosol particles using a dielectric barrier discharge reactor. *J. Hazard. Mater.* **2010**, *175*, 417–422.
49. Huang, H.; Ye, D.; Guan, X., The simultaneous catalytic removal of VOCs and O3 in a post-plasma. *Catal. Today* **2008**, *139*, 43–48.
50. Kundu, S. K.; Kennedy, E. M.; Gaikwad, V. V.; Molloy, T. S.; Dlugogorski, B. Z., Experimental investigation of alumina and quartz as dielectrics for a cylindrical double dielectric barrier discharge reactor in argon diluted methane plasma. *Chem. Eng. J.* **2012**, *180*, 178–189.
51. Abedi, K.; Ghorbani-Shahna, F.; Jaleh, B.; Bahrami, A.; Yarahmadi, R., Enhanced performance of non-thermal plasma coupled with TiO2/GAC for decomposition of chlorinated organic compounds: influence of a hydrogen-rich substance. *Journal of Environmental Health Science and Engineering* **2014**, *12*, 119.
52. Zhu, T.; Li, R. R.; Ma, M. F.; Li, X., Influence of energy efficiency on VOCs decomposition in non-thermal plasma reactor. *Int. J. Environ. Sci. Technol.* **2017**, *14*, 1505–1512.
53. Ye, Z.; Zhang, Y.; Li, P.; Yang, L.; Zhang, R.; Hou, H., Feasibility of destruction of gaseous benzene with dielectric barrier discharge. *J. Hazard. Mater.* **2008**, *156*, 356–364.
54. Li, Y.; Fan, Z.; Shi, J.; Liu, Z.; Shangguan, W., Post plasma-catalysis for VOCs degradation over different phase structure MnO2 catalysts. *Chem. Eng. J.* **2014**, *241*, 251–258.
55. Abd Allah, Z.; Whitehead, J. C.; Martin, P., Remediation of Dichloromethane (CH2Cl2) Using Non-thermal, Atmospheric Pressure Plasma Generated in a Packed-Bed Reactor. *Environ. Sci. Technol.* **2014**, *48*, 558–565.
56. Schmidt, M.; Jõgi, I.; Hołub, M.; Brandenburg, R., Non-thermal plasma based decomposition of volatile organic compounds in industrial exhaust gases. *Int. J. Environ. Sci. Technol.* **2015**, *12*, 3745–3754.
57. Ghorbani Shahna, F.; Bahrami, A.; Alimohammadi, I.; Yarahmadi, R.; Jaleh, B.; Gandomi, M.; Ebrahimi, H.; Ad-Din Abedi, K., Chlorobenzene degeradation by non-

thermal plasma combined with EG-TiO2/ZnO as a photocatalyst: Effect of photocatalyst on CO2 selectivity and byproducts reduction. *J. Hazard. Mater.* **2017**, *324*, 544–553.
58. Zhu, R.; Mao, Y.; Jiang, L.; Chen, J., Performance of chlorobenzene removal in a nonthermal plasma catalysis reactor and evaluation of its byproducts. *Chem. Eng. J.* **2015**, *279*, 463–471.
59. Magureanu, M.; Mandache, N. B.; Eloy, P.; Gaigneaux, E. M.; Parvulescu, V. I., Plasma-assisted catalysis for volatile organic compounds abatement. *Appl. Catal. B* **2005**, *61*, 12–20.
60. Chen, J.; Xie, Z.; Tang, J.; Zhou, J.; Lu, X.; Zhao, H., Oxidation of toluene by dielectric barrier discharge with photo-catalytic electrode. *Chem. Eng. J.* **2016**, *284*, 166–173.
61. Jiang, L.; Nie, G.; Zhu, R.; Wang, J.; Chen, J.; Mao, Y.; Cheng, Z.; Anderson, W. A., Efficient degradation of chlorobenzene in a non-thermal plasma catalytic reactor supported on CeO2/HZSM-5 catalysts. *J. Environ. Sci.* **2017**, *55*, 266–273.
62. Nguyen, H. H.; Kim, K.-S., Combination of plasmas and catalytic reactions for CO2 reforming of CH4 by dielectric barrier discharge process. *Catal. Today* **2015**, *256*, 88–95.
63. Ma, C.; Dai, B.; Liu, P.; Zhou, N.; Shi, A.; Ban, L.; Chen, H., Deep oxidative desulfurization of model fuel using ozone generated by dielectric barrier discharge plasma combined with ionic liquid extraction. *J. Ind. Eng. Chem.* **2014**, *20*, 2769–2774.
64. Mok, Y. S.; Lee, S.-B.; Oh, J.-H.; Ra, K.-S.; Sung, B.-H., Abatement of Trichloromethane by Using Nonthermal Plasma Reactors. *Plasma Chem. Plasma Process.* **2008**, *28*, 663–676.
65. Kim, H.-H.; Lee, Y.-H.; Ogata, A.; Futamura, S., Plasma-driven catalyst processing packed with photocatalyst for gas-phase benzene decomposition. *Catal. Commun.* **2003**, *4*, 347–351.
66. Song, Y.-H.; Kim, S.-J.; Choi, K.-I.; Yamamoto, T., Effects of Adsorption and Temperature on a Nonthermal Plasma Process for Removing VOCs. *J. Electrostat.* **2002**, *55*, 189–201.
67. Hayashi, K.; Yasui, H.; Tanaka, M.; Futamura, S.; Kurita, S.; Aoyagi, K., Temperature Dependence of Toluene Decomposition Behavior in the Discharge–Catalyst Hybrid Reactor. *IEEE Trans. Ind. Appl.* **2009**, *45*, 1553–1558.
68. Jarrige, J.; Vervisch, P., Plasma-enhanced catalysis of propane and isopropyl alcohol at ambient temperature on a MnO2-based catalyst. *Appl. Catal. B* **2009**, *90*, 74–82.
69. Kim, H.-H.; Ogata, A.; Futamura, S., Atmospheric plasma-driven catalysis for the low temperature decomposition of dilute aromatic compounds. *J. Phys. D Appl. Phys.* **2005**, *38*, 1292.
70. Yue, W.; Lei, W.; Dong, Y.; Shi, C.; Lu, Q.; Cui, X.; Wang, X.; Chen, Y.; Zhang, J., Toluene degradation in air/H2O DBD plasma: A reaction mechanism investigation based on detailed kinetic modeling and emission spectrum analysis. *J. Hazard. Mater.* **2023**, *448*, 130894.

71. Dors, M.; Izdebski, T.; Tański, M.; Mizeraczyk, J., The influence of hydrogen sulphide and configuration of a DBD reactor powered with nanosecond high voltage pulses on hydrogen production from biogas. *European Chemical Bulletin* **2014**, *3*, 798–804.
72. Yan, X.; Sun, Y.; Zhu, T.; Fan, X., Conversion of carbon disulfide in air by non-thermal plasma. *J. Hazard. Mater.* **2013**, *261*, 669–674.
73. Karatum, O.; Deshusses, M. A., A comparative study of dilute VOCs treatment in a non-thermal plasma reactor. *Chem. Eng. J.* **2016**, *294*, 308–315.
74. Guo, Y.-F.; Ye, D.-Q.; Chen, K.-F.; He, J.-C.; Chen, W.-L., Toluene decomposition using a wire-plate dielectric barrier discharge reactor with manganese oxide catalyst in situ. *J. Mol. Catal. A Chem.* **2006**, *245*, 93–100.
75. Chen, H. L.; Lee, H. M.; Chen, S. H.; Chang, M. B.; Yu, S. J.; Li, S. N., Removal of volatile organic compounds by single-stage and two-stage plasma catalysis systems: a review of the performance enhancement mechanisms, current status, and suitable applications. *Environ. Sci. Technol.* **2009**, *43*, 2216–2227.
76. Mei, D.; Zhu, X.; He, Y.; Yan, J. D.; Tu, X., Plasma-assisted conversion of CO2 in a dielectric barrier discharge reactor: Understanding the effect of packing materials. *Plasma Sources Sci. Technol.* **2015**, DOI: 10.1088/0963-0252/24/1/015011.
77. Mahammadunnisa, S.; Reddy, E. L.; Reddy, P. R. M. K.; Subrahmanyam, C., A facile approach for direct decomposition of nitrous oxide assisted by non-thermal plasma. *Plasma Process. Polym.* **2013**, *10*, 444–450.
78. Sultana, S.; Vandenbroucke, A. M.; Leys, C.; De Geyter, N.; Morent, R., Abatement of VOCs with Alternate Adsorption and Plasma-Assisted Regeneration: A Review. *Catalysts* **2015**, *5*, 718–746.
79. Tang, S.; Yuan, D.; Rao, Y.; Li, N.; Qi, J.; Cheng, T.; Sun, Z.; Gu, J.; Huang, H., Persulfate activation in gas phase surface discharge plasma for synergetic removal of antibiotic in water. *Chem. Eng. J.* **2018**, *337*, 446–454.
80. Chang, C.-L.; Bai, H.; Lu, S.-J., Destruction of Styrene in an Air Stream by Packed Dielectric Barrier Discharge Reactors. *Plasma Chem. Plasma Process.* **2005**, *25*, 641–657.
81. Xu, M.; Fukuyama, Y.; Nakai, K.; Liu, Z.; Sumiya, Y.; Okino, A., Characteristics of Double-Layer, Large-Flow Dielectric Barrier Discharge Plasma Source for Toluene Decomposition. *Plasma* **2023**, *6*, 212–224.
82. Chang, C.-L.; Lin, T.-S., Decomposition of Toluene and Acetone in Packed Dielectric Barrier Discharge Reactors. *Plasma Chem. Plasma Process.* **2005**, *25*, 227–243.
83. Lee, J. E.; Ok, Y. S.; Tsang, D. C. W.; Song, J.; Jung, S.-C.; Park, Y.-K., Recent advances in volatile organic compounds abatement by catalysis and catalytic hybrid processes: A critical review. *Sci. Total Environ.* **2020**, *719*, 137405.
84. Wright, A.; Taglioli, M.; Montazersadgh, F.; Shaw, A.; Hemaka Bandulasena, H. C., Microbubble-Enhanced DBD Plasma Reactor: Design, Characterisation and Modelling. *Chem. Eng. Res. Des.* **2019**, *144*, DOI: 10.1016/j.cherd.2019.01.030.
85. Onyshchenko, I.; De Geyter, N.; Morent, R., Improvement of the plasma treatment effect on PET with a newly designed atmospheric pressure plasma jet. *Plasma Process. Polym.* **2017**, *14*, 1600200.

86. Pasolari, R. S.; Papadopoulos, P. K.; Svarnas, P.; Giannakopoulos, E.; Krontiras, C., Macroscopic modeling of plasma effects on heat and fluid flow in a dielectric barrier discharge based process for biosolid stabilization. *AIP Adv.* **2020**, *10*, 045021.
87. Abdulkadirov, R.; Lyakhov, P., Estimates of Mild Solutions of Navier–Stokes Equations in Weak Herz-Type Besov–Morrey Spaces. *Sci. China Ser. A Math.* **2022**, *10*, 680.
88. Dincer, M. S.; Tezcan, S. S.; Duzkaya, H.; Dincer, S., Synergism analysis in dielectric strength of CO2+N2+O2 ternary mixtures. *Alex. Eng. J.* **2022**, *61*, 3747–3756.
89. Duzkaya, H.; Tezcan, S. S.; Acarturk, A.; Yilmaz, M., Environmental and Physiochemical Properties of Gaseous Dielectrics Alternatives to SF6. *El-Cezeri Fen ve Mühendislik Dergisi* **2020**, *7*, 1460–1470.
90. Stancu, G. D.; Kaddouri, F.; Lacoste, D. A.; Laux, C. O., Atmospheric pressure plasma diagnostics by OES, CRDS and TALIF. *J. Phys. D Appl. Phys.* **2010**, *43*, 124002.
91. Walsh, J. L.; Kong, M. G., Portable nanosecond pulsed air plasma jet. *Appl. Phys. Lett.* **2011**, *99*, DOI: 10.1063/1.3623487.
92. Deng, X. L.; Nikiforov, A. Y.; Vanraes, P.; Leys, C., Direct current plasma jet at atmospheric pressure operating in nitrogen and air. *J. Appl. Phys.* **2013**, *113*, 023305.
93. Xiao, D.; Cheng, C.; Shen, J.; Lan, Y.; Xie, H.; Shu, X.; Meng, Y.; Li, J.; Chu, P. K., Characteristics of atmospheric-pressure non-thermal N2 and N2/O2 gas mixture plasma jet. *J. Appl. Phys.* **2014**, *115*, 033303.
94. Butterworth, T.; Allen, R. W. K., Plasma-catalyst interaction studied in a single pellet DBD reactor: dielectric constant effect on plasma dynamics. *Plasma Sources Sci. Technol.* **2017**, *26*, 065008.
95. Liang, W.; Li, J.; Li, J.; Jin, Y., Abatement of toluene from gas streams via ferroelectric packed bed dielectric barrier discharge plasma. *J. Hazard. Mater.* **2009**, *170*, 633–638.
96. Peeters, F. J. J.; van de Sanden, M. C. M., The influence of partial surface discharging on the electrical characterization of DBDs. *Plasma Sources Sci. Technol.* **2015**, *24*, 015016.
97. Huo, W. G.; Zhang, X.; Gu, J. L.; Ding, Z. F., Experimental studies of breakdown characteristics in pulse-modulated radio-frequency atmospheric discharge. *Phys. Plasmas* **2016**, *23*, 123515.
98. National Institute of Health Sciences, Acute Exposure Guideline Level for Selected Airborne Chemicals. n.d.

Publication list

Journal paper (Reviewed)

1. **Mao Xu,** Yuito Mori, Chishi Ryu, Yohei Fukuyama, Yuki Sumiya, Tianzhuo Zhan, Akitoshi Okino. Design and Characterization of an Upscaled Dielectric Barrier Discharge-Based Ten-Layer Plasma Source for High-Flow-Rate Gas Treatment, Applied Sciences, Vol. 14, No. 1, p. 27, Dec. 2023.
2. Tianzhuo Zhan, **Mao Xu,** Zhi Cao, Chong Zheng, Hiroki Kurita, Fumio Narita, Yen-Ju Wu, Yibin Xu, Haidong Wang, Mengjie Song, Wei Wang, Yanguang Zhou, Xuqing Liu, Yu Shi, Yu Jia, Sujun Guan, Tatsuro Hanajiri, Toru Maekawa, Akitoshi Okino, Takanobu Watanabe. Effects of Thermal Boundary Resistance on Thermal Management of Gallium-Nitride-Based Semiconductor Devices: A Review, micromachines, Vol. 14, No. 11, p. 2076, Nov. 2023.
3. **Mao Xu,** Yohei Fukuyama, Kazuki Nakai, Zhizhi Liu, Yuki Sumiya, Akitoshi Okino. Characteristics of Double-Layer, Large-Flow Dielectric Barrier Discharge Plasma Source for Toluene Decomposition, Plasma, MDPI, Vol. 6, Issue 2, pp. 212-224, Apr. 2023.

Book

4. Chishi Ryu, Motoaki Yamauchi, Taiki Osawa, **Mao Xu,** AKITOSHI OKINO. 大気圧プラズマを用いたポリイミドフィルムの親水化処理, ポリイミドの高機能設計と応用技術, 技術情報協会, pp. 354-361, Aug. 2022.

International Conference (Reviewed)

5. **Mao Xu,** Yohei Fukuyama, Chishi Ryu, Motohide Aoki, Akitoshi Okino. Developments of air purification device featured with dielectric barrier discharge for VOCs abatements, The 7th International Symposium on Biomedical Engineering (ISBE2022), Nov. 2022.
6. **Mao Xu,** Yohei Fukuyama, Zhizhi Liu, Akitoshi Okino. Decomposition of high-density Toluene in water-vapor- mixed Nitrogen/Air using dielectric barrier discharge, 75th Annual Gaseous Electronics Conference (GEC 2022/ICRP-11), Oct. 2022.
7. **Mao Xu,** Yuito Mori, Motohide Aoki, Tomonari Umemura, Akitoshi Okino. Decomposition of large flow toluene using multilayer dielectric barrier discharge, The 49th IEEE International Conference on Plasma Science (ICOPS 2022), May 2022.
8. Yohei Fukuyama, **Mao Xu,** Yuki Sumiya, Akane Yaida, Motohide Aoki, AKITOSHI OKINO. Decomposition of large-flow and high-concentration VOCs using large-area dielectric barrier discharge, The 8th International Symposium on Biomedical Engineering, Nov. 2023.
9. Zhizhi Liu, Taiki Osawa, **Mao Xu,** Yuriko Matsumura, Atsuo Iwasawa, Akitoshi Okino. Simultaneous irradiation device of low-temperature plasma and ultraviolet light for surface treatment and sterilization, 25th International Symposium on Plasma Chemistry, May 2023.

Domestic Conference (Reviewed)

10. **Mao Xu,** Zhi Cao, Akitoshi Okino, Tianzhuo Zhan. Effects of Annealing on Thermal Boundary Resistance of Low-k Interlayer Dielectrics, The 70th JSAP Spring Meeting 2023, Extended abstracts of the 70th JSAP spring meeting, The Japan Society of Applied Physics, 16p-A403-18, Mar. 2023.
11. **Mao Xu,** Yohei Fukuyama, Zhizhi Liu, Akitoshi Okino. Decomposition experiments of toluene in humidified air using intermittent pulse barrier discharge, The 83rd JSAP Autumn Meeting 2022, Sept. 2022.
12. **Mao Xu,** Yuito Mori, Akitoshi Okino, Motohide Aoki, Tomonari Umemura. Development of large flow air purification devices based on dielectric barrier discharge plasma, 令和 3 年度生体医歯工学共同研究拠点成果報告会/第 12 回 IDEA 連携シンポジウム, 令和 3 年度生体医歯工学共同研究拠点成果報告会, 生体医歯工学共同研究拠点成果報告会, Mar. 2022.
13. Yohei Fukuyama, **Mao Xu,** AKITOSHI OKINO. 大面積誘電体バリア放電を用いた加湿空気および窒素中高濃度トルエンの分解実験, 2022 年放電学会年次大会, Dec. 2022.
14. Chishi Ryu, Motoaki Yamauchi, **Mao Xu,** Taiki Osawa, AKITOSHI OKINO. 紫外/赤外線-プラズマ同時処理に向ける透明電極誘電体バリア放電装置の開発と基礎特性評価, 2022 年第 83 回応用物理学会秋季学術講演会, Sept. 2022.

Domestic Conference (Not reviewed / Unknown)

15. Zhizhi Liu, Taiki Osawa, **Mao Xu,** Akitoshi Okino. Measurement of and Hydrophilic Effect and Spectroscopic Property of Ultraviolet and Low-temperature Plasma Simultaneous Irradiation Device, 2022 年度日本分光学会年次講演会, 2022 年度日本分光学会年次講演会要旨集, Oct. 2022.
16. Motoaki Yamauchi, **Mao Xu,** Taiki Osawa, Kenichi Yamazaki, AKITOSHI OKINO. 循環型プラズマ処理のためのマルチ電極プラズマアクチュエータの開発, 令和 4 年 電気学会 A 部門大会, Sept. 2022.
17. Yohei Fukuyama, **Mao Xu,** Koki Hihara, Motoaki Yamauchi, AKITOSHI OKINO. 大面積バリア放電を用いた亜酸化窒素の分解実験, 電気学会東京支部カンファレンス学生研究発表会, Aug. 2022.
18. Motoaki Yamauchi, **Mao Xu,** Taiki Osawa, Kenichi Yamazaki, AKITOSHI OKINO. プラズマ化した気体の循環のためのマルチ電極プラズマアクチュエータの開発, プラ研若手会第二回講演会, July 2022.
19. Motoaki Yamauchi, **Mao Xu,** Taiki Osawa, Kenichi Yamazaki, AKITOSHI OKINO. プラズマ化した気体の非接触制御のためのマルチ電極プラズマアクチュエータの基礎実験, 2022 筑波セミナー, June 2022.